Molecular Dissection of the Retinal Projectome

Submitted by

Yvonne Kölsch

Dissertation der Graduate School of Systemic Neurosciences
der Ludwig-Maximilians-Universität München

April 2019

First reviewer and supervisor

Prof. Dr. Herwig Baier

Genes- Circuits - Behavior

Max Planck Institute of Neurobiology

Second reviewer

Prof. Dr. Rüdiger Klein

Molecules – Signaling - Development

Max Planck Institute of Neurobiology

External reviewer

Prof. Dr. Stephan Neuhauss

Institute of Molecular Life Sciences

University of Zurich

Submission of dissertation

April 1st 2019

Defense

September 9th 2019

Ever tried. Ever failed. No matter. Try Again. Fail again. Fail better.
- Samuel Beckett

ABSTRACT

Keywords: cell type classification, retinal ganglion cells, molecular markers, visual pathways, behavior

The retina transforms visual sensation into perception. Extracted visual features are encoded by retinal ganglion cells (RGCs), the output neurons of the eye, and sent to the brain in parallel processing channels. Morphologically, RGCs fall into more than fifty diverse types, which innervate distinct brain areas. Such visual pathways differentially regulate various behaviors. However, the genetic determinants of RGC type diversity are unknown and thus we lack genetic access to study visual pathways. A generation of a more comprehensive RGC type atlas integrating molecular, morphological and functional properties is essential to dissect the functional architecture of the visual system.

In a collaborative effort, I used single cell transcriptomics to molecularly classify RGCs during larval and adult stages. RGC types segregate into many discrete transcriptional clusters each with a unique molecular composition. Relatedness of clusters revealed a molecular taxonomy, in which RGC types are arranged into major RGC groups that comprise subclasses and diversify into individual types. This organization of RGC type diversification underlies a code of gene expression patterns, composed primarily of transcription factors. Differential gene expression analysis identified dozens of novel cluster-specific genetic markers for RGC types. Comparison of transcriptional signatures revealed that larval RGCs exhibit higher molecular diversity, which facilitates segregation of similar types, while adult RGCs maintain a core molecular identity suggesting a tight correspondence between larval and adult RGC types.

Next, I mapped transcriptional clusters to RGC morphotypes. Select candidate markers were exploited as genetic entry points in a CRISPR-Cas9 transgenesis approach. To restrict labeling specifically to cluster-specific RGC types, I established a genetic intersection with a broad RGC marker. This intersectional transgenic approach allowed to correspond various clusters to distinct morphologically classified RGC types. I generated two transgenic lines using RGC subclass markers, one of which is based on the transcription factor *eomesa* expressed by RGC types routing to visual areas in hypothalamus, pretectum and tectum.

Based on homologies to RGC types characterized in other species, I hypothesized that *eomesa*$^{+}$ RGCs constitute intrinsically photosensitive RGCs and have non-image forming functions. I tested this hypothesis by characterizing their response

profiles to a battery of visual stimuli and found that they are not tuned to canonical pattern stimuli. Rather *eomesa*$^{+}$ RGCs encode ambient luminance levels corroborating my hypothesis. I further tested their necessity in non-image forming behavior, specifically visual background adaptation, which by initial investigation appears to not be affected by chemogenetic ablation of *eomesa*$^{+}$ RGCs.

In conclusion, this thesis presents a strong foundation for a RGC type atlas and reconciles molecular, morphological and functional features of discrete cell types. This comprehensive molecular classification of RGC types, together with the identified markers and newly established transgenic tools, provides a rich resource towards a better understanding of visual pathway function.

ACKNOWLEDGEMENT

The past years as a PhD student clearly were an exciting and adventurous period of my life. I have grown personally and professionally, have advanced my technical skills and expanded my knowledge base inside and outside of neuroscience. I would not have come this long way if it was not for the contribution of the people I was surrounded by. Many have left their mark on my life and deserve heartfelt thanks:

I am very grateful to Herwig Baier for giving me the opportunity to perform my graduate studies in his lab, which has allowed me to become a confident scientist. Over the course of my entire PhD, I have had the invaluable privilege of intellectual and experimental freedom to let my scientific creativity develop and run free. I am very glad I could immerse myself in studying cell types in the visual system from a molecular and developmental perspective - and furthermore bridge my project to functional analyses. Thank you, Herwig, for your consistent supervision and scientific advice as I traversed through these themes of Neuroscience. Many thanks for all inspiration and guidance during the past years!

I wish to thank my thesis committee members Herwig Baier, Rüdiger Klein and Claire Wyart for guidance, critique, discussions and fruitful input to my thesis during our annual meetings. I further thank Herwig Baier, Rüdiger Klein and Stephan Neuhauss for evaluation of this thesis.

I feel tremendously fortunate for having had the opportunity to collaborate with Joshua Sanes and his lab members. I contemplate this development of my PhD as a once-in-a-lifetime opening, which I was more than happy to take! I often think back to my experiences at Harvard. My visits were certainly amongst the most educational, busy, inspiring and encouraging periods of my PhD. Thank you, Herwig, for the support and thank you, Josh, for welcoming me in your lab!

I would like to express my deep appreciation to Irene for her friendly, warm, and patient support during my visits and the valuable experimental advice that made a great contribution to the realization of this collaborative project. I would like to express my sincere gratitude to Karthik, Anna and Wenjun, who made great efforts on the computational side of the project to make this a success. My further acknowledgement is directed to Emily, Mallory, Yirong and Dustin for lending their

helping hands on occasions. Also, thanks to all Sanes lab members for the great time I got to spend at Harvard.

I feel blessed for having such inquisitive, smart and fun minds as my colleagues. I have always enjoyed the passionate and heated discussions during lab meetings. I am particularly thankful for the direct contributions of Manuel, Shriya, Thomas, Eva and Irene to my PhD project. Thanks to all past and present Baier lab members with further special mention of Estuardo, Miguel, Eliane and Anna.

Many thanks to Michael, Duncan, Manuel, Greg and Shriya for comments and discussions on this thesis.

I owe the deepest acknowledgement to my mother Marion, my father Torsten, my aunt Doris and to Paul, who tolerated my focus on my PhD project with great understanding and who continue to show their relentless unconditional support for me.

Thank you for all the encouragement!

Contents

LIST OF FIGURES AND TABLES

ABBREVIATIONS

AF	arborization field
AC	amacrine cell
BAC	bacterial artificial chromosome
BC	bipolar cell
Cas	CRISPR-associated
CRISPR	clustered regularly interspaced short palindromic repeats
crRNA	CRISPR RNA
DNA	deoxyribonucleic acid
dpf	days post fertilization
FACS	fluorescence-activated cell sorting
GCL	ganglion cell layer
gRNA	guide RNA
HC	horizontal cell
INL	inner nuclear layer
IPL	inner plexiform layer
ONL	outer nuclear layer
OPL	outer plexiform layer
PAM	protoadjacent motif
PBS	phosphate buffered saline
PC	projection class
PCA	principal component analysis
PFA	paraformaldehyde
PR	photoreceptor
RGC	retinal ganglion cell
RNA	ribonucleic acid
SAC	stratum album centrale
SFGS	stratum fibrosum et griseum superficiale
SGC	stratum griseum centrale
SO	stratum opticum
SPV	stratum periventriculare
tracrRNA	trans-activating crRNA
t-SNE	t-stochastic neighbor embedding

1 INTRODUCTION

1.1 Neuronal cell type classification to better understand brain function

Our brain is the most complex organ and is central to all bodily tasks and higher cognitive functions. One particular aspect of today's neuroscience aims to better understand how the brain processes perception and transforms it into behavioral adaptations.

The nervous system is composed of a myriad of neurons, the fundamental elements of the brain, which are interconnected to form intricate neuronal networks and communicate with each other. Each neuron within a circuit executes a specified task to compute and transmit information. To allow for such processing, neurons differ in their molecular, morphological and physiological properties. The rich diversity of neuronal cell types was already recognized in early studies by Santiago Ramón y Cajal [1–3]. The founding father of modern neuroscience employed a sparse labeling technique in various brain parts across animal species and demonstrated that neurons come in varying shapes and differ greatly in their morphological properties. In looking at the retina, the nervous tissue that lines the back of our eye and enables us to perceive the visual world, Cajal described distinct neuronal classes that are connected to each other and proposed pathways of visual information flow. Cajal thus characterized all major retinal cells [2] shown in Figure 1A: Photoreceptors sense light, bipolar cells convey information from photoreceptors onto retinal ganglion cells, which send visual perception to the brain, as well as local horizontal cells and amacrine cells and Müller glia.

How can we dissect the vast diversity of cell types assembling the brain to fully comprehend neural circuit function? Today, it is in common agreement that, in order to understand how the brain works, comprehensive accounting and definition of its component cell types is key [4–8] . Once a robust cell type atlas has been built, it will advance research in numerous ways [5]: First, a clear reference frame will allow to unequivocally identify same types and compare results across studies. Second, unbiased global characterization of tissue components will lead to the discovery of new types. Third, comparison of cell type atlases across species will allow to identify analogous, evolutionary conserved types. Fourth, and most significant to the present thesis, molecular classification will provide researchers with genetic access to cell types, which facilitates their specific investigation.

What could a cell type atlas look like? Numerous studies are underway to classify cell types present in all kinds of tissues from model organisms to humans. But conceptual foundations for a cell type classification scheme are still highly debated. The prevailing idea is to catalog types into a hierarchical tree - a cellular taxonomy [5,6]. Here, cell types can be distinguished by virtue of their characteristics from a higher degree of shared features to discrete properties unique to a cell type. At higher order, types are grouped into classes, composed by subclasses at intermediate level, which split into terminal branches that represent individual cell types on lowest order. Given the rich current knowledge, an extensive type atlas of the retina as illustrated in Figure 1B is within reach and could prove as an ideal substrate for conceptualization of cell types. Prospective empirical data, however, will need to be integrated into and harmonized within atlases to substantiate and manifest accurate representation of cell types.

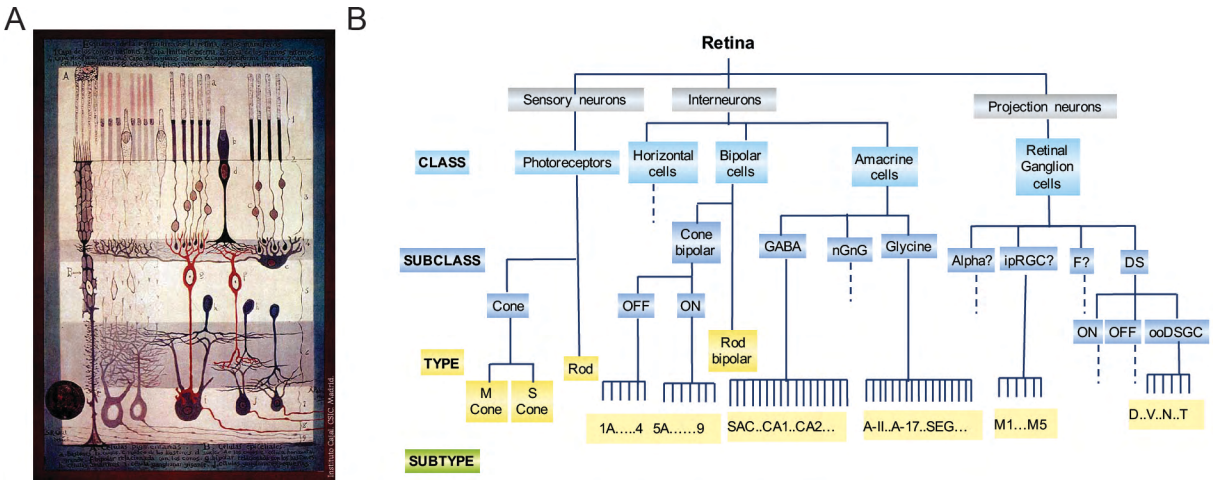

Figure 1: Approach for classification of neuronal cell type diversity.

A) Drawing from Ramón y Cajal demonstrating neuronal cell type diversity in the retina. Taken from the Instituto Cajal. **B)** Cellular taxonomy of the retina – a proposed hierarchical design of a cell type atlas. Cell types are arranged from top to bottom by virtue of degree of commonalities to increasing discreteness. Taken from Zeng and Sanes, 2017 [5].

1.1.1 What is a neuronal cell type?

How exactly is a cell type defined? A universal consensus as to how to unambiguously discriminate cell types has not been reached yet. Thus, the genuine definition of a cell type is contentious to date. However, the notion that a cell type occupies a unique functional niche is at the core of ongoing debates. In other words, neurons belong to

the same type population if they have homogeneous properties but differ from the properties of other type populations. [4,5,8–12]

In finding a definition of a cell type, diverse neuronal properties should be cut down into different categories such as anatomical localization, developmental origin, molecular signature, morphology, connectivity, physiology and function. These modalities are synergistic and interdependent and all cellular properties together should build a unique entity, which determines a cell type [5].

It is interesting to note that there are opposing opinions regarding which criterion should be prioritized. Some argue that functional properties are superior to genetic properties [7], while others consider a cell's genetic repertoire as the all underlying determinant of type identity and function [4,5]. Ideally, cell type atlases will be polythetic - an aggregate of all modalities accommodating different criteria from molecules to function. Because it is currently unclear if all criteria can be reconciled in the same cellular taxonomy, there is need to investigate how different classification criteria correspond to each other. For example, will a morphologically classified type have a unique molecular composition and correlate with a distinctive physiological profile?

1.1.2 Comprehensive type classification by large-scale molecular profiling

Apart from the conceptual challenges described above, there are also technical obstacles towards systematic classification of cell types. While descriptions of cell types based on connectivity [13], physiology [14,15] or morphology [16,17] are precedent, large-scale classification using such approaches has been hampered by technical constraints.

In contrast, transcriptional profiling has been more widely used to investigate cell types. As briefly mentioned above, a cell's identity is largely rooted in its molecular composition [4] and thus identifying the ensemble of mRNA molecules transcribed from active genes within a cell facilitates classification. Early studies began to unravel bulk genetic differences of purified neuronal populations using microarray [18–20] or RNA-Sequencing [21,22], but great cell heterogeneity within these samples had obscured identification of actual types. As methods became sensitive to low RNA content, scientists moved on to sequence single cells using a variety of techniques based on manual or automatic isolation of individual cells prior to RNA-Sequencing [23–33]. Although unique genetic features associated with distinct neurons became evident,

these techniques were still limited in throughput, which prevented comprehensive classification of types within a neuronal population.

Recent advances in the field of single cell transcriptomics, however, have revolutionized cell type classification approaches now allowing for simultaneous molecular characterization of thousands of cells. Such massively parallel RNA-Sequencing assays established since 2015. In particular, Drop-Seq [34], inDrop [35] and the commercialized 10X Genomics system [36] have leveraged the ability to profile the transcriptome of single cells at unprecedented large scale. The shared basic concept of these methods is a microfluidic platform as depicted in Figure 2A. The chip consists of micro-channels arranged in a pathway to allow for automated mixing of input components. One lane carries hydrogel beads harboring distinctly barcoded oligonucleotides. In parallel, another lane is loaded with a single cell suspension. Individual cells are co-encapsulated with one hydrogel bead into a droplet and carried away in oil. Inside the droplet, the cell is lysed and its poly-adenylated RNA is captured by barcoded oligonucleotides. All barcodes on a hydrogel share the first nucleotides forming a 'cell barcode', which is followed by a distinct sequence functioning as unique molecular identifier (UMI) for each transcript within a cell. During reverse transcription, these barcodes are tagged to individual RNA molecules so as to uniquely barcode each cell's transcriptome. Using this microfluidic preparation, thousands of such droplets can be collected into a single reaction tube and, subsequently, a cDNA library can be prepared in bulk. The barcoding system allows to assemble RNA molecules by cell of origin and digitally count transcript numbers during following bioinformatic analyses.

Droplet-based RNA-Sequencing has been proven a successful approach to classify cell type identities in the murine retina [34]. In this pioneering study, Macosko *et al.* characterized the mRNA composition of close to 45.000 retinal cells captured by Drop-Seq. The authors performed bioinformatic analyses including principal component analysis, a density clustering approach and dimensionality reduction using t-stochastic neighbor embedding to parse molecular diversity into defined cell types. In doing so, they identified thirty-nine distinct transcriptional clusters (Figure 2B), which directly correspond to described retinal cell types as determined by selective expression of known molecular markers.

The field remains very active and methods are constantly improved or modified. Alternative versions of droplet-RNA-Sequencing protocols allow, for example, to use fixed cells enabling to profile rare types from archived samples [37]. Besides, new approaches for cell type classification, complementary to droplet-based

RNA-Sequencing techniques, are being developed such as microwell-based expression profiling systems [38,39] or spatial transcriptomics [40,41].

Taken together, droplet RNA-Sequencing methods provide researchers with an extremely powerful tool to comprehensively analyze transcriptional composition, identify cell types and build molecular atlases as a foundation to systematically investigate brain function.

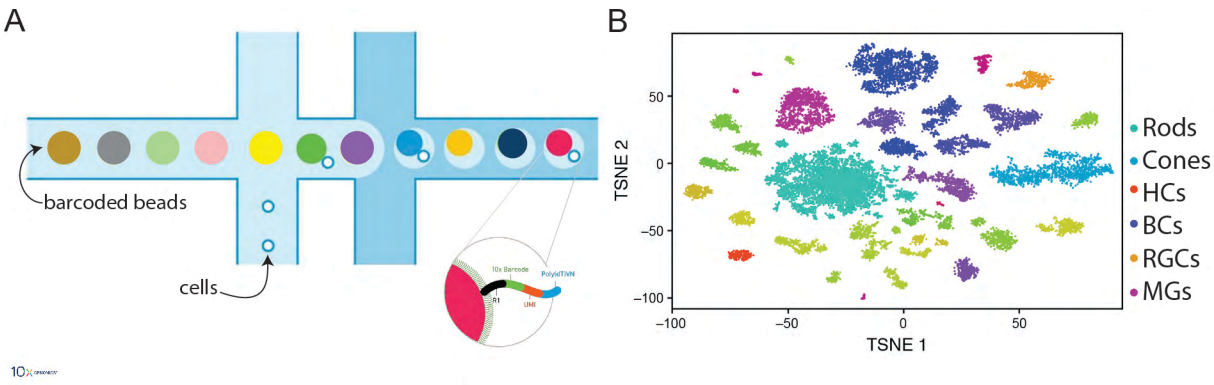

Figure 2: Molecular cell type classification by large-scale transcriptomic profiling.

A) Concept of high-throughput single cell RNA-Sequencing using a microfluidic device. The device has three input lanes: One carries barcoded hydrogel beads, another lane is loaded with a single cell suspension and oil fills the output lane. Single cells are co-encapsulated with a barcoded hydrogel and thousands of cell-hydrogel droplets can be collected from the output channel. Cells are lysed inside the droplet and each cell's transcriptome is uniquely barcoded during reverse transcription for subsequent bulk preparation and sequencing. Figure used with permission from 10X Genomics. **B)** Molecular classification of mouse retina cell classes and types using a high-throughput single cell RNA-Sequencing method. Bioinformatic analyses grouped transcriptomic profiles of more than 40.000 cells into thirty-nine distinct transcriptional clusters, which directly correspond to rods, cones, horizontal cells (HCs), bipolar cells (BCs), retinal ganglion cells (RGCs) or Müller glia (MGs). Figure modified from Macosko et al., 2014 [34].

1.1.3 Current advances in molecular cell type classification of the retina

Since its introduction, high-throughput single cell RNA-Sequencing has been widely applied for cell type classification in various tissues from organoids to model organisms to humans [42–44]. I will restrict myself to review recent progress on molecular cell type classification in the retina across organisms, in particular of bipolar cells (retinal interneurons) and retinal ganglion cells (the output neurons of the eye), and highlight valuable lessons learned from these studies:

Because there is detailed molecular prior knowledge, the mouse retina served as a proving ground for the ability to resolve cell types using Drop-Seq [34]. As

mentioned above, several thousand sequenced retinal cells were segregated into distinct clusters based on their transcriptional profile. Of note, retinal ganglion cells (RGCs) were represented by a single cluster (see Figure 2B), while bipolar cells (BCs) or amacrine cells (ACs) formed multiple clusters. The smallest cluster comprises as little as fifty cells and was identified as astrocytes, which had associated with axons. The overall size of the clusters correlated well with the proportions of cell classes characterized by histology. Conceivably, highly abundant cell types are captured more frequently and represent a larger proportion of the total dataset. The authors further demonstrate that cell type resolution is dependent on number of analyzed cells. In other words, the more cells are sequenced, the more evident become transcriptional differences and the better a cell type forms a segregated cluster. Consequently, rare cell types, such as RGCs comprising only 1% of the mouse retina [45], were underrepresented and lumped into one cluster in this dataset. The heterogeneity of the RGC cluster was further dissected by consecutive supervised clustering. [34]

Owing to transcriptional profiling by single cell RNA-Sequencing, murine BCs likely form the best classified neuronal population to date. Purified retinal cells were sequenced to median depth and, following contaminant removal, BCs were clustered into fourteen domains, which represent putative BC types [46]. Differential gene expression analysis identified markers that are strongly enriched in specific clusters. Using previously characterized genetic markers in addition to experimental validation of new markers, BC transcriptional clusters could be matched to BC morphotypes in a one-on-one fashion. This orthogonal investigation from molecules to morphology also led to the discovery of a new BC type, which masquerades as an amacrine cell. Analysis of cluster relationships resulted in a taxonomic tree, where the major branch splits two groups each comprising BC types with shared physiological and axonal features. Apart from these biological insights, the authors confirm that a large number of cells is required to differentiate molecularly similar types. Moreover, they further demonstrate that deep sequencing of fewer cell numbers is not satisfactory to classify cell types. Altogether, Shekhar et al. generate an experimental and bioinformatical framework for cell type classification. [46]

Classification studies of mouse BCs present a particularly exciting and encouraging case, because different approaches investigating different criteria, specifically morphology [46–48], physiology [15] and genetics [46], identified same or almost same numbers of BC types, indicating that reconciliation of distinct modalities is possible [5].

Similarly to BCs, a study pursued categorization of mouse retinal ganglion cells (RGCs), which are much more diverse than BCs. Using the commercialized 10X Genomics platform, more than 6.000 RGCs were sequenced and forty clusters were retrieved after bioinformatic clustering analysis [49]. Interestingly, examination of cluster-specific marker genes suggested that RGC types are defined by a code of transcription factor expression. Relatedness of these clusters generated a hierarchical tree, forming intermediate RGC subpopulations (conceptually equivalent with the above-mentioned term 'subclasses'), which harbor several individual clusters (equivalent to the concept of a 'type'). Notably, RGC subclasses differentially express transcription factors. For example, a particular subclass is defined by expression of Eomes, a marker for well characterized intrinsically photosensitive RGC types, and harbors five individual clusters.[49]

More recently, single cell transcriptomics has been applied to primate and human retinas to establish a molecular classification of higher vertebrate retinas [50]. This research was expanded to evolutionary conservation across species. Comparison of retinal cell types between macaques and mice disclosed that, with exception of RGCs, most retinal cell classes can be readily matched between species. Strikingly, despite similar transcription factor codes across RGC clusters, there is no close molecular correspondence between mouse and macaque RGC types. Merely intrinsically photosensitive RGCs, an evolutionary ancient RGC subset, exhibit a comparable transcriptional repertoire between the examined species.[50]

These scientific efforts together show that key methodological advancements in single cell transcriptomics allow for a definition of cell types based on increasingly detailed descriptions of their properties. In reconciliation of molecular classification with the rich prior histological and functional knowledge, full classification of the mouse retina is within reach. Except for primate retina [50], however, other model organisms remain little explored, which precludes further assessment of conserved cell types, their genetic markers and organizing principles of type diversification.

1.2 The molecular toolbox for neuronal circuit dissection in zebrafish

Since its introduction in the 1980's [51], the zebrafish, *Danio rerio*, appeals as a vertebrate model organism with genomic and structural homologies to other vertebrates including humans [52]. The zebrafish facilitates research with several key advantages [53]: First, zebrafish are easy to maintain and breed in a cost-efficient manner. Second, the embryo develops externally and a full body plan is established rapidly. Third, the larvae remain transparent allowing for many experimental measurements including the visualization of developmental processes as well as the anatomy of the nervous system or the recoding of neuronal activity. Fourth, zebrafish are amenable to genetic modifications and manipulations. A great variety of transgenic lines and mutants is available to the community to study gene and tissue function in diverse contexts. Fifth, without compromise of cell type diversity, the zebrafish brain has a modest size easing inspection of neurons.

1.2.1 Labeling, characterizing and manipulating neurons using transgenic tools

Zebrafish are a well suited model organism for neuronal circuit dissection and tools are available to label, functionally characterize and manipulate neurons of interest. Most of its applications are based on transgenic lines, which allow to express a genetically encoded tool in a tissue-specific and timely-controlled manner. Binary expression systems, like the Gal4/UAS system adapted from yeast, offer a versatile platform, where any tissue-specific driver line can be combined with a desired reporter line (Figure 3A). Here, a driver line expresses the transcription factor Gal4 under control of a specific promoter. Gal4 binds to its consensus sequence named UAS and activates reporter expression of a tool of interest [54]. To date, an extensive library of Gal4-driver lines and UAS-reporter lines is available to the community [55–57]. Notably, some drawbacks of the Gal4/UAS-system have been reported over the past decades that include variegation of gene expression due to positional integration effects or silencing over generations [55]. Thus, an alternative binary expression system was introduced recently and promises more robust gene expression [58,59]. The Q-system, originating form a gene cluster in a fungus, acts equivalently to the Gal4/UAS-system and consists of the QF2 transcription factor and its QUAS consensus sequence [60,61].

Using these transgenic systems, neuronal circuits can be readily observed in the transparent zebrafish brain (Figure 3B) and dissected at various levels. Regarding anatomy, for example, cellular morphology can be reconstructed by sparse labeling

techniques [62–67]. At the functional level, physiology of neurons can be characterized by measuring their activity patterns. The method of choice for functional characterization is a genetically-encoded calcium sensor such as GCaMP. GCaMPs consist of a fusion of GFP and calmodulin, where the latter inactivates the fluorescent state by default [68]. When a neuron becomes active and intracellular calcium concentrations rise, calmodulin undergoes a conformational change and no longer inhibits GFP florescence. Hence, GCaMP fluorescence levels serve as a proxy for neuronal activity and can be measured *in vivo* over time using a two-photon microscope [69–71]. Moreover, causal relationship of a specific neuronal population to a behavior or biological effect can be demonstrated by manipulating neural circuits. Chemogenetic ablations, for example, facilitate such necessity tests by inducing cell death of neurons of interest. In detail, cells express the bacterial enzyme nitroreductase, which converts its substrate, when applied to the fish water, into a DNA-intercalating compound ultimately leading to cell death [72–74].

In summary, scientists can draw from versatile resources of driver and reporter lines and diverse, optimized genetic techniques to inspect different aspects of neural circuit function ranging from development, anatomy, physiology to regulation of behavior.

1.2.2 Cell type specific markers provide genetic access for circuit analysis

Availability of genetic markers is essential to the analysis of neuronal circuits. Such defined markers can be exploited as genetic entry points and enable precise interrogation of cell types through reliable, robust and reproducible labeling of the same type. Cell type specific driver lines, which rest on promoter regulation of genetic markers, can be combined with tools described above for characterization and manipulation.

Various approaches were implemented to generate such tissue-specific driver lines. For example, screening efforts for random insertion of transgenes generated a large array of lines, in which transgene expression is regulated by trapped enhancers [57,66,75]. Insertion sites of most enhancer trap lines, however, remain unknown and hence, genes reflected by a given expression pattern are not identified. More precise and gene-oriented transgenesis was made possible through the development of bacterial artificial chromosomes (BACs) [76,77]. BACs are large genomic clones and carry a gene of interest together with large flanking regions that include its promoter.

BACs can be modified so as to achieve transgene transcription under control of the genes' endogenous promoter and integrated into the zebrafish genome to generate stable transgenic lines. Most of the BAC lines largely reproduce the endogenous expression pattern of the desired gene [77]. This way, cells expressing a marker of interest can be labeled throughout the larval zebrafish. Some examples of lines reflecting expression of transcription factors, neurotransmitters, neuropeptides or axon guidance molecules are shown in Figure 3B. Many of the available transgenes have been registered in an atlas and are digitally searchable [70,78–81].

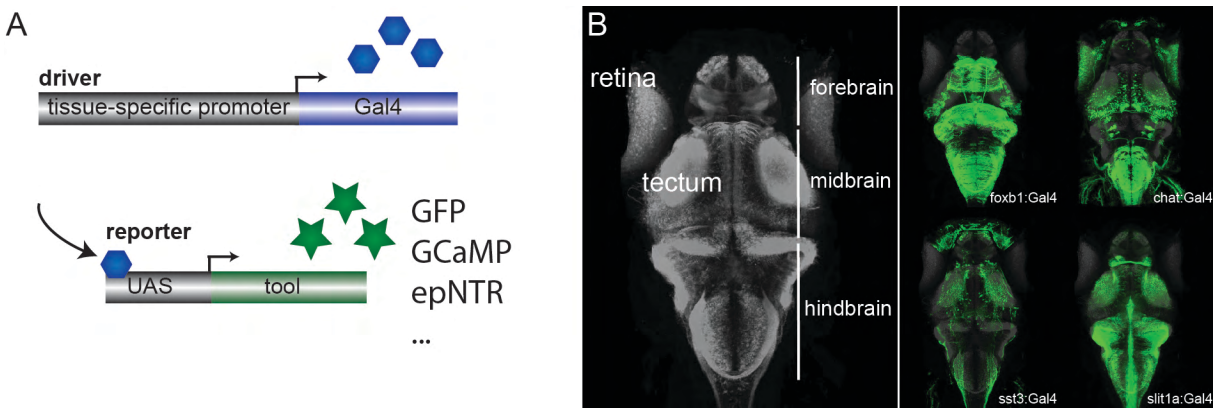

Figure 3: Transgenic tools for neuronal circuit dissection in zebrafish.

A) Using the binary Gal4/UAS expression system, a tissue-specific promoter expresses the yeast transcription factor Gal4, which in turn binds to its UAS consensus sequence to activate expression of a genetically encoded tool. **B)** Coarse structure of the translucent larval zebrafish brain. A versatile library of transgenic driver and reporter lines aids the visualization, functional characterization and manipulation of specific neuronal populations and cell types. Examples show a selection of Gal4 driver lines labeling different brain areas. Images were taken from a zebrafish brain atlas resource (Kunst et al. [81], under review).

An important caveat, though, is that most of the genes hold functions in diverse tissues and are expressed across several areas of the brain. Thus, to specifically target a defined cell type, transgene expression thus needs to be further refined. The prevailing consideration as to how to restrict expression is by genetic intersection. Here, two transgenes present in the same cell together result in activated expression of a reporter. In a more specific example of this two-component system, a driver line initiates expression of an intersectional reporter that consists of a default cassette and a conditional cassette. A second transgene modifies the reporter transgene effecting in removal of the default cassette. Ultimately, combined driver expression and reporter modification creates a logic AND gate and refines transgene expression to specific cell

types. Such combinatorial finesse has been successfully applied to zebrafish [80,82], but technical limitations have prevented its widespread use.

Yet, genetic markers for individual cell types or markers for combinatorial intersection have not been identified comprehensively. Today, advanced molecular techniques, in particular droplet RNA-Sequencing, together with optimized transgenic tools give hope to better define, target and access cell types making headway for specific circuit analysis.

1.2.3 Precise genome engineering using the CRISPR-Cas9 system

The traditional transgenic technologies described above, although straightforward in implementation, often do not recapitulate the endogenous expression pattern of a gene of interest in a faithful manner because promoter elements are incomplete [83]. In addition, many transgenes show highly variegated quality of expression probably due to integration at random and sometimes silenced positions in the genome [66]. In recent years, more advanced genome engineering methods were developed [84–86], which promise highly faithful mimicry of gene expression achieved by direct knockin of a transgene to the endogenous site. These methods are built upon nucleases, which are guided to target DNA by a sequence-specific component, where they induce site-specific DNA cleavage. Cellular DNA damage repair pathways are erroneous and can lead to insertions or deletions or to the integration of a transgenic fragment at the desired locus.

Due to its ease of implementation, the CRISPR-Cas9 system has transformed genome engineering applications [87,88]. This versatile system originates from the bacterial and archaeal adaptive immune system [89] and comprises mainly two components, which together result in a dual RNA-guided endonuclease complex: the genomic CRISPR (clustered regularly interspaced palindromic repeat) array and the CRISPR-associated protein 9 (Cas9). DNA of invading viruses is incorporated into spacers within the CRISPR array and used as template for RNA transcription of crRNA (CRISPR RNA). crRNA and trans-activating RNA (tracrRNA) form a RNA duplex, which in turn builds a ribonucleoprotein complex with the Cas9 protein. Cas9 induces DNA double strand breaks in the invader DNA matching the twenty nucleotides sequence of crRNA. [90] Based on this detailed understanding of CRISPR-Cas9 system function, it could be reprogrammed to target any genomic locus in eukaryotic cells [91–

[93]. Today, CRISPR-Cas9 is adapted in many systems across biology, biotechnology and medicine to induce site-specific DNA modifications.

In fact, the CRISPR-Cas9 system has been successfully applied to zebrafish transgenesis and will likely become the standard procedure. Yet, insertion of transgenes is not used routinely and many efforts are underway to improve protocols. For example, insertion can be targeted to various genomic regions such as upstream of the gene [83,94] , to transcribed regions disrupting gene function [95] or as a linker to the end of the transcript. Moreover, laboratories have different preferences regarding use of Cas9 protein [95] versus mRNA [83,96] or use of flanking homology arms in the donor [97] or claim bait sequences for highly efficient cleavage [96]. Notably, a successful integration event does not guarantee optimal transgene expression as there is a 50% chance of reverse integration and if inserted to coding sequence even less due to possible out-of-frame integration [83]. All these points considered, a universal protocol for CRISPR-Cas9 knock-in remains to be established.

Nonetheless, the CRISPR-Cas9 system provides a promising method to edit the zebrafish genome. It will likely become the standard procedure to generate transgenic lines. Because the transgene is integrated directly to the natural promotor site, it will recapitulate the endogenous pattern with high confidence.

1.3 The visual system – a starting point to comprehensively catalog cell types

1.3.1 Why study the visual system?

The visual system is the part of the brain that perceives and processes all information of our visual environment and is the best studied sensory system. Visual information is sensed by the retina located in the eye. Its structure and function is extremely well described owing to several key advantages that facilitate experimental investigation [12,98]: First, the retina is anatomically separated from the brain and presents an easily accessible part of the nervous system. Second, there are only six principal retinal cell classes, which are arranged in a clearly defined laminar architecture. Photoreceptors (PRs), bipolar cells (BCs), horizontal cells (HCs), amacrine cells (ACs), retinal ganglion cells (RGCs) and Müller glia cells can be readily identified and discriminated based on morphology and laminar position. Third, each laminar structure can be associated with a specific stage of visual processing.

Furthermore, it is generally known that diverse retinal cell types build complex neuronal networks, which act as image processors to extract relevant features of the visual percept [99–101]. The retina achieves perception in a complete computational circuit: It has a sole source of input from photoreceptors and a sole output channel formed by retinal ganglion cell types, which relay preprocessed visual information to several distinct brain nuclei. These downstream processing sites in the brain initiate appropriate motor commands allowing an animal to constantly adapt to the visual environment [102].

Experimental advantages together with a wealthy prior description of morphology and function make the retina an ideal proving ground for cell type classification studies. The retina is likely to be the first neuronal tissue with full inventory of cell types and their correspondences of molecular, morphological and functional features.

1.3.2 The retina transforms sensation into perception

The retina, as indicated above, contains an intricate neural network of specified cell types that process images from incoming light signals [99–101]. In other words, the retina transforms sensation into perception. How does it work?

The structure and function of the retina is evolutionary conserved [103] and underlies a common principle [98,104–107] : The retina is a highly organized neuronal structure that comprises three nuclear layers, where retinal cell bodies reside, and two plexiform layers, which harbor synaptic connections between retinal neurons. These layers are stacked on top of each other and arranged from outside in: outer nuclear layer (ONL), outer plexiform layer (OPL), inner nuclear layer (INL), inner plexiform layer (IPL) and ganglion cell layer (GCL). Each of these retinal layers harbors different retinal cell classes, which execute specific functions in transmission and computation of visual information (Figure 4). In brief, photoreceptors in the ONL sense light and pass the information to bipolar neurons in the INL, which in turn relay it to retinal ganglion cells, the output neurons of the eye. This excitatory parallel pathway is modulated laterally by inhibitory neurons - the horizontal cells form connections within the OPL and amacrine cells extend their neurites within the IPL. As a consequence, the visual image is successively compressed, spatially and temporally filtered to ultimately encode salient features, which are relayed to the brain in parallel visual processing streams by diverse RGC types. In the following, I describe the successive mechanisms of image formation and review relevant cell types of the zebrafish retina:

In general, all retinal cell classes comprise diverse cell types, which come in molecular, morphological and physiological variants. With few exceptions, each cell type is tiled across the entire retina in a mosaic manner, so that all fields of the visual scene are sampled by a broad set of information-processing cell types.

Photoreceptors sense light photons and transduce visual signal into neuronal activity. They are distinguished into cones and rods, which act in different visual modes [103]. Cones convey photopic vision in bright light and are less sensitive to light and less prone to bleaching, whereas rods mediate scotopic vision in dim light and are able to sense low light levels. Zebrafish exhibit one type of rod photoreceptors and four types of cone photoreceptors [108]. Each distinct cone type either senses UV, blue, red, or green light [109]. Interestingly, in zebrafish, rods seem to be only physiologically relevant from juvenile stages onwards [108]. In the dark, photoreceptors signal through continuous release of glutamate, but light activation inhibits this steady current. At synaptic terminals of photoreceptors, within the OPL, the signal is relayed to BCs and HCs.

Bipolar cells (BCs) are glutamatergic interneurons residing in the INL, which contact every other retinal neuron class [110]. Each BC extends a dendrite to the OPL to receive input from multiple photoreceptors and projects its axon to the IPL to pass

visual information like luminance or color onto retinal ganglion cells (RGCs) and amacrine cells (ACs) [111]. BCs are subdivided into two major groups - OFF and ON BCs - in addition to rod BCs. The latter BC types predominantly form contacts with rods [111], but feed the signal into the cone ON BC pathway [112]. OFF and ON BCs can be clearly distinguished based on their signaling properties with OFF BCs encoding light decrements and ON BCs signaling light increments [113]. These complementary responses to light stimuli depend on the type of glutamate receptor they express. OFF BCs express the ionotropic glutamate receptor and are depolarized by the continuous glutamate release from PRs. Conversely, ON BCs express a metabotropic glutamate receptor, which inhibits neuronal firing in presence of glutamate and leads to a sign inversion. ON BCs thus depolarize upon light stimulation when glutamate release by PRs is decreased [113]. The functional distinction of BCs correlates with morphological features. Importantly, BC inputs partition the IPL into a distal OFF and proximal ON region, where BC axons ramify accordingly. Sparse labeling studies in the zebrafish retina found a total of seventeen morphologically distinct types of BCs [114,115]. Their most distinctive feature is the axon ramification pattern within IPL sublaminae. There are seven OFF BC types and six ON BC types [114,115]. Interestingly, four BC types possess multistratified axon terminals in both ON and OFF IPL regions [114,115], but mostly have either ON or OFF responses [111].

Horizontal cells (HCs) are located in the distal part of the INL and form mainly inhibitory synaptic triads with photoreceptors and bipolar cells within the OPL [116]. In the zebrafish retina, four HC types are reported [116], which are categorized into axon-bearing (cone HCs) and axon-less neurons (rod HCs) [114,116,117]. HCs play a fundamental role in color opponency and contrast enhancement and thus contribute to shaping visual information at the first synapse within the IPL [118,119].

The IPL is the main site of visual signal processing. Here, axons from bipolar neurons, neurites from amacrine cells and dendrites from RGCs synapse. Their synaptic connections are arranged into IPL sublayers, of which there are at least ten in the zebrafish [110]. There is accumulating evidence that IPL sublayers are highly organized and reflect functional segregation. Stratification pattern of cell types within the IPL may thus be indicative of physiological properties. For example, OFF and ON partitioning by BCs dictates the activity profile of the cell types that co-stratify and connect with them. For example, RGCs elaborating dendrites in the proximal ON IPL region will respond to light increments. Also, transient and sustained signals of ACs and RGCs are spatially segregated [120]. Moreover, colors are processed in different IPL layers [121].

Amacrine cell neurites synapse to BC axon terminals and RGC dendrites within the IPL and contribute largely to shaping the response of RGCs [122]. Most ACs are positioned in the proximal part of the INL, whereas a group of displaced amacrine cells sits in the GCL [123]. Neurochemically, ACs are vastly inhibitory interneurons with a larger GABA-ergic population and a glycinergic population [110]. Immunohistochemical staining suggests that displaced ACs are exclusively GABA-ergic [123]. Morphological classification of zebrafish ACs groups the twenty-eight types based on their dendritic width into narrow-field, medium-field and wide-field ACs [114,123]. Both molecular and morphological observations strongly suggest that each AC type acts in a highly dedicated fashion: They form connections at specific sublaminar positions to connect to a given set of BC and RGC types, they exhibit a defined combination of molecules and some AC types control narrow while other control wide visual fields [122].

Retinal ganglion cells (RGCs) residing in the GCL are the sole output neurons of the retina and therefore play a pivotal role in the visual system. RGCs extend their dendrites within the IPL to receive dendritic input from co-stratifying BCs and ACs and transmit visual information via their axons to a variety of retinorecipient brain nuclei. RGCs are the most diverse retinal population with current estimates exceeding fifty types [16,124,125]. At the most basic level of classification, RGCs are grouped into ON, OFF or ON-OFF RGCs according to their dendritic stratification pattern and correlating physiology [126]. Each RGC type is thought to be the output channel of a specialized intra-retinal circuit that extracts a relevant feature from the visual scene. Thus, a local selective connectivity with BC and AC types renders RGC types feature-selective [101,127,128] to, for example, direction of motion [129–131], the orientation of an object [132,133], local edges [134] or differential object motion [135–137] and so forth.

Taken together, the retina computes images from incoming light signals by various, specialized cell types. There may well be more than one hundred diverse cell types [103,107,138], but the exact number remains disputed until a comprehensive and conclusive cell type inventory is available. Of note, the visual system uses the pre-processed information in two ways: most of the information contributes to the formation of images in higher brain areas, but some of the RGC types do not see patterns and function in more basal, non-image forming pathways.

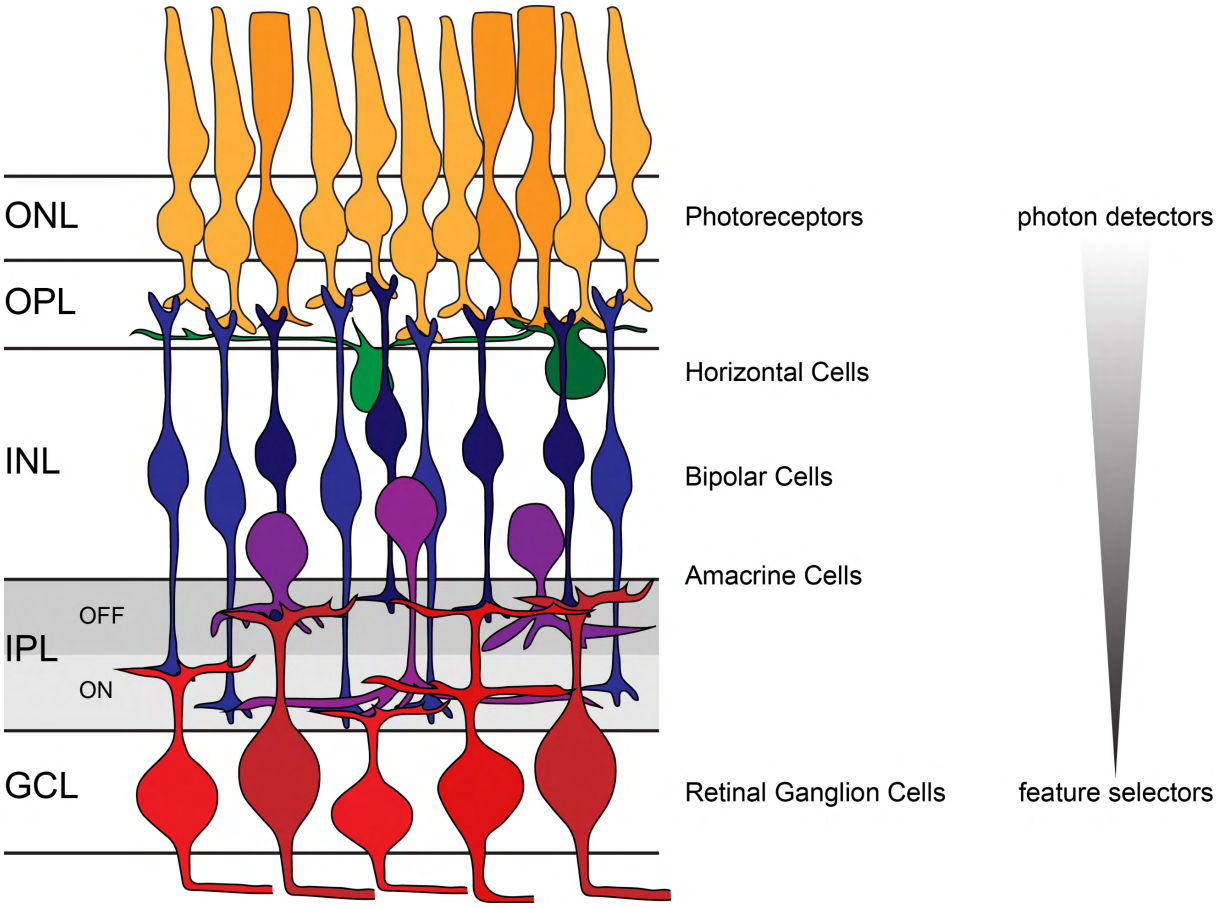

Figure 4: The retina transforms visual sensation into perception.

Schematic representation of the laminar structure of retina. Each layer harbors different retinal cell classes: PRs sit at the back of the eye in the ONL; HCs, BCs and ACs reside in the INL; and RGCs are located in the GCL. Visual signal is conveyed from PRs to BCs via their synapses in the OPL. There are two groups of BCs: ON BCs encode light increments and terminate in the proximal IPL, whereas OFF BCs relay light decrement signals to the distal IPL. BC input is received by RGC dendrites within the IPL. The vertical, excitatory information flow from PRs via BCs to RGCs is modulated by lateral interactions from inhibitory HCs in the OPL and ACs in the IPL. Intra-retinal circuits formed by diverse cell types extract visual features, which are encoded by RGC types and send to the brain in parallel processing channels. Müller glia and other non-neuronal cells are omitted in this schematic. PRs: photoreceptors, HCs: horizontal cells, BCs: bipolar cells, ACs: amacrine cells, ONL: outer nuclear layer, INL: inner nuclear layer, GCL: ganglion cell layer, OPL: outer plexiform layer, IPL: inner plexiform layer.

1.3.3 Central projections of RGCs in the zebrafish brain

In zebrafish, RGC axons encounter each other at the optic chiasm and cross entirely to project to the contralateral hemisphere. Here, RGCs terminate in ten distinct retinorecipient brain nuclei termed arborization fields (AFs) depicted in Figure 5A [63,67,139]. AFs were numbered progressing from the ventral AF1 to the dorsal AF10, which is best known as the optic tectum. The optic tectum is the main innervation site of

RGCs, where axons form laminar innervation domains named from superficial to deep (Figure 5B): stratum opticum (SO), stratum fibrosum et griseum superficiale (SFGS), stratum griseum centrale (SGC) and stratum album centrale/stratum periventriculare (SAC/SPV). While the SO domain consists of two sublayers and SFGS domain can be divided into a total of six sublaminae (SFGS1-6), SGC and SAC/SPV each form a single lamina. Taking all tectal layers and extratectal AFs into account, there are eighteen potential innervation sites of RGC axons.

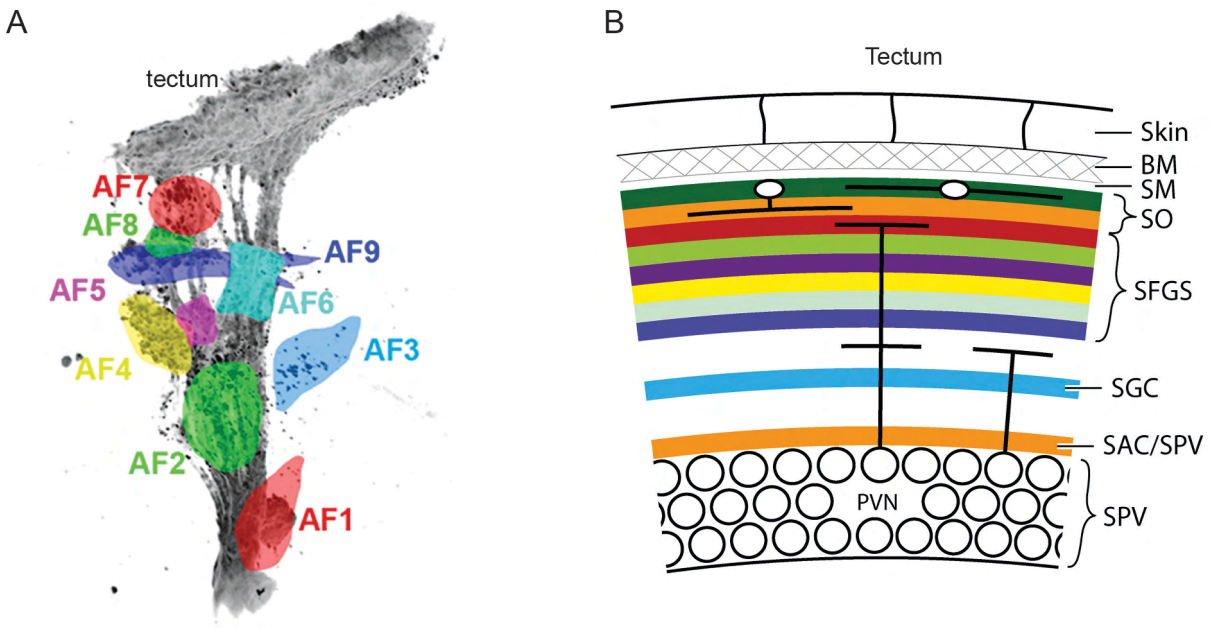

Figure 5: Anatomy of zebrafish visual pathways.

A) 3D view of the optic tract and retinorecipient brain nuclei in the zebrafish. Arborization fields (AFs) innervated by RGC axons are numbered from ventral to dorsal. AF10, the tectum, is the main innervation side of RGCs. Figure taken with permission from Robles et al., 2014 [16]. **B)** Schematic representation of the tectum. RGC axons terminate in distinct laminated innervation domains (here colored) named from superficial to deep: SO (stratum opticum), SFGS (stratum fibrosum et griseum superficiale), SGC (stratum griseum centrale) and SAC/SPV (boundary between stratum album centrale and stratum periventriculare). Downstream periventricular neurons (PVNs) reside in the SPV region and extend their neurites within the tectal neuropil. BM (basal membrane); SM (stratum marginale). Figure taken with permission from Baier, 2013 [138].

In general, RGC axon termination is organized in a topographic manner. To clarify, neighboring RGCs terminate in neighboring positions within the tectum to preserve spatial information of visual stimuli [140]. Thus, nasal RGCs project to the posterior tectum and temporal RGCs terminate anteriorly. But there are few interesting exceptions [16]: AF1, AF4 and AF8 receive predominant input from the ventral retina while AF6 is innervated by RGCs originating from the dorsal retina and

AF7 has a strong characteristic innervation from RGCs enriched in the temporal field. It is well possible that this asymmetric bias of RGC projections is linked to functional demands. For example, AF7, which is strongly implicated in hunting behavior, receives input predominantly from temporal RGCs, where prey images fall [141] or RGC types surveying ambient luminance levels are enriched in the ventral retina and project to AF1, which connects to hypothalamic nuclei that set the circadian clock.

1.4 Retinal ganglion cell type diversity

At single cell resolution, it becomes evident that RGC types are highly diverse. The multitude of RGC types comes in different shapes, where each type elaborates unique patterns of dendritic and axonal projections, possesses a distinctive molecular repertoire and encodes a specific visual feature relevant for regulation of behavior [142]. In the following, I review our current knowledge on RGC type diversity in zebrafish and how their structural diversity provides insights on the functional architecture of the visual system.

1.4.1 The retinal projectome defines ground truth of RGC type diversity

In zebrafish, the morphological connectivity pattern of RGCs has been comprehensively catalogued at cellular resolution. This study, referred to as the retinal projectome, presents a complete wiring diagram from the retina to brain, which, to date, is not available in any other vertebrate model organism and, more importantly, provides a ground-truth of RGC cell types fundamental to the present work. [16]
More than four hundred single GFP-labeled RGCs were classified by their dendritic stratification pattern and their axonal projection pattern. RGC types exhibit precise stereotyped morphologies and more than fifty morphological types can be distinguished. This number far exceeds previous estimates of cell type quantities in the retina [101].

RGCs extend their dendrites within five sublayers of the IPL to form synaptic connections with BCs and ACs. Dendritic stratification patterns can be categorized into monostratified, bistratified and diffuse structures (Figure 6A). In total, fourteen morphologically distinct dendritic classes have been defined: There are four monostratified classes, five bistratified classes and four diffuse classes. These individual classes can be distinguished based on the depth of their stratification within the IPL. One class, the biplexiform RGC types, falls out of this categorization and extends dendrites through the IPL and INL to terminate in the OPL.

RGC axonal projections can be distinguished into twenty definite projection classes (PCs). The vast majority of RGC axons terminates in the tectum, where planar arborizations remain restricted to a specific lamina (Figure 6B). Seven PCs exhibit dedicated input and exclusively innervate a tectal target lamina. In contrast, twelve PCs form axon collaterals to extratectal AFs en route to the tectum. For example, PC2 extends an axon collateral into AF7 and terminates in the SO layer. Other RGC types

innervate a combination of several AFs such as PC20, which targets AF1, AF2, AF3, AF4, AF9 and tectal SAC/SPV. This complex projection principle allows single RGC axons to innervate multiple brain areas through axon collaterals, suggesting signal divergence for parallel processing. One projection class (PC15) stands out in that it does not terminate in the tectum and was classified by axonal collateralization to AF4 and termination in AF9. This particular PC was observed less frequently in the study and is likely associated with rare RGC types.

Individual RGC morphotypes can be unambiguously defined by their unique combination of one dendritic class with one axonal class (Figure 6B). A dendritic class can be associated with one to twelve axonal classes and, conversely, an axonal class is combined with one to eight dendritic classes.

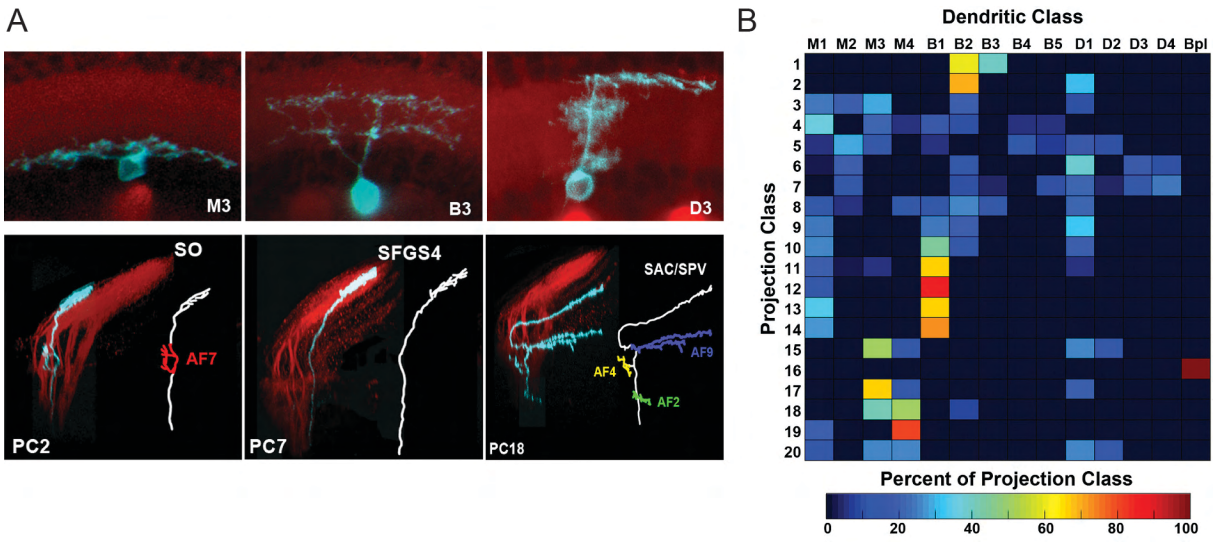

Figure 6: The retinal projectome provides a morphological RGC type atlas.

A) Examples of diverse RGC morphologies. RGC dendrites fall into fourteen different morphological classes categorized as monostratified, bistratified or diffuse. Their axons differentially innervate AFs and twenty projection classes have been classified. Each RGC axon innervates a specific tectal layer. Some types form en route axon collaterals to extratectal AFs. **B)** Matrix summarizes all RGC types classified in the 'retinal projectome'. RGCs can be uniquely defined by stereotyped combination of dendritic structure and axonal projection. Figures adapted from Robles et al., 2014 [16].

Importantly, molecular distinctions between diverse RGC types remain elusive. Given that molecular description of RGC types is poor, genetic access to individual RGC types or a defined RGC subset is lacking and precludes further analysis of e.g. their function and role in behavior.

Taken together, the retinal projectome provides a comprehensive RGC type classification at morphological level. The data build a strong foundation and reference to generate a RGC type atlas and integrate molecular and functional properties of cell types.

1.4.2 Visual representations are specific to brain areas

The eye sends visual information to the brain in parallel processing channels represented by diverse RGC types, which encode visual features extracted by retinal computation. As shown above, RGC axonal projections carry such defined visual information and serve it to a dedicated set of retinorecipient relay stations. An intriguing insight from the retinal projectome is that visual representations are brain area specific [16]. In other words, each AF is innervated by a unique set of RGC types and thus receives a different image of the outside world.

In this regard, the tectal SO layer, for example, is innervated by a total of four RGC morphotypes, two of which elaborate axon collaterals to AF7. The deepest tectal SAV/SPV layer, on the other hand, receives input from thirteen different types, all of which route via AF9 and a combination of other AFs. On the more extreme end, AF2 as well as AF9 are each innervated by as many as sixteen distinct RGC types. [16]

In fact, AF9 can be subdivided into two innervation zones, AF9 dorsal (AF9d) and AF9 ventral (AF9v) [16,139]. In line with the notion that AFs receive a dedicated visual modality, functional imaging unraveled that AF9 subdivisions receive functionally opposed inputs. Responses in AF9d neuropil are predominated by ON RGCs, whereas AF9v receives a mixture of ON and OFF inputs [16].

It is believed that this pattern of innervation by a unique set of RGC types serves functional purposes, in particular the regulation of visually evoked behaviors. Simply put, an AF which transforms prey perception into capture behavior does not require information about e.g. photopic regimes, but is innervated by prey-sensing RGC types. Conversely, an AF implicated in circadian rhythm receives input by RGCs conveying luminance levels.

In the following, I provide two, out of several known, examples of visual pathway function, which, for the most part, I borrow from the mouse visual system.

1.4.3 RGC types selectively encode direction of motion

Direction-selective (DS) RGC types belong to the best described RGC population and most of what we know of them has been discovered in the mouse retina [130,131]. They are named after their tuning selectivity to particular directions of moving objects. In the mouse retina, there are four types of ON-OFF DS RGCs (ooDS) and three types of ON DS RGCs [143].

The former group, ooDS, has bistratified dendrites in both ON and OFF sublayers of the IPL and projects to various brain targets including the superior colliculus, a main visual area homologous to tectum [20]. Molecularly, ooDS can generally be distinguished from all other RGCs by expression of cocaine-and-amphetamine-related transcript in addition to finer molecular fingerprints more specific to individual ooDS types [20]. Each of the four ooDS types selectively responds to one particular motion – upward, downward, forward or backward [129]. The role of ooDS in behavior has not been investigated, but it is conceivable to speculate that they are essential to image formation and a variety of behaviors such as orientation towards an attract object.

ON-DS RGCs differ from ooDS in several aspects. On DS RGCs elaborate a single dendritic arbor in the ON region of the IPL and project to the accessory optic system, a set of brainstem nuclei different than the ones innervated by ooDS. Just like ooDS, ON DS RGCs can be distinguished into three types according to their preferred direction - either upward, forward or downward. In contrast to ooDS, they prefer slower kinetics of motion stimuli and respond to whole field motion. Interestingly, these anatomical and physiological properties match well with their function in the optokinetic response - an innate reflex for image stabilization during self-motion [144].

In zebrafish, three DS RGC types have been reported [145,146]. In this study, zebrafish larvae were presented with bars moving in different directions and neuronal activity was recorded from RGC axons. The stimulus elicited responses specifically in a RGC population, which terminates in superficial SFGS. Precisely, DS RGC types show distinctive tuning profiles to the drifting bars and encode upward, forward or downward motion, respectively. The authors further posit a possible role of the DS RGC subset in the optokinetic response, but this hypothesis remains untested as no specific access to this population is available.

1.4.4 RGC types exhibit intrinsic photosensitivity

Intrinsically photosensitive RGCs (ipRGCs) form an atypical group of RGCs found across many species. They likely comprise the most ancient RGC type [50,147,148] and are evolutionary conserved [50]. First indications of the existence of ipRGCs arose when mice lacking photoreceptors retained some visual functions, in particular ability to adapt their circadian rhythm [149–152]. The long-standing view that photoreceptors are the sole light sensors of the retina was then changed when expression of photopigments, so-called melanopsins, was detected in a rare set of RGCs [153–155]. Melanopsin is today known as key characteristic feature of ipRGCs, which renders them intrinsically photosensitive. Accordingly, ipRGCs depolarize upon photo-stimulation and encode ambient luminance levels [154]. ipRGCs thus play essential roles in the regulation of non-image forming behaviors such as circadian photoentrainment. [147,156,157]

In mouse, there are five types of ipRGCs named M1 to M5, which contribute only 1-2% of the entire RGC population [158]. In addition to characteristic expression of melanopsin, ipRGCs are molecularly defined by the transcription factor Eomes, also known as Tbr2, and other genetic markers [21,22,34,49,159,160]. ipRGCs differ in their dendritic stratification pattern with M1 elaborating monostratified arbors into the OFF IPL region, M3 being bistratified in ON-OFF and M2, M4 and M5 extending monostratified dendrites in the most proximal ON layer. Despite their intrinsic photosensitivity, all five RGC types receive synaptic ON inputs from BCs [161–163]. In fact, although M1 stratifies in the OFF layer, ON BCs relay ON signal through en passant synapses [164,165]. Their sustained, sluggish, durable, linear responses to light, however, is a major feature distinguishing ipRGCs from other RGC types [166]. Mouse ipRGCs project through the retino-hypothalamic optic tract to innervate many visual brain targets, mostly non-image forming brain areas such as the master circadian pacemaker, the suprachiasmatic nucleus (SCN), or the olivary pretectal nucleus (OPN) involved in the pupillary light reflex [158,167]. They do, however, also target image forming visual areas such as the lateral geniculate nucleus and the superior colliculus [167]. In line with this physiology and anatomy, ipRGCs were causally linked to a variety of non-image forming functions of the visual system. Targeted ablation of M1 ipRGCs severely disrupts circadian rhythm and the pupillary light reflex [168–170]. Intriguingly, these functions are differentially mediated by two distinct subtypes of M1, which are characterized by presence or absence of the transcription factor Brn3b. A Brn3b$^-$ M1 subpopulation targets the SCN and regulates circadian rhythm while Brn3b$^+$ M1 ipRGCs innervate the OPN and control the pupillary light reflex [171]. The behavioral

relevance of M2 to M5 ipRGC types is unknown. Recent studies suggest roles in pattern vision [172] and color opponency [173].

While expression of melanopsins by zebrafish RGCs has been reported [174,175], ipRGCs remain yet to be identified. One study suggests that RGCs projecting to AF4 are intrinsically photosensitive and regulate light-seeking behavior [176].

1.4.5 Visual pathways regulate behavior

The retinal projectome – a classification of RGC morphotypes - revealed a fundamental organizing principle of the visual system: structural diversity of RGC types generates functional segregation into visual pathways illustrated in Figure 7. Visual pathways are thought to regulate behavior by routing behaviorally relevant information to dedicated brain nuclei, where the information is further transformed into the appropriate behavioral output.

Already at early larval stages, zebrafish exhibit a number of diverse, innate and adapted, visually evoked behaviors [102,177,178]. For example a repertoire of innate reflexive behaviors has been characterized in psychophysical experiments including the optokinetic reflex (OKR), the optomotor response (OMR), phototaxis or visual background adaptation (VBA) and many more. Each of these described behaviors serves a specific purpose in adapting to the larva's visual environment. In detail, OKR moves the eyes to compensate for retinal slip during self-motion and steady the gaze [179–182]. Similarly, OMR stabilizes the fish's position with respect to a drifting visual environment [179–181]. Phototaxis, on the other hand, is a navigational behavior that the larva executes to target preferred light conditions (zebrafish larvae perform both positive and negative phototaxis) [183–185]. VBA is an interesting neuroendocrine response, in which the larva adjusts its skin pigments to camouflage against their background and ambient light levels [179,186]. VBA is strongly dependent on RGCs [180] and thought to be regulated through a retino-hypothalamic pathway [179]. Besides, the zebrafish larva also performs a great variety of more complex behaviors driven by conscious computation and integration of pattern vision such as prey capture [141,187–190], escape responses [191,192] or object approach and avoidance [193].

How are these diverse visual behaviors regulated by RGC types? Due to the lack of genetic access to visual pathways, we have very little understanding of how a concise set of RGC types contributes to transformation of vision into behavior. Past

attempts to dissect visual pathway function utilized genetic or chemical perturbations [179,180,183,194–196] or laser ablations [186].

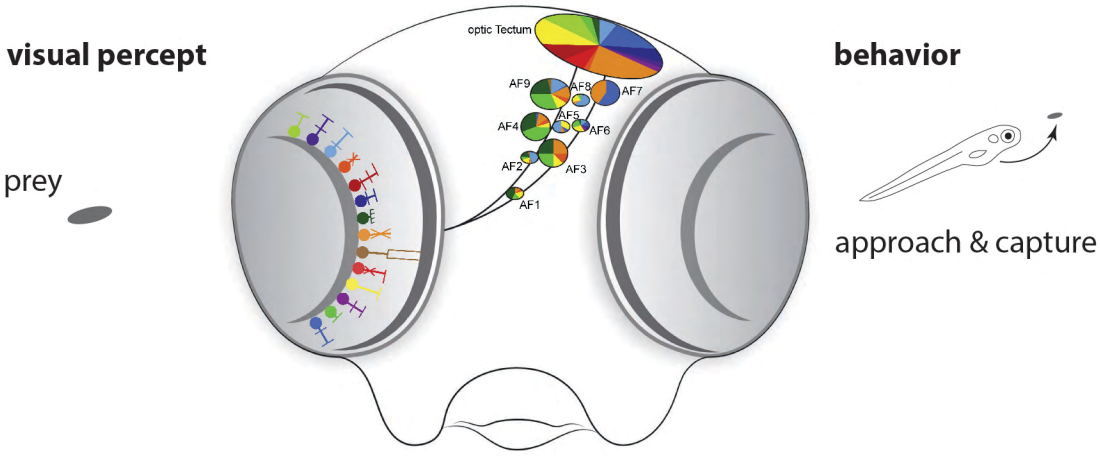

Figure 7: Functionally segregated visual pathways differentially regulate behavior.

RGC structural diversity creates diverse visual pathways with distinct connectivity patterns within the retina and stereotyped axonal projection patterns to retinorecipient brain nuclei. Relative contributions of distinct dendritic types to AFs are color-coded. Each AF is innervated by a dedicated set of RGC types and receives a different image of the outside world. These visual pathways encode behaviorally relevant visual features, which are transformed into appropriate behavioral output by dedicated processing sites. Prey, for instance, specifically activates a visual pathway to AF7 and tectal SO to initiate approach and capture strikes.

For example, mutagenesis screens isolated a mutant, *no optokinetic response c* (*nrc*), named after its disability to perform OKR [197]. The *nrc* mutant is characterized by abnormal photoreceptor terminals, which disrupt retinal ON signaling. Together with pharmacological blocking of the ON pathway these observations show that OKR is controlled by ON RGCs [198]. Likewise, a study on phototactic behavior using the *nrc* mutant suggests that the ON pathway also mediates light-seeking navigation [184]. Another interesting example of genetic disruption to identify the neural substrate of visual behavior addressed regulation of VBA. Few identified mutants, *sleepy* and *grumpy* [179,199,200] or *wait until dark* and *yoimachi* [180], show severe pathfinding errors, impaired retinal structure or defective photoreceptors. Accordingly, these mutant strains fail to perform OKR and OMR [179,180]. Intriguingly, however, they retain ability to adapt to background [179]. Considering these observations, it could be speculated that VBA is mediated by zebrafish ipRGCs projecting along the retino-hypothalamic pathway.

In addition to genetic mutagenesis screens, laser ablation experiments probed the importance of the tectum in several behaviors. Disruption of tectal innervation,

however, did not have strong effects on OKR, OMR or VBA performance, suggesting that extratectal AFs are dedicated to regulate these behaviors [186].

By thorough behavioral analysis in conjunction with functional imaging, specific visual pathways could be well attributed to regulation of prey capture and escape responses. Owing to these investigations, we now know that the pathway formed by RGCs to AF7 and SO tectal layer is strongly implicated in prey capture [141], while RGCs terminating in deep SFGS detect looming stimuli and likely form part of a circuit for escape responses [191].

Prospectively, transgenic markers for genetically defined visual pathways, which allow for reproducible investigation of genetically identified RGC subsets or types, will be an invaluable asset to better understand their function and behavioral relevance.

2 THESIS OBJECTIVES

One of the greatest challenge in contemporary neuroscience is to classify each and every cell type that forms the brain. A comprehensive description of neuronal cell types will pave way for a holistic understanding of brain function. Cell types, however, exhibit heterogeneous and highly complex features across molecular, morphological and functional properties. Thus, there is need to investigate how different modalities of cell types correspond to each other in order to develop conceptual principles underlying the generation of cell type atlases.

My thesis tackles cell type classification of retinal ganglion cells (RGCs), which route visual information from the eye to the brain. These neurons fall into more than fifty morphologically classified types. Diverse RGC types form parallel diverging pathways that encode specific visual features to regulate distinct aspects of behavior. In the past, functional analyses of visual pathways have been hampered by the lack of genetic access.

On these notes, several key questions remain yet unanswered: What are molecular distinctions of diverse RGC morphotypes? Does this diversity underlie a higher-order logic, for example a taxonomical organization? Are there molecular markers for individual RGC types? Can such genetic markers be exploited as entry points to study visual pathway function? How are transcriptional profiles of distinct RGC types causally related to morphotypes and functional properties?

The zebrafish model is uniquely suited to orthogonally investigate molecular composition, morphological features and functional properties of cell types in the retina. Altogether, the results of my thesis show that molecular, morphological and functional properties can be integrated into a cell type taxonomy derived from large scale transcriptional profiling. Novel molecular markers identified in this RGC type atlas yield genetic access to specific visual pathways and enable systematic investigation of their physiological properties and behavioral relevance.

2 Thesis objectives

My thesis project can be divided into following key parts:

Part I Molecular profiling of RGCs

I collaborated with the laboratories of Joshua Sanes and Aviv Regev to perform high-throughput single cell RNA-Sequencing to molecularly classify RGCs. Computational analysis of thousands of single cell transcriptome profiles of larval and adult RGCs derived transcriptionally distinct clusters representing putative RGC types. The molecular relationships between these clusters revealed hierarchical organizing principles of RGC diversity. Differential gene expression analysis identified cluster-specific markers, which provided the basis to relate morphological (Part II) and functional (Part III) properties to transcriptional clusters.

Part II Mapping novel molecular markers to RGC morphotypes

In a team effort, I exploited cluster-specific markers as genetic entry points in a CRISPR-Cas9 knockin approach to label cellular processes and map morphological identity to transcriptional profiles. I established a novel transgenic line based on the RGC subclass marker *eomesa*. This transcription factor is specifically expressed by RGCs projecting to a dedicated set of brain targets including pretectum and deep tectal layer.

Part III Functional characterization of RGC types

Based on conserved features in mouse RGCs, I hypothesized that *eomesa*$^{+}$ RGCs constitute intrinsically photosensitive RGCs in zebrafish and are implicated in non-image forming functions. In collaboration, I assessed this possible role of *eomesa*$^{+}$ RGCs by characterizing their response profiles to visual stimuli and by testing their necessity in visual background adaptation.

3 EXPERIMENTAL PROCEDURES

3.1 Zebrafish

All animal experiments performed at the Max Planck Insitute of Neurobiology near Munich were approved by governmental (Regierung von Oberbayern) and institutional (Max Planck Institute of Neurobiology) administrations (protocol 31-2016 and 101-12). Experiments carried out at Harvard laboratories in Cambridge, MA, USA were approved by Harvard University/Faculty of Arts & Sciences Standing Committee on the Use of Animals in Research and Teaching (IACUC, protocol #24-10). Zebrafish were maintained under standard facility conditions at 28.5°C in a 14/10 hour day/night cycle. Embryos were bred in Danieau buffer (17 mM NaCl, 2 mM KCl, 0.12 mM MgSO4, 1.8 mM Ca(NO_3), 1.5 mM HEPES, pH 7.6) and raised in the facility from 5 dpf on. The transgenic lines used in the present work are listed in Table 1.

Table 1: Transgenic lines

Transgenic line	**Reference**
ath5:Cre	Förster et al., 2017 [77]
ath5:QF2	generated in the present study
eomesa:QF2	generated in the present study
isl2b:GFP	Pittmann et al., 2008 [201]
isl2b:tagRFP	Horndli et al., 2012 [202]
mafaa:QF2	generated in the present study
QUAS:epNTR-tagRFP	generated in the present study
QUAS:GCaMP6s	generated in the present study
QUAS:GFPcaax	generated in the present study
QUAS:switchG6s	generated in the present study
QUAS:switchNTR	generated in the present study
ßact:loxP-GFP-loxP-RFP	Marquart et. al., 2015 [79]
tbx20:Gal4	Förster et al., 2017 [77]
UAS:Dendra	Arrenberg et al., 2009 [203]
vsx1:GFP	Kimura et al., 2008 [204]

3.2 High-throughput single cell RNA-Sequencing

3.2.1 Isolation of retinal cells

Solutions described below for isolation of retinal cells were prepared freshly, sterile-filtered and kept at a physiological pH 7,5. Ames buffer (Sigma A1420) was supplemented with sodium bicarbonate (Sigma S5761) and oxygenated prior to the experimental procedure. Retinas from adult or larval transgenic euthanized zebrafish were dissected in Ames and transferred into chilled Ames on ice until tissue collections were completed. Retinas were transferred to activated dissociation solution containing papain (Worthington LS003126) at 20U/ml, DNAse I (Sigma D4527) at 10U/ml and 5mM L-cysteine (Sigma C1276) in Ames. Retinas were then dissociated in a 28°C water bath for forty to fifty minutes while inverting the mixture at regular intervals. After tissue fragments settled down, dissociation solution was replaced by papain inhibitor solution containing ovomucoid (Worthington LS003087) at 15mg/ml, BSA (Sigma A9418) at 15mg/ml and DNAse I at 10U/ml in Ames. The tissue was triturated using a flamed glass pipette until a single cell suspension was obtained. Cells were pelleted at 300g for 10min and resuspended in oxygenated Ames supplemented with 0.4% BSA (Sigma A9418). Viability was assessed using trypan blue (Thermo Fisher 15250061) and cell density was adjusted to 1M/ml for subsequent fluorescence-activated cell sorting (FACS). Cells were stained with the viability probe calcein blue (Thermo Fisher C1429) at 1μg/ml. Viable single cells were isolated at the FACS machine at a low pressure of 20psi with a 100μm nozzle and sorted into oxygenated Ames, 0.4% BSA. Cells were then pelleted at 250g for 10 minutes and resuspended in PBS, 0.04%BSA. The concentration and viability was assessed on a hemocytometer immediately prior to loading the cell suspension onto the microfluidic platform for high-throughput single cell RNA-Sequencing.

3.2.2 Droplet formation and cDNA library preparation

The high-throughput single cell RNA-Sequencing experiments were performed using the commercial 3' Single Cell Chromium platform (10X Genomics; PN-120233). The cDNA libraries were prepared according to the manufacturer's instructions with no modifications. In brief, each cell's poly-adenylated RNA was reverse transcribed and barcoded inside the nanoliter droplet. Following droplet breakage, full length cDNA was purified and PCR amplified. cDNA library construction entailed enzymatic

fragmentation, end repair, A-tailing, adaptor ligation and PCR to obtain constructs equipped with P5/P7 binding sites, a sample index and Read1 and Read2 oligonucleotides. Final paired-end sequencing was performed at the Broad Institute (Cambridge, MA) using an Illumina HiSeq platform.

3.2.3 RNA-Sequencing data analysis

The bioinformatic analysis of single cell RNA-Sequencing data was performed by our collaborators Karthik Shekhar (Regev lab, Broad Institute), Anna Sappington (Regev lab, Broad Institute) and Wenjun Yan (Sanes lab, Center for Brain Science, Harvard). The Cell Ranger software [205] converted BCL sequencing files obtained from Illumina sequencing into FASTQ files to then transform raw sequencing data into a gene expression matrix, where gene counts for each cell were listed for further analysis. Sequences were aligned to the zebrafish reference transcriptome (genome assembly Zv82), duplicated PCR amplicons were collapsed based on UMI sequences and detected transcripts were separated as per their cell of origin based on each cell's barcode. The final gene-cell expression matrix was used for further analysis using custom-written scripts and R tools. Sequencing reads were normalized to give read counts as transcript per million (TPM). Cells with less than 350 for BCs and 450 for RGCs genes detected or with a mitochondrial transcript content of more than 5% were filtered out. Genes of very low abundance were also removed. Following the identification of highly variable genes, a principal component analysis was implemented to reduce dimensionality of data. The distribution of cells along most relevant principal components was used to create a k-nearest neighbor graph and cluster cells into transcriptionally distinct domains. These clusters were visualized in two dimensions by t-stochastic neighbor embedding. All data combined from different replicate runs were batch corrected. Genetic markers for clusters were identified by differential expression analysis between the cells of a cluster and the rest of the cells based on a bimodal and binominal test.

3.3 Genetic constructs and transgenesis

3.3.1 Transgenic constructs

The generation and modification of transgenic constructs presented in this study will be described in the following:

For the establishment of the binary Q-system a Tol2-QUAS:MCS-polyA;cmlc2:mCherry vector was generated holding a multiple cloning site (MCS) for reporter insertion and a RFP transgenesis heart marker using the cmlc2 promoter. The promoter sequence consists of five copies of the natural QF binding site GGGTAATCGCTTATCC [60]. This vector was used in a classical restriction-ligation method to insert PCR amplified GFPcaax, GCaMP6s or epNTR-tagRFP fragment downstream of QUAS, respectively. The QF2 coding sequence was obtained from Addgene (Plasmid #61312) to construct a template vector for BAC recombineering equipped with a Kanamycin resistance and cmlc2:Cerulean cassette. A PCR amplified QF2;cmlc2:Cerulean fragment was used to generate an ath5:QF2 BAC using clone DKEY-111E19 by BAC recombineering as described previously [77].

For the RGC-specific intersectional approach via Cre intersection, the ath5 BAC DKEY-111E19 was recombineered with a Cre;cmlc2:Cerulean cassette [77]. For the intersectional reporter construct QUAS:switchNTR, a floxed GFPcaax fragment [77] and an epNTR-tagRFP fragment [206] were PCR amplified and subsequently cloned into the Tol2-QUAS;cmlc2:mCherry vector by In-Fusion cloning (Clontech 63890). For the intersectional reporter construct QUAS:switchG6s, a floxed tdTomatocaax fragment [77] and a GCaMP6s fragment [207] were PCR amplified and subsequently cloned into the Tol2-QUAS;cmlc2:mCherry vector by In-Fusion cloning.

Donor plasmids for the CRISPR-Cas9-mediated knockin approach were cloned by Golden Gateway Cloning methods [208]. Entry vectors (pGGEVs) carrying fragments of interest were generated by restriction-ligation cloning and used for assembly into the destination plasmid pGGDest. Here, we used pGGEV-1 as a linker containing the eGFP-bait sequence [96], pGGEV2 to insert target-specific gRNA sequences, pGGEV3 for the basal promoter e1b, pGGEV4 for QF2, pGGEV5' for a terminating polyA-signal. The final eGFP-bait; gRNA; e1b:QF2-polyA pGGDest plasmid contained was used as donor plasmid in the CRISPR-Cas9-mediated knockin approach. The sequences of gRNAs used in this study are listed in Table 2.

3.3.2 Tol2-mediated transgenesis

Transgenic constructs for either transient mosaic expression or for the generation of a stable transgenic line were delivered to the organism by microinjections. Eggs were collected at one-cell stage and mounted in a 2% agarose (Biozym 840001) injection mold for injection with 2-3 nl of freshly prepared solutions containing phenol red (Sigma P0290) for visibility. Tol2-plasmids were injected at 25ng/μl together with tol2 mRNA at 50-100ng/μl synthesized from pCS-zT2TP plasmid [76]. For sparse labeling, plasmid concentration was adjusted to 2-5ng/μl. BAC DNA was injected at 100ng/μl together with tol2 mRNA at 50-100ng/μl.
Larvae showing transient expression were raised and adult fish were screened for germline transmission by outcrossing.

3.3.3 CRISPR-Cas9-mediated locus-specific knockins

The gRNA target sites for targeted insertion of transgenes were selected using the CRISPR-Cas9 target predictor tool CCTop [209] and are listed in Table 2.

Table 2: gRNA targets

gene	Ensembl reference	position	gRNA target sequence including PAM
barhl1b	ENSDARG00000019013	exon	GCTTCACGCAAGCAGCAGTGTGG
barhl1b	ENSDARG00000019013	intron	AAGTCATGTTATGGCGTCAAAGG
barhl1b	ENSDARG00000019013	upstream	TGCCGCTTTGCTTCTGTCCGTGG
bhlhe22	ENSDARG00000058039	exon	TATGGACAGGAGAATAAACTTGG
eomesa	ENSDARG00000006640	upstream	ACCTGAGCGCACGAATTGCGCGG
eomesa	ENSDARG00000006640	exon	GGACAGGTTGTAGAAGGTCTTGG
mafaa	ENSDARG00000044155	exon	TGCGCTCATGGCGAGATCGGTGG
tbr1b	ENSDARG00000004712	upstream	TGTGTGCCGAATATAATCGGAGG
tbx3a	ENSDARG00000002216	upstream	CTGCACTCCATGGGCTTCGGCGG

For microinjections, CRISPR-Cas9 reagents were prepared freshly as follows: tracrRNA (IDT 1072534) was mixed at equimolar ratio with target-specific crRNA (IDT, customized) in nuclease-free duplex buffer (IDT 11-01-03-01) and annealed. Cas9 protein (IDT 1081060) was dissolved in Cas9 working buffer (20mM HEPES; 150mM

KCl, pH 7.5) to an equimolar concentration of gRNA (typically 1.5μM). Annealed gRNA and Cas9 protein were mixed at a 1:1 ratio and incubated at 37°C for 15 minutes to form the ribonucleoprotein complex. Solutions were placed on ice and donor plasmid was added to a final concentration of 20ng/μl.
In order to establish a stable transgenic line, fish sorted for successful integration of the construct were raised to sexual maturity and screened for germline transmission by outcrossing.

3.5 Histological methods

3.5.1 Tissue clearing using CLARITY

CLARITY staining was performed in collaboration with Eva Laurell (MPI Neurobiology, Baier lab). Adult brains were dissected in PBS from euthanized fish and immediately transferred to hydrogel solution containing 1% acrylamide (BioRad 161-0140), 0.25% VA-044 Initiator (Wako 017-19362), 4% PFA (Alfa Aesar 43368) in PBS. The hydrogel solution was diffused through brain tissue for about forty-eight hours at 4°C. Brain samples were then deoxygenized in hydrogel solution and acrylamide was polymerized for three hours at 37°C. Next, brains were cleared in clearing solution consisting of 200mM boric acid (Merck 10043-35-3), 4% SDS (Sigma L3771) at pH 8,5 for two weeks at 37°C. Cleared samples were washed six times in PBT prior to immunohistochemical staining.

3.5.2 Immunohistochemistry

If samples were not processed by CLARITY, larvae were euthanized and fixed in 4% PFA in PBS buffer supplemented with 0.25% Triton-X 100 (Sigma Roth 6683.1), hereafter PBST, either for three hours at room temperature or overnight at 4°C. Samples were washed at least three times in PBST to remove residual PFA. If necessary, retinal pigment epithelium was bleached by incubation in 1% hydrogen peroxide (Merck 107209) in PBST followed by subsequent washing in PBST.
For tissue sectioning, samples were incubated in 35% sucrose (Sigma S8501) in PBS at 4°C overnight for cryoprtection. Tissue was then embedded in TissueTek (VWR 25608-930) and sectioned at a cryostat.

For immunohistochemical staining, the samples were permeabilized in PBST containing Trypsin-EDTA (Gibco 15400) at a 1:20 dilution on ice. The duration of permeabilization depends on tissue size. 5 dpf larvae were permeabilized for 45 minutes. Permeabilizing agents were removed in a series of five washes in PBST. Samples were blocked in blocking buffer containing 5% goat serum (Sigma G9023), 1% BSA (Sigma A3912) and 0,1% DMSO (Sigma D8418) in PBST for at least two hours at room temperature (for adult brains overnight). Antigen detection by primary antibodies diluted in blocking buffer (Table 3) was then allowed for up to seven days (for adult brains two weeks). Samples were washed in PBST at least six times for ten minutes. A fluorophore-conjugated secondary antibody diluted in PBST was incubated for up to three days (for adult brains one week). Samples were rigorously washed in PBST and post-fixated in 4% PFA in PBST for 20 minutes. For tissue clearance, samples were transferred to 80% glycerol (Roth 4043.1) in ascending steps for imaging and long-term storage.

Table 3: Antibodies

Antibody	**Source**	**Dilution factor**
chicken α-GFP	Invitrogen A10262	1:500
DAPI	Sigma D9542	300 nM
goat α-chicken Alexa488	Invitrogen A11039	1:1.000
goat α-mouse Alexa647	Invitrogen A21235	1:1.000
goat α-rabbit Alexa555	Invitrogen A21428	1:1.000
mouse α-znp1	ZIRC	1:400
rabbit α-tagRFP	Invitrogen R10367	1:500

3.5.3 Miscellaneous staining procedures

In order to stain the synaptic layers in the retina, larvae were bathed in 20mM Bodipy-TR Ceramide (Invitrogen D7540) in Danieaus for thirty to sixty minutes in the dark prior to *in vivo* imaging.

Retinal projections were labeled by injections of lipophilic tracer DiD (Invitrogen D307) dissolved to 1% in dimethylformamide (Sigma D4551). Larvae were fixed in 4% PFA in PBS for one to three hours at room temperature and mounted in 1% agarose in

PBS for dye injections into the retina. Larvae were stored in PBS at 4°C to let the dye diffused throughout the entire optic tract over night for imaging the next day.

3.6 Confocal imaging

Confocal images were acquired using a Zeiss LSM 780 or a Leica Sp8 system. For *in vivo* imaging, larvae were mounted in 1-2% low-melting agarose (Invitrogen 16520-100) in Danieaus and, if necessary, anesthetized using tricaine (Sigma A-5040). For imaging of stained samples, specimens were mounted in 3% low-melting agarose in 80% glycerol in PBS. Images were processed using FIJI [210], Imaris (Bitplane), Adope Photoshop or Adobe Illustrator.

3.7 Functional analyses

3.7.1 Functional imaging

Larvae expressing the Ca-reporter GCaMP6s were immobilized in 2% melting agarose and mounted on a stage at a 2P-microscope (Femtonics 3DRC microscope, Femtonics, Tuzlo, Hungary). GCaMP6s signals were recorded during visual stimulation, which was designed using the PsychoPy tools [211] and presented to the larva monocularly on a white diffusive screen using the red channel of a LED projector (LG, Model No. PA72G). The stimulus sequence was as follows: OFF (black screen, 10 seconds, t0), ON (black to bright red, 10 seconds, t10), OFF (red to black, 10 seconds, t20), grating (10° black bars interspaced at 30°,stationary, 5 seconds, t30), upward motion (grating moves upward at 20°/sec, 5 seconds, t35) followed by forward, downward and backward motion each interleaved by a stationary grating, OFF (10 seconds, t70), prey-like stimulus (3° dot sweeping across screen at 90°/sec, four repetitions, 20 seconds, t80), brightening (dark to bright red in 5 seconds, t100), ON (10 seconds, t105), loom (disc expanding at 30°/second to reach screen frame, two repetitions, 30 seconds, t115), dimming (bright red to dark in 5 seconds, t145), OFF (10 seconds, t150). The total stimulus duration is 160 seconds.

Imaging data were analyzed by Thomas Helmbrecht (MPI Neurobiology, Baier lab). In brief, the recordings were corrected for motion of the larva. Regressors for each stimulus were designed and convolved with a GCaMP6s kernel. Next, correlation of response traces of each pixel to the designed regressors was calculated using a linear

regression and resulted in two values – a $\Delta F/F$ coefficient and R^2 as a measure of fit to the regressor. The score is calculated by multiplication of these values and normalized to the global maximum of the recording. Pixels scored <0.2 were discarded from analysis. Traces were then clustered and visualized according to cluster assignment across the recorded neuropil.

3.7.2 Chemogenetic ablations

Larvae expressing the enzyme nitroreductase were incubated in 7.5 mM metronidazole (Sigma M3761), 0.2% DMSO (Sigma D8418) in Danieaus. As control groups, one group of larvae expressing nitroreductase were incubated in 0.2% DMSO in Danieaus and another group of larvae not expressing nitroreductase was incubated in 7.5 mM Mtz, 0.2% DMSO in Danieaus. Treatment occurred for 24 hours in a light-protected tray, after which larvae were washed in Danieaus three times and given a recovery time overnight. Efficient ablation was validated by *in vivo* confocal imaging before and after treatment on a random basis.

3.7.3 Visual background adaptation assay

To test visual background adaptation, dark adapted larvae were placed on a white sheet of paper and allowed to adapt to the bright background for 45 minutes. Adaptation was assessed visually by several lab members, who were blinded to group identities. Individual larvae of all groups were scored in grades from 0 to 10, where 0 relates to a pale adapted wildtype larva and 10 to a lakritz mutant with dispersed melanophores.

In a different approach, individual larvae were sorted into wells of a round-shaped 96-well plate (Sigma CLS3799) in 30 μl of Danieaus. Larvae were then placed on a white background at a transparent stage illuminated by a light source (Lumitronix, Multibar 35) from below. Larvae were allowed to adapt to bright background for at least 30 minutes. Pictures were taken from each larvae using a 50 mm lens (Edmund Optics, 56-531) and a high-performance camera (IDS, PointGrey) at same illumination standards and exposure time. Individual larvae were selected as region of interest (ROI) from each image and the mean grey values were calculated using FIJI [210] to determine the overall state of melanophore dispersion or aggregation.

4 RESULTS

4.1 Molecular profiling of RGCs

Acknowledgement
The results presented in Part I "Molecular profiling of RGCs" were obtained in a collaborative effort. I performed single cell RNA-Sequencing experiments. Karthik Shekhar and Anna Sappington analyzed sequencing data, completed clustering analysis and provided custom-written R scripts to investigate and plot data. Immunohistochemical staining of adult brains was carried out with help of Eva Laurell.

4.1.1 Purification of zebrafish retinal neurons

How can live single neurons be purified from the intact retina? Conventionally, a population of interest can be collected from dissociated tissue by specific labeling thereof in conjunction with fluorescence-activated cell sorting (FACS).

With this intention, I made use of the transgenic lines *vsx1:GFP* expressing in bipolar cells [115,212] and *isl2b:tagRFP* labeling RGCs [213] presented in Figure 8A and 8B. The section of an adult *vsx1:GFP, isl2b:tagRFP* retina shows characteristic GFP labeling of bipolar cells (BCs) and RFP-expressing retinal ganglion cells (RGCs) with nuclear and synaptic counterstains to visualize laminar structures. I established and optimized a cell dissociation protocol to purify healthy retinal cells and maximize cell yield.

Using this protocol, about ten thousand retinal cells could be purified from a larval retina and about one million retinal cells from an adult retina. A representative example of a single cell suspension typically used as FACS input is demonstrated in Figure 8C. At the FACS machine, cell suspensions were gated for live singlets to purify GFP-labeled BCs or RFP-labeled RGCs for subsequent droplet RNA-Sequencing. In adult retinal suspensions, the BC population constituted about 40% of the overall suspension, whereas the RGC population was represented by approximately 2-4%. These proportions reflect our estimates of cell class proportions in the intact retina and are close to quantification of class distributions in the larval retina [214]. Both labeled BCs and RGCs clearly separated from other retinal cells in the FACS scatter plots (Figure 8C and 8E, respectively).

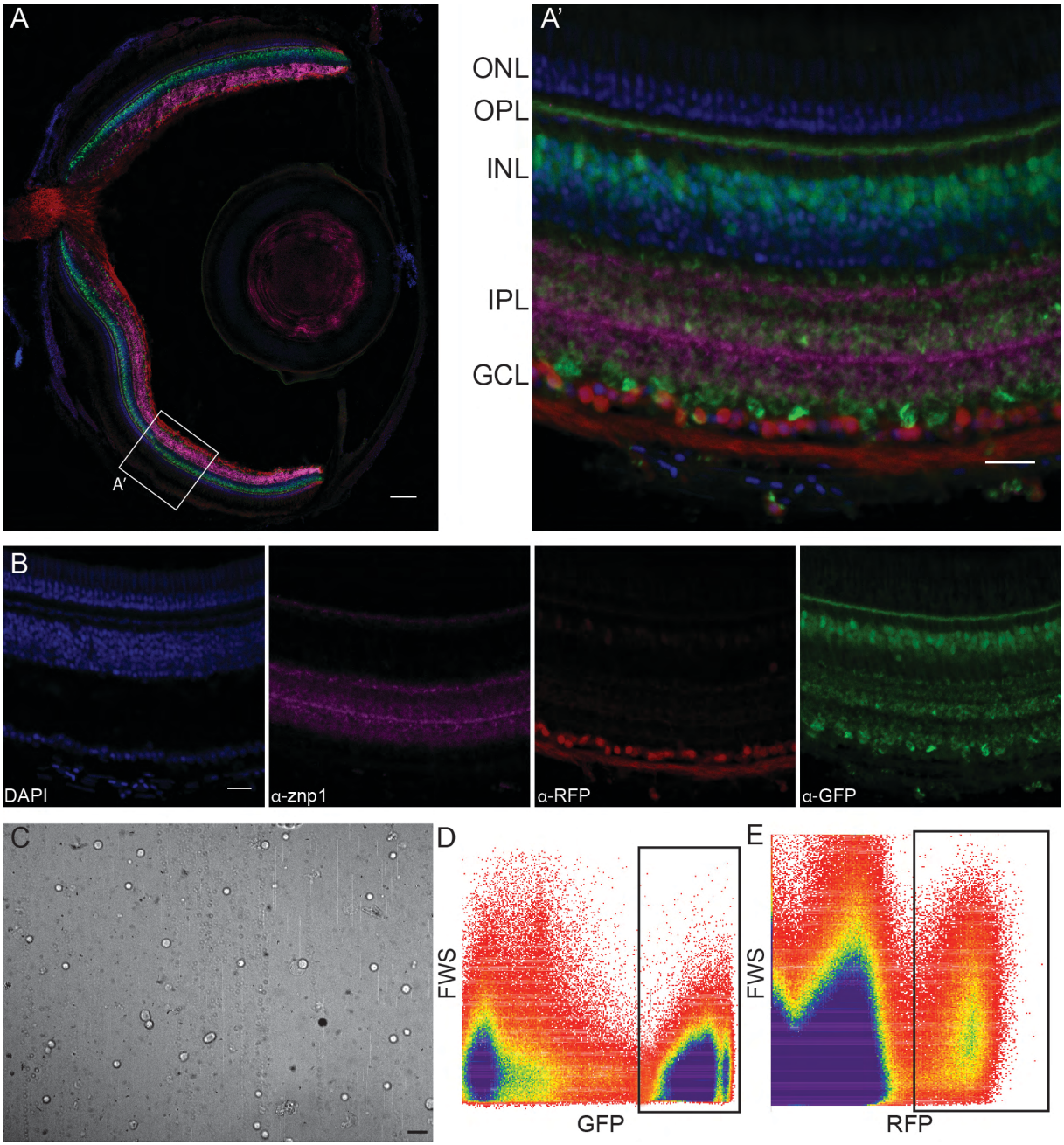

Figure 8: Purification of bipolar cells and retinal ganglion cells.

A) Overview of an adult retina section of *vsx1:GFP* and *isl2b:tagRFP* double transgenics. BCs are GFP-labeled; RGCs are RFP-labeled. **A')** Magnified region in A to examine labeling across retinal layers. **B)** Individual channels of the image in A'. DAPI and znp1 staining serve as reference for nuclear and synaptic layers, respectively. **C)** Representative image of a retinal cell suspension obtained from dissociated adult retinas. The majority of cells are singlets. **D)** FACS scatter plot of *vsx1:GFP* labeled BCs. The gating strategy for BC collection is indicated. **E)** FACS scatter plot of *isl2b:tagRFP* labeled RGCs. The gating strategy for RGC collection is indicated. ONL: outer nuclear layer; OPL: outer plexiform layer; INL: inner nuclear layer; IPL: inner plexiform layer; GCL: ganglion cell layer. Scale bar in A is 100µm, in A' and B 20µm, in C 10µm.

Thus, cell suspensions could be greatly enriched for single living BCs or RGCs. Quality of collected cells was assessed before cells were processed by droplet RNA-Sequencing shortly after FACS enrichment.

4.1.2 Transcriptional profiling facilitates molecular classification of bipolar neurons

The present study is amongst the first research endeavors using a droplet-based RNA-Sequencing technique for classification of zebrafish neurons, which differ greatly from the type of cells that were characterized previously. In fact, zebrafish retinal cells measure only 5-10 μm in diameter and have less RNA content, an essential parameter in this assay, than a comparable mammalian cell [215]. This factor confronted us with the question if droplet RNA-Sequencing is powerful enough to classify retinal cell types.

Hence, we first tested the performance of the assay and ability to classify cell types on zebrafish bipolar neurons. Bipolar neurons were chosen as subject for this pilot study for several reasons: First, there is good prior knowledge regarding cell type diversity. Bipolar neurons are morphologically classified into seventeen types presenting a moderately complex retinal cell population. Second, there are canonical markers specific to a subset of BC types, which can be utilized to verify molecular classification by single cell RNA-Sequencing. Expression of these subset markers is expected to be represented in the clustered RNA-Sequencing data accordingly. Third, BCs make up a large proportion of the retina and can be purified easily utilizing vsx1:GFP, which labels all morphologically described BC types [115].

We performed droplet-based single cell RNA-Sequencing on adult BCs and sequenced a total of 16.432 cells across eight replicates. The derived 9.103 genes x 16.432 cells expression matrix was analyzed bioinformatically. Briefly, principal component analysis was performed using the most highly variable genes across the dataset and subsequent graph clustering groups cells according to similarity of their transcriptional profile. On average, 804 transcripts as defined by UMI counts and 502 genes were detected per cell. Basal contaminants, in particular Müller glia, rods and amacrine cells, were identified by known retinal cell class markers in the initial clustering analysis and removed (data not shown). During this initial process, only 258 cells were removed demonstrating a bipolar cell purity of 98.4%. The remainder 16.174 bipolar cells were subjected to further clustering analysis, which yielded twenty transcriptional domains, or clusters, shown in Figure 9A. These clusters are defined by

a unique molecular composition and represent putative BC types. Clusters are numbered by size with cluster 1 being the biggest cluster across the dataset and cluster 20 the smallest. Consequently, cluster numbers may correspond to the abundance of a certain BC type.

General markers characteristic for BCs like the transcription factor *vsx1* [115], the vesicular glutamate transporter *slc17a7* (*vglut1)* [216], the ribbon synapse associated protein *ribeye a* [217] or calcium-binding proteins such as *cabp2a* and *cabp5a* [218] are broadly distributed across clusters (Figure 9B). In contrast, known cell type specific molecular markers are selectively expressed in specific clusters according to prior knowledge and aid in identifying them. Interestingly, the transcription factor *pax6a*, a key factor in the maintenance of retinogenic progenitors [219,220], is markedly enriched in cluster 16. This observation indicates early retinal progenitor cell (RPC) identity of this cluster. However, cluster 16 cannot be uniquely identified as such, because co-expression of other RPC markers like *rx1* or *vsx2* is lacking. There is a possibility that cluster 16 represents a specific BC type, which exhibits continued *pax6* expression [221]. Next, I investigated distribution of indicators for OFF- and ON-BC identity across clusters. The ionotropic glutamate receptors expressed by OFF-BCs [222] *grin1b* (NMDA receptor) or *grik1a* (AMPA receptor) are enriched and co-expressed in several clusters (2, 4-10, 13, 12, 19), whereas the metabotropic glutamate receptor *grm6b* characteristic for ON-BCs [222] is enriched in most of the remaining clusters (1, 3, 11, 12, 15, 17, 18). Other known ON-BC markers such as the transcription factor *isl1* [115,223], the dendritic synapse-associated protein encoded by the *nyx* gene [224–226] as well as *prkca* (protein kinase C) [222,227] align with *grm6b* expression. This co-expression further corroborates ON-BC cluster identity and accuracy of the molecular classification approach. Moreover, reported differential expression is reflected across BC clusters accordingly. For example, the neuronal intermediate filament *inaa* [228] is specific to cluster 14 as well as the differentially expressed scaffolding protein *lin7a* [229] is reflected at varying levels across the clusters. While many clusters likely correspond to distinct cell types, there is a possibility that defined transcriptional clusters represent doublets, a methodological artefact currently unavoidable in droplet RNA sequencing. Noticeably, there are several observations that led to assume that cluster 20 contains doublet cells. First, formation of doublets occurs rarely and cluster 20 is the smallest cluster. Second, cluster 20 shows a higher average number of transcripts consistent with more RNA content originating from two cells rather than singlets. Third, and most indicatively, cluster 20 expresses a mixed signature of all cluster-specific markers described below.

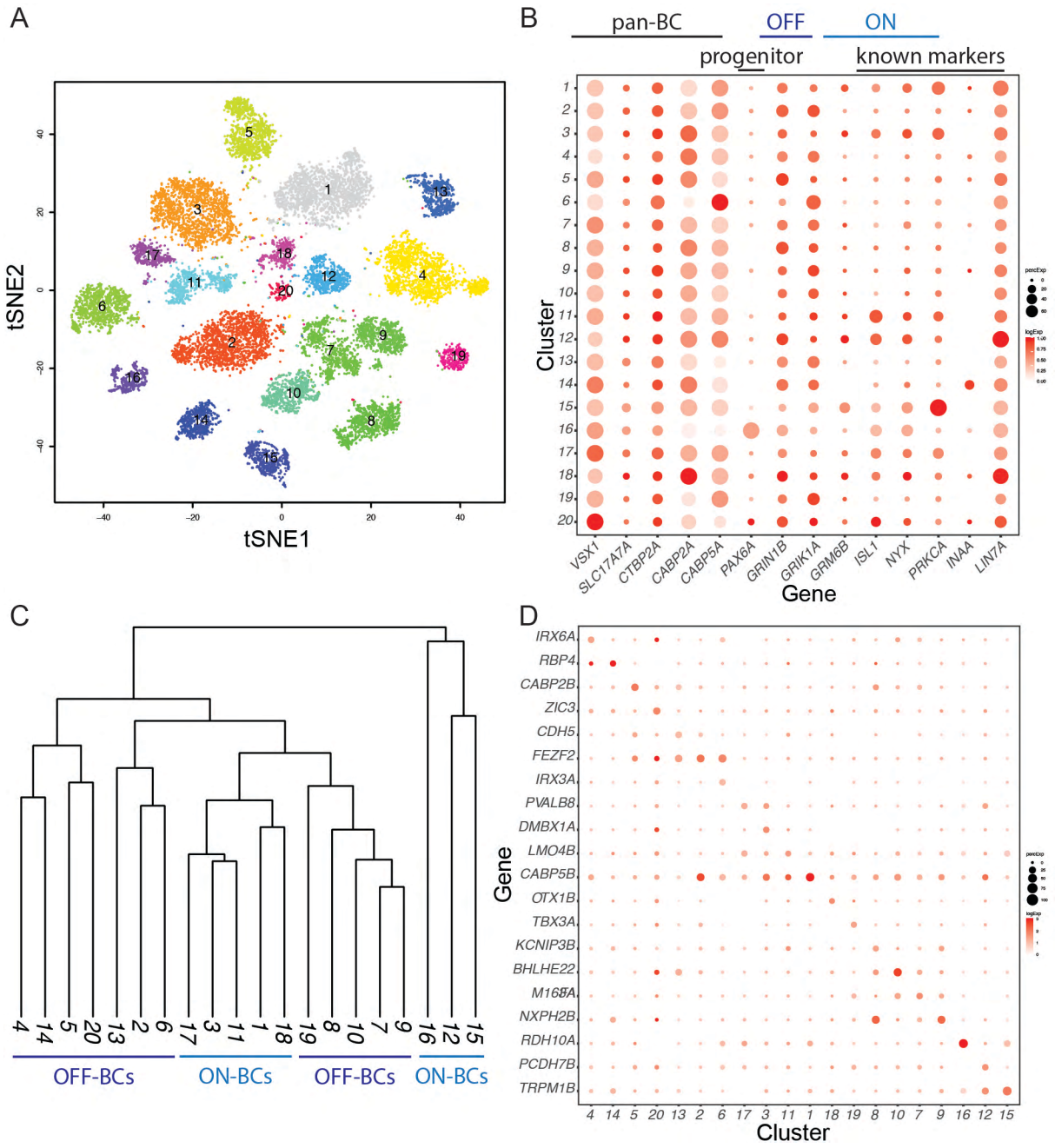

Figure 9: Molecular classification of bipolar neurons.

A) Two-dimensional visualization of adult bipolar cell transcriptional clusters derived from more than 16.000 cells using t-SNE. Each dot corresponds to a cell and is colored according to cluster correspondence. Clusters are ordered by size. **B)** Gene expression patterns of major BC markers and known subset markers across clusters. OFF and ON BC markers show enrichment in specific subsets of clusters. **C)** Hierarchical clustering of average BC cluster gene signatures indicates taxonomical organization of types into subclasses, where OFF or ON BC types are each other's closest relatives, respectively. **D)** Expression pattern of identified top novel molecular markers for BC types across clusters.

We further analyzed the molecular relationship between clusters by hierarchical clustering based on the cluster's average gene signatures. This molecularly-derived taxonomy of putative BC types shown in Figure 9C demonstrates a hierarchical organization of BC diversification. Several BC subclasses diversify further into BC clusters. Provocatively, subclasses correspond to ON or OFF BC subsets, where the identified ON-BC or OFF-BC clusters are each other's closest relatives. Thus, molecular profiles underlying functional properties ON versus OFF appears to be a main discriminating feature.

While subclass markers have been described previously, there are no known markers for individual BC types. To identify cluster-specific markers, we performed a differential gene expression analysis. Virtually every cluster is defined by a novel unique molecular marker (Figure 9D). These markers include genes from different categories like transcription factors (*irx6a, zic3, fezf2, irx3a, dmbx1a, lmo4b, otx1b, tbx3a* or *bhlhe22*), cell adhesion molecules (*cdh5* or *pcdh7b*) or physiologically relevant genes (*cabp2b, pvalb8, cabp5b* or *kcnip3b*).

Taken together, droplet RNA-Sequencing enabled molecular classification of zebrafish adult BCs so as in effect transcriptional profiles of putative BC types segregate and known molecular distinctions can be recognized across clusters accordingly.

4.1.3 The *isl2b:tagRFP* transgene labels RGCs in larval and adult stages

As previously discussed, the transgene *isl2b:tagRFP* [213] is reported to label virtually all RGCs [201] and photoreceptors inside the retina [202] and thus can be used as a tool to purify RGCs. For the purpose of molecular profiling of RGC types at different stages, I first characterized the transgenic expression pattern in the larval and adult animal to confirm maintenance of broad and unbiased RGC labeling.

In *isl2b:tagRFP* larvae, all or the vast majority of RGCs express RFP as is evident from retina sections depicted in Figure 10A where RFP expression is broadly distributed throughout the ganglion cell layer. In addition, the transgene drives RFP expression in photoreceptors, but at lower fluorescence levels than RGCs. In line with pan-RGC labeling, axonal RGC projections labeled by *isl2b:tagRFP* show innervation of all described retinorecipient brain areas (Figure 10B).

In the six-month old adult *isl2b:tagRFP* fish, this pan-RGC labeling is maintained. Immunohistochemical staining in optically cleared brains revealed RFP-

labeled axonal processes in major retinorecipient nuclei such as the tectum (Figure 10C and magnification in 10F), AF9 (Figure 10D) and AF7 (Figure 10E). The tectal planes clearly show RGC projections terminating in all described innervation domains (SO, SFGS, SGC and SAC/SPV). These observations confirm continuous labeling of RGCs in a broad manner throughout investigated stages.

As can be concluded from this characterization, the *isl2b:tagRFP* transgene is suitable for unbiased purification of all RGC types for molecular classification.

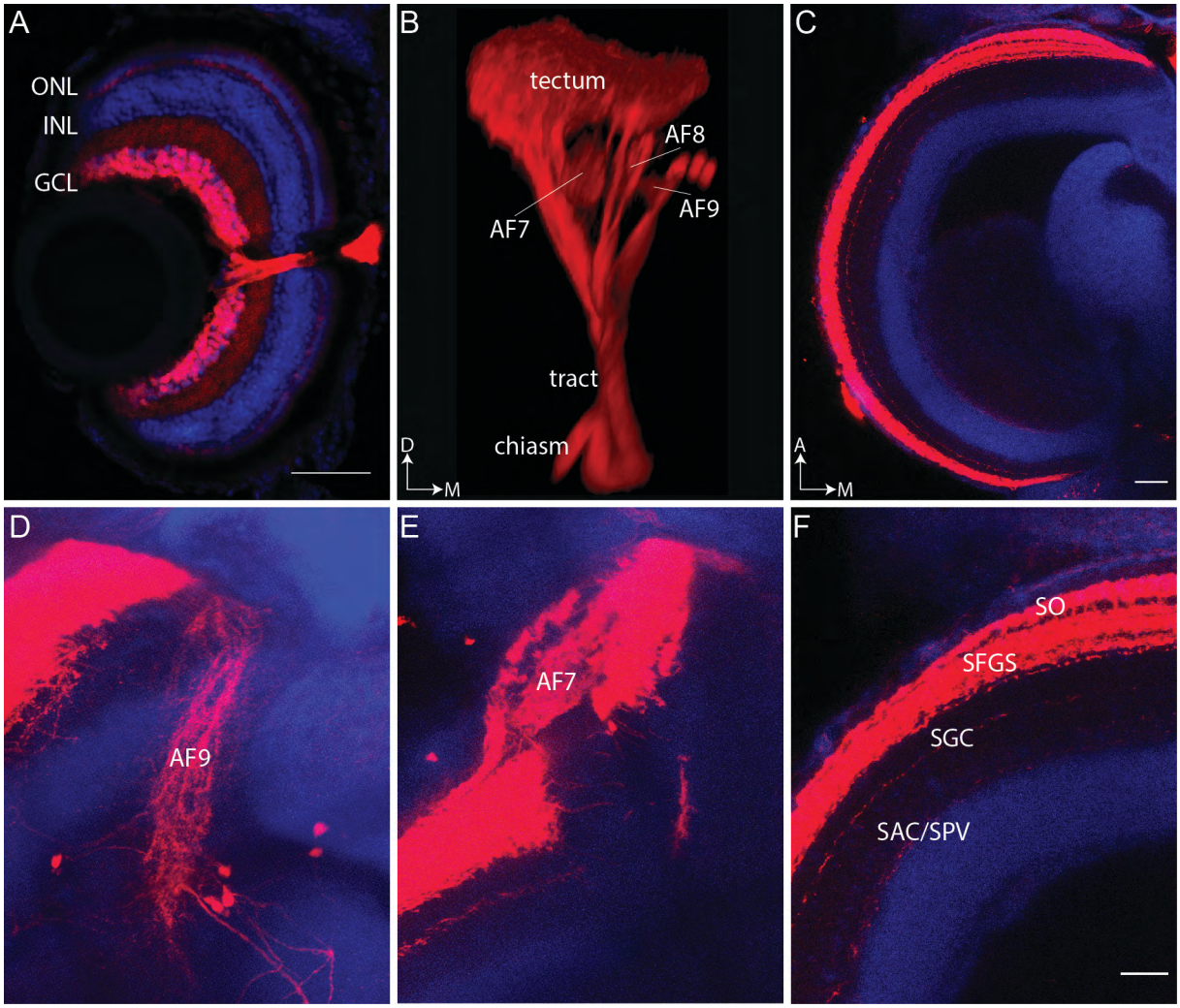

Figure 10: *isl2b:tagRFP* labels retinal ganglion cells in the larval and adult zebrafish.

A-B) *isl2b:tagRFP* labeling in the 6 dpf larva. **C-F)** Transgenic labeling of RGCs in the adult brain. **A)** Retina section of the 6 dpf larval *isl2b:tagRFP* retina stained for the nuclear counterstain DAPI and RFP. All RGCs are RFP-labeled as well as very few INL cells and photoreceptors. **B)** 3D view of RGC projections in the larval *isl2b:tagRFP* fish. All AFs are innervated by *isl2b* labeled RGC types. **C)** Tectal plane of a 6 month adult *isl2b:tagRFP* brain stained for DAPI and RFP. *isl2b:tagRFP* maintains expression into adulthood. **D)** Plane in the adult brain at level of AF9. **E)** Plane in the adult brain at level of AF7. **F)** Adult plane magnified from C with retinotectal innervation domains SO (stratum opticum), SFGS (stratum fibrosum et griseum superficiale), SGC (stratum griseum centrale) and SAC/SPV (boundary between stratum album centrale and stratum periventriculare). Scale bar in A is 50 µm, in C 100 µm and in F 100 µm.

4.1.4 Transcriptional profiling identifies putative RGC types

In pursuance of a comprehensive classification of RGC types at molecular level, we devised a strategy as illustrated in Figure 11. RGCs were molecularly profiled at two stages: At 5 dpf, when the visual system is fully functional, but developmental programs are still in process and transcriptional diversity is high, and in the adult retina, when the visual system is fully matured. Using bioinformatics, both datasets were analyzed in parallel, independent of each other.

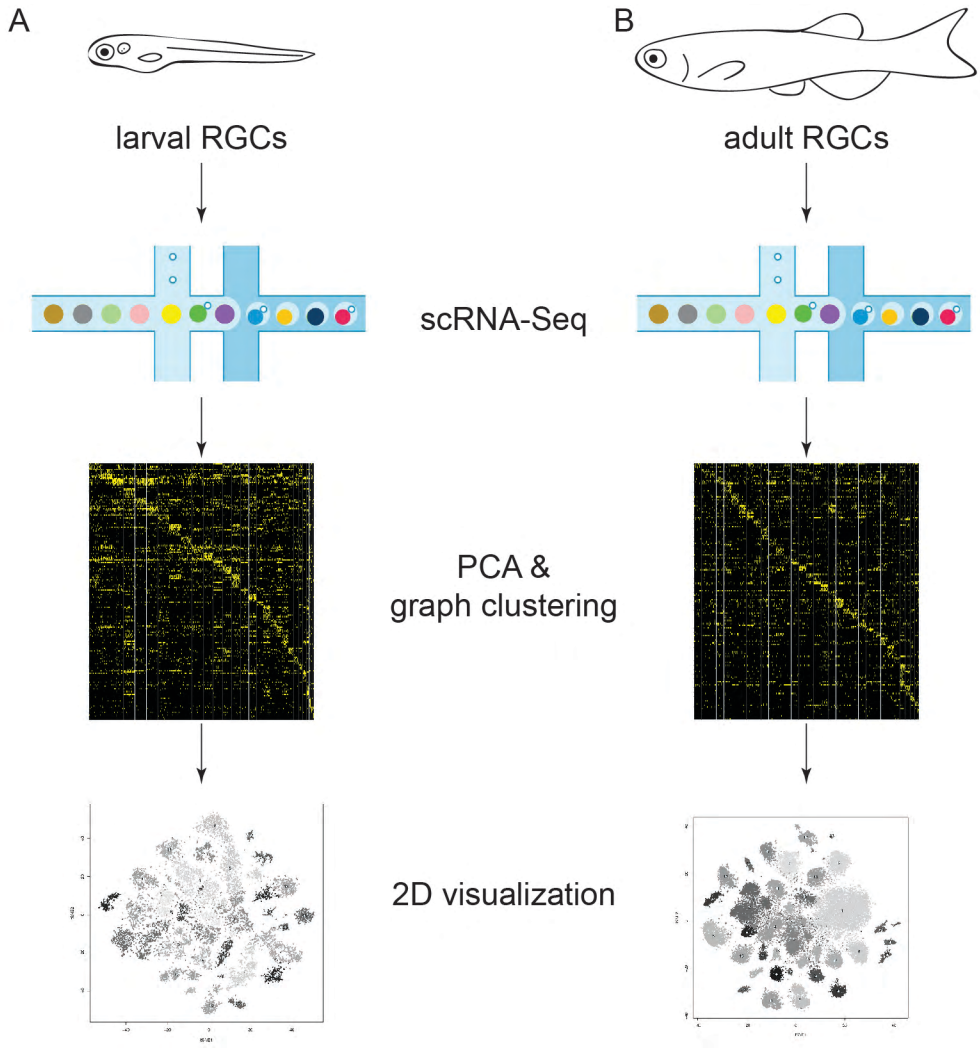

Figure 11: Workflow for comprehensive molecular classification of retinal ganglion cells.

RGCs were purified from **A)** larval and **B)** adult zebrafish retinas and processed by single cell RNA-Sequencing in parallel. Sequences were arranged into a cell x gene expression matrix. Highly variable genes were identified and used for a principal component analysis followed by graph clustering to group cells based on similarity of their transcriptional profile. Clusters are visualized in 2D using t-SNE. Both datasets were analyzed independently of each other.

Each dataset possesses distinct advantages: On the one hand, because larval RGCs undergo neuronal assembly programs they likely show higher transcriptional diversity than mature neurons. Such transcriptional differences ease bioinformatic segregation of cell types as it has been reported for Drosophila neurons [230]. Moreover, the retinal projectome was acquired using 5 to 7 dpf larvae and a transcriptional profiling of RGCs during this stages will aid comparison of molecular composition and morphology. On the other hand, RGCs in the mature retina may exhibit a higher degree of shared transcriptional programs, but are more numerous and thus types can be resolved by capturing large cell numbers to complete sampling [46].

In the following sections, I describe the two complementary larval and adult RGC datasets along with the insights offered.

For larval RGC classification, we captured RGC transcriptional profiles using 6 dpf *isl2b:tagRFP* retinas across three single cell RNA-Sequencing replicates. cDNA libraries were sequenced to a depth of ~20.000 reads per cell. Including all cells with more than 450 detected genes, we derived a gene expression matrix of 12.398 genes across 12.693 cells. During initial analysis, data were clustered to investigate potential contaminants. We identified several small contaminant clusters using known markers for retinal cell classes such as *vsx1* for bipolar cells, *rho* for photoreceptors, *slc6a9* (a glycine transporter) for amacrine cells, *glula* for Müller glia and *olig2* for oligodendrocytes (data not shown). While these contaminant clusters provide internal controls, data will be omitted for clarity. The obtained dataset demonstrated 97.7% purity of RGCs since only 295 contaminant cells were identified and removed. Larval RGCs showed on average 1.949 transcripts and 1.023 genes per cell. Following contaminant removal, further bioinformatic analysis clustered cells based on transcriptional similarity. Briefly, 4.230 highly variable genes were used to identify significant principal components to build a k-nearest neighbor graph. This clustering analysis yielded twenty-nine molecularly distinct larval RGC clusters, which are ordered by decreasing cluster size and depicted in two dimensions using t-stochastic neighbor embedding (t-SNE) in Figure 12A. Each of these transcriptional clusters is defined by a unique molecular composition and represents a putative RGC type.

Adult RGC data were processed in same manner to obtain pure RGC clusters. From fifteen replicates of single cell RNA-Sequencing, we derived a gene expression matrix of 16.552 genes across 48.535 cells. Most identified contaminants were photoreceptors possibly captured because their RFP intensity falls into the RGC gate

during FAC sorting. After contaminant removal, a total of 39.095 RGCs remained indicating a cell purity of 80.6%. A total of 1.118 highly variable genes was used for principal component analysis suggesting fewer transcriptional variance than in the larval RGC dataset. On average, adult RGCs showed 2.426 transcripts and 1.137 genes per cell. Clustering of pure RGC single cell data classified types into thirty-three transcriptional clusters shown in the t-SNE plot in Figure 12B.

In conclusion, transcriptomic profiling of both larval and adult RGCs allowed to classify molecularly distinct RGC types into separately partitioned transcriptional clusters.

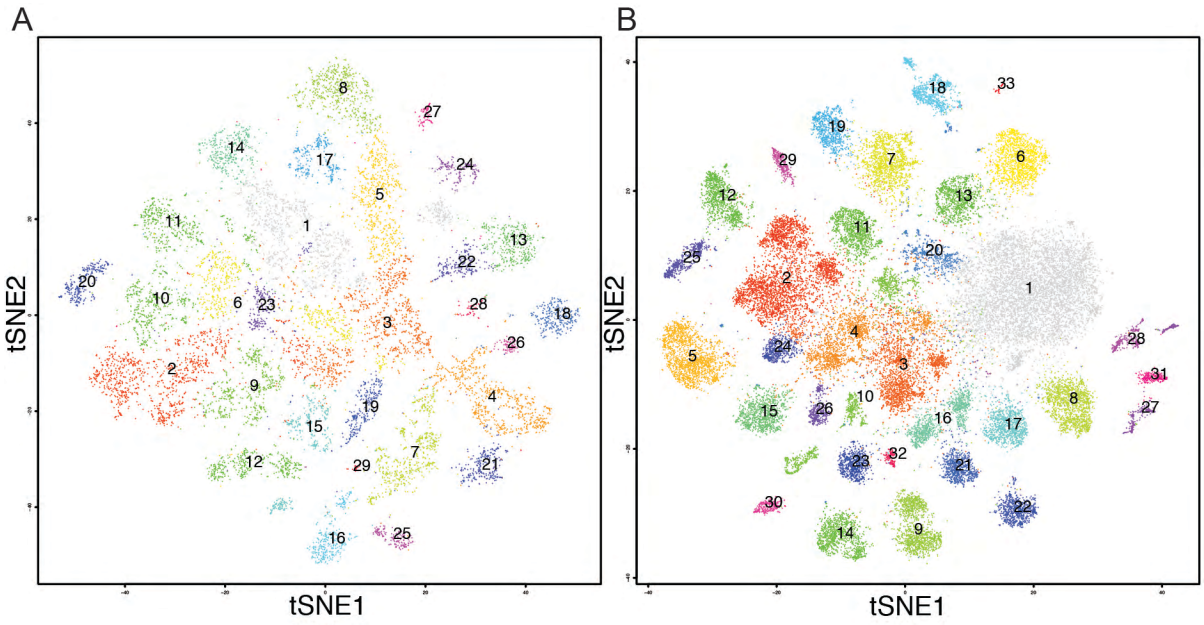

Figure 12: Clustering of single cell transcriptional profiles classifies putative RGC types.

A) 2D visualization of 29 larval transcriptional RGC clusters using t-SNE obtained from more than 12.000 RGCs. Each dot corresponds to a single cell and is color coded according to its cluster assignment. Clusters are ordered by size. **B)** 2D visualization of 33 adult RGC clusters using t-SNE obtained from more than 39.000 RGCs.

4.1.5 Molecular taxonomy identifies main genetic distinctions of RGC types

The successful segregation of putative RGC types into distinct transcriptional clusters led us to next explore the following questions: What exactly are the molecular commonalities or distinctions of RGC types? How are RGC types inter-related? And does RGC type diversity underlie a higher-order logic?

To address these questions, we performed hierarchical clustering analysis to first investigate global relatedness of RGC clusters. The derived molecular taxonomies

revealed fundamental organizing principles of RGC type diversity for both the larval and adult clusters.

The dendrogram in Figure 13A shows a taxonomic tree of RGC diversification based on average gene signature of larval RGC clusters. It appears that diverse RGC types form four major groups, perhaps relating to major functional groups as observed in BC types [46]. Cluster 27, 28 and 29 appear not to be closely related to any RGC clusters. Upon closer inspection, I noted that these clusters are defined by upregulated metabolic genes and are likely outlier clusters as an artefact from cell purification. The major groups split further into RGC subclasses, which harbor closely related RGC type clusters that are positioned together in the dendrogram. To put it differently, RGC diversification follows a hierarchy from major groups to RGC subclasses to RGC types.

The dotplot aligned with the dendrogram illustrates gene expression across clusters, which are ordered according to their position in the dendrogram. The size of the dot indicates the fraction of cells in a given cluster in which particular marker transcripts were detected and the color code indicates average number of transcripts.

Unlike for BCs, known markers for RGC subsets are scarce. Generally, RGC identity is evident from the expression pattern of pan-RGC markers across clusters. For example, the genes *rbpms2b* [231], *robo2* [232], *isl2b* [201] or *slc17a6b* (*vglut2a*) [216] all are reported to be expressed throughout RGCs and are distributed across clusters accordingly. The transcription factor *pou4f3* (also known as *brn3c*) is a known marker for RGCs terminating in the SFGS innervation domain and labels approximately 40% of RGCs [233]. Interestingly, this marker appears enriched in a set of related clusters (3, 12, 15, 19 for instance) and begins to demonstrate molecular distinctions and reliable representation of gene expression across clusters.

Next, I investigated whether genetic commonalities within major groups or subclasses underlie the relationships of putative RGC types. Specifically, I examined the expression pattern of genes known to be implicated in determination of cell type identity, namely transcription factors (TFs) or cell adhesion molecules (CAMs). Several observations suggest that, indeed, genetic signatures are associated with RGC type diversification. For instance, there is a non-overlapping pattern of three POU domain homeobox TFs. Both *pou4f1* and *pou4f2* define major groups 1 and 2 in addition to a subclass in major group 4. In contrast, *pou2f2a* is expressed by *pou4f1*/*pou4f2*- subclasses in major group 3. Besides, there are multiple additional TFs, which are characteristic for specific subclasses. The TF *tfap2d* is associated with a subclass in major group 1 or *foxp2* enrichment aligns well with a subclass in major group 2 and 4. As further illustration, I highlight the TFs *mafaa* and *eomesa*. *mafaa* expression is linked to a

subclass comprising three clusters in group 2 and one additional cluster. Similar to this case, *eomesa* (*eomesodermin homolog a*; also known as *tbr2*) is expressed by a total of five larval RGC clusters and uniquely identifies a RGC subclass in group 3. Strikingly, this finding relates well to mouse RGC type diversification, where the mouse homolog Eomes is a marker for a subclass (termed superclusters in the referred study) of five clusters [49]. Apart from TFs, only two genes encoding for cell adhesion molecules, *pcdh11* and *pcdh19*, showed an enrichment in particular RGC groups. So is *pcdh11* expressed at high levels by clusters in group 1 and 2.

Considering these remarkable genetic commonalities shared by related clusters, I next assessed physiologically relevant genes and their distribution across RGC cluster taxonomy. I found that, for instance, the calcium binding protein *cabp5b* has higher expression levels in group 1 and 2 than in the remainder clusters. Furthermore, the expression of glutamate receptors *grm4*, *grin1a*, *grin1b*, *gria2b*, and *gria4a* does not follow taxonomic differences since these genes were detected in every cluster, yet to different expression levels. Likewise, other neurotransmitter receptors are broadly distributed. GABA receptors do not show a striking specificity as exemplified by *gabra2* or *gabra5* expression as well as the dopamine receptor *drd2b*, the glycine receptor *glra4a* or the acetylcholine receptor *chrnb3b,* which were broadly detected across clusters. An exceptional case is the serotonin receptor *htr1ab*, which shows specific enrichment to the *eomesa*$^{+}$ subclass.

In the adult, a similar molecular taxonomy organizes putative adult RGC types into five major groups (Figure 13B) suggesting that complexity of inter-cluster relationship increases in the mature retina. While most clusters showed some degree of relatedness to other clusters, cluster 10 forms a distinct solitary cluster and is not related to any other RGC clusters. This cluster contains RGC progenitor cells as I describe below. Some, but not all, of the distinguishing molecular features identified in the larval clusters continue to discriminate RGC types. For example, POU transcription factors show a non-overlapping pattern, where *pou2f2a* is characteristic to group 1 including *eomesa*$^{+}$ clusters while *pou4f1* and *pou4f2* are enriched in group 2 to 5. A compelling observation is that the intra-subclass organization is largely maintained from larval to adult datasets. As an illustration of this point, *mafaa*$^{+}$ clusters remain each other's closest relatives in the adult RGC clusters just as *eomesa*$^{+}$ clusters are positioned in the same subclass. Strikingly, however, there are merely two *eomesa*$^{+}$ clusters present in the adult RGC data as opposed to five *eomesa*$^{+}$ clusters found in the larval data.

Taken together, the global relatedness of putative RGC types is defined by a hierarchical organizing principle of type diversity – a molecular taxonomy, which intriguingly is explained by underlying characteristic genetic commonalities.

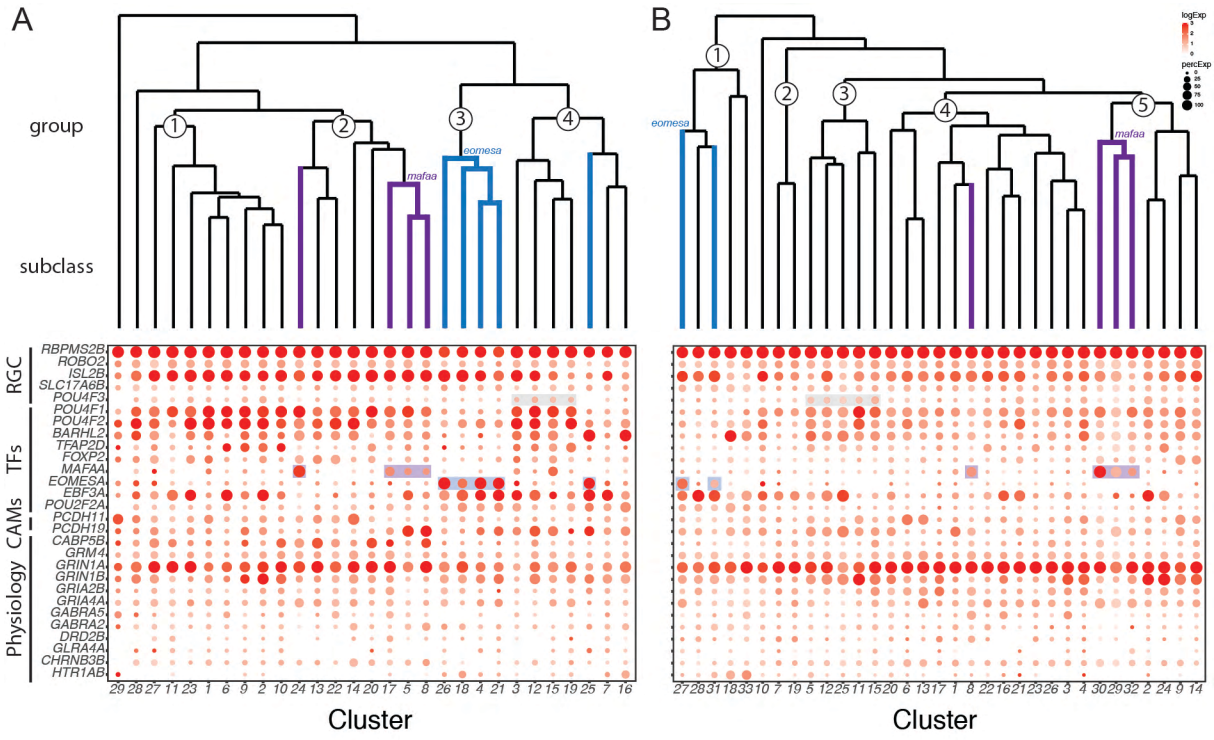

Figure 13: Molecular-derived taxonomy and underlying gene signatures of RGC types.

A) Hierarchical clustering of average gene expression patterns reveals taxonomic relationships of larval RGC clusters and underlying genetic commonalities. Plotted are known RGC markers, transcription factors (TFs), cell adhesion molecules (CAMs) and genes related to physiological functions including different neurotransmitter receptors. Pattern of gene expression, in particular that of TFs, aligns well with organization into groups and subclasses. For example, TFs *mafaa* and *eomesa* each label a RGC subclass. **B)** Hierarchical clustering of average gene expression patterns demonstrates relatedness of adult RGC clusters. Same genes as in the larval dataset are plotted. Gene expression patterns underlying the global relatedness of RGC clusters appear to be maintained in the mature retina. For example, *mafaa* and *eomesa* each continue to be expressed by molecularly related RGC cluster.

4.1.6 Cluster-specific genes provide novel molecular markers for RGC types

As shown above, RGC clusters exhibit distinctive gene signatures and can be differentiated or grouped based on such markers. But is there a unique molecular marker for each individual RGC type?

Addressing this question, we performed differential gene expression analysis to identify genes unique to specific clusters. Prospectively, such cluster-specific genes can be utilized as genetic entry point to RGC types. Indeed, virtually each cluster can

be defined by expression of a unique gene, which is highly expressed in the respective cluster but shows basal, if any, expression in the rest. These genetic markers include a variety of ontological categories like transcription factors, cell adhesion molecules or neuropeptides. I describe the identified top novel molecular markers presented in dotplots for the larval (Figure 14A) and the adult (Figure 14B) RGC clusters separately.

Most of the larval cluster-specific markers are transcription factors (*lmo1, meis1b, foxp1b, bhlhe22, tfap2d, mafaa, skor1b, eomesa, irx5b, tbx20, tbr1b* or *casz1*). Other cluster-specific genes encode cell adhesion molecules (*cdh6, pcdh17, kirrel3a*) or are implicated in synaptogenesis (*shisa9a, shisa9b, olfm3a*). Few markers can be attributed to physiological processes such as the potassium channel *kcn3* or the opsin *tmtops2a*. The remaining set of markers are genes involved in cellular processes (*fam19a1a, ntrk3b, cd82a*) or have unknown functions. As noted above, three clusters, cluster 27, 28 and 29, are defined by genes related to metabolism (*calca, junba* and *apoeb*), possibly upregulated during the purification procedure, and are unlikely to represent RGC types.

Likewise, the majority of differentially expressed genes between adult RGC clusters are transcription factors (*eomesa, skor1b, atoh7, zic3, lmo1, barhl1b, tbr1b, bhlhe22, mafa, foxp1b, irx4b, tbx3a, mafaa, etv1, foxp2, foxp4*). Other markers are neuropeptides (*pdyn, tac1*) or include a variety of genes related to physiology (*cabp7, grm6b, gabra5, pvalb8, icn*). Strikingly, cluster 10 can be clearly identified as differentiating RGCs. This cluster expresses the proneural transcription factor *atoh7* (better known as *ath5*), the transcription factor *zic3* and the *alcamb* (also known as *neurolin b)*. All three genes hold functions in RGC differentiation and development. *atoh7* is a known marker for RGC fate determination [234], *zic3* is expressed in a gradient from the peripheral stem cell niche to center and is involved in intra-retinal axon pathfinding [235] and *alcamb* encodes an adhesion molecule involved in differentiation and axonal pathfinding of RGCs [236].

The identified cluster-specific markers from both RGC datasets provide a complementary list of potential RGC type markers during developmental and mature stages. The majority of top markers encompass transcription factors. Interestingly, the larval top markers tend to include developmentally relevant genes, particularly cell adhesion molecules or proteins involved in synaptogenesis. In contrast, the adult top markers comprise genes determining physiological properties and some neuropeptides, which do not fall under criteria of top marker genes in larval RGCs.

While some markers appear unique to either larval or mature RGCs, other markers are shared and maintain cluster-specific expression. For example, the gene *c1ql3a*, which is reported to play a role in synapse numbers and density [237], is highly

enriched in the larval cluster 16 and the adult cluster 18. There are a number of transcription factors that show continuous cluster-specific expression: *lmo1, bhlhe22, mafaa, eomesa* and others. However, the number of clusters defined by these TFs is reduced in the adult dataset when compared to the larval clusters. The most striking example is *eomesa*, which is expressed by a total of five larval clusters (4, 18, 21, 25 and 26), but enriched in only two adult clusters (27 and 31). We investigated the relationships of specifically *eomesa* clusters in more detail below.

In summary, differential gene expression analysis revealed cluster-specific genes, which provide RGC type markers at unprecedented depth. These identified novel markers will be exploited to gain genetic access to specific types.

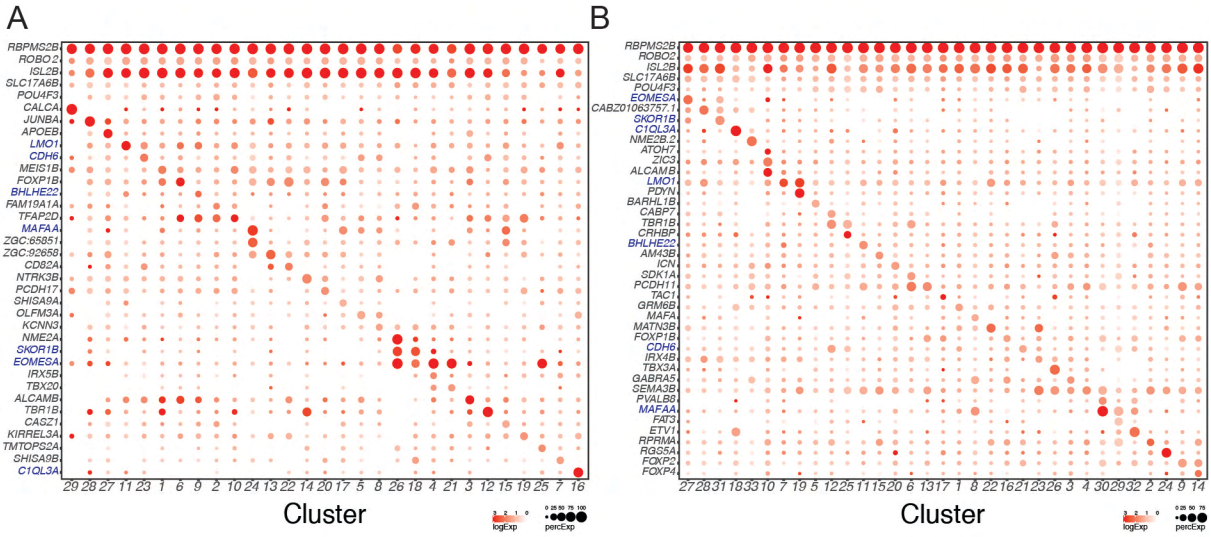

Figure 14: Differentially expressed genes serve as cluster-specific RGCs markers.

A) Best cluster-specific markers enriched in larval RGC clusters are aligned to known RGC markers presented in the top five rows. Genetic markers mostly include transcription factors, cell adhesion molecules and genes related to synaptogenesis. Top markers shared by larval and adult RGC clusters are highlighted blue. **B)** Best cluster-specific markers enriched in adult RGC clusters. Vast majority of markers code for transcription factors or neuropeptides.

4.1.7 RGC types maintain core molecular identity from larval to adult stages

The transcription factor *eomesa* is expressed in a total of five larval clusters, but enriched in only two of the adult clusters. How do these clusters relate between larval and adult stages? What are their differences? And how many types are defined by *eomesa* exactly?

Across the larval dataset, five clusters express the marker *eomesa* and together contain about 1.500 cells (Figure 15A). Four of these clusters (cluster 4, 18, 21 and 26)

are transcriptionally related and form a RGC subclass described in Figure 13, whereas cluster 25 is positioned more distantly in this molecular taxonomy. We identified individual cluster-specific gene signatures within *eomesa*$^{+}$ clusters at greater precision to better distinguish types. As depicted in Figure 15C, each larval *eomesa*$^{+}$ cluster exhibits a unique molecular composition. For example, the highly related four clusters co-express the neuropeptide *nmbb*, while cluster 25 lacks this feature. Moreover, cluster 18 and 26 share expression of the transcription factor *skor1b* while cluster 4 and 21 unite expression of transcription factor *onecut1*. Strikingly, cluster 25 expresses several transcription factors including *barhl2*, *vax1* or *zfhx4*, but also the *tmtops2a*, a teleost member of the opsin gene family [175,238]. The expression of *barhl2*, which is involved in RGC development [239], and the distant taxonomic position of cluster 25 suggest that RGCs in this cluster are *eomesa*$^{+}$ RGC precursors. Cluster 26 is defined by expression of the kinase *nme2a* as well as transcription factors *irx5a* and *tbx2b*. In addition, the most interesting molecular feature of cluster 18 is expression of the serotonin receptor *htr1ab*, but other markers include cellular components as *grapa* or *dio1*. Furthermore, cluster 4 and cluster 21 are highly similar and share expression of transcription factors *tbx20, irx1a, irx5b, irx6b*. Intriguingly, there are molecular indications of intrinsic photosensitivity as these clusters express opsins encoded by *opn5* as well as *tmtopsb* and produce *rdh10a*, an enzyme important to the visual cycle of chromophores.

Undersampling of cell types with high transcriptional similarity can result in merged clusters that contain two or more cell types [46]. An elegant approach to disentangle merged clusters is to perform iterative clustering analysis [25,215,230,240]. Indeed, the two adult *eomesa*$^{+}$ clusters are highly heterogeneous and a second iteration of clustering segregated the 731 cells into four subclusters (Figure 15B). These subclusters are transcriptionally highly similar and most of their gene signatures are evenly distributed across the subclusters. However, individual cluster-specific markers identified from larval *eomesa*$^{+}$ clusters maintain differential expression across the adult *eomesa*$^{+}$ subclusters and allow for direct comparison and identification (Figure 15D). Visual inspection of these markers predicts that adult subcluster 1 maps to larval *tbx20*$^{+}$ cluster 21, subcluster 2 corresponds to larval cluster 18, subcluster 3 to larval cluster 4 and subcluster 4 to larval cluster 26. No correspondence for the developmental *eomesa*$^{+}$ RGCs represented in larval cluster 25 could be found.

Collectively, these data strongly suggest that integrating transcriptome differences during developmental stages is key to molecular classification and facilitates resolving cell types with high molecular similarity. Larval *eomesa*$^{+}$ RGCs

exhibit higher transcriptional diversity and readily segregated into multiple clusters, which exhibit clear molecular distinctions. In contrast, splitting of adult *eomesa*$^{+}$ RGCs required supervised clustering. RGC types within this specific subclass, however, maintain molecular identity and continue to express specific markers. The data suggest that eomesa is a marker for three to five RGC types.

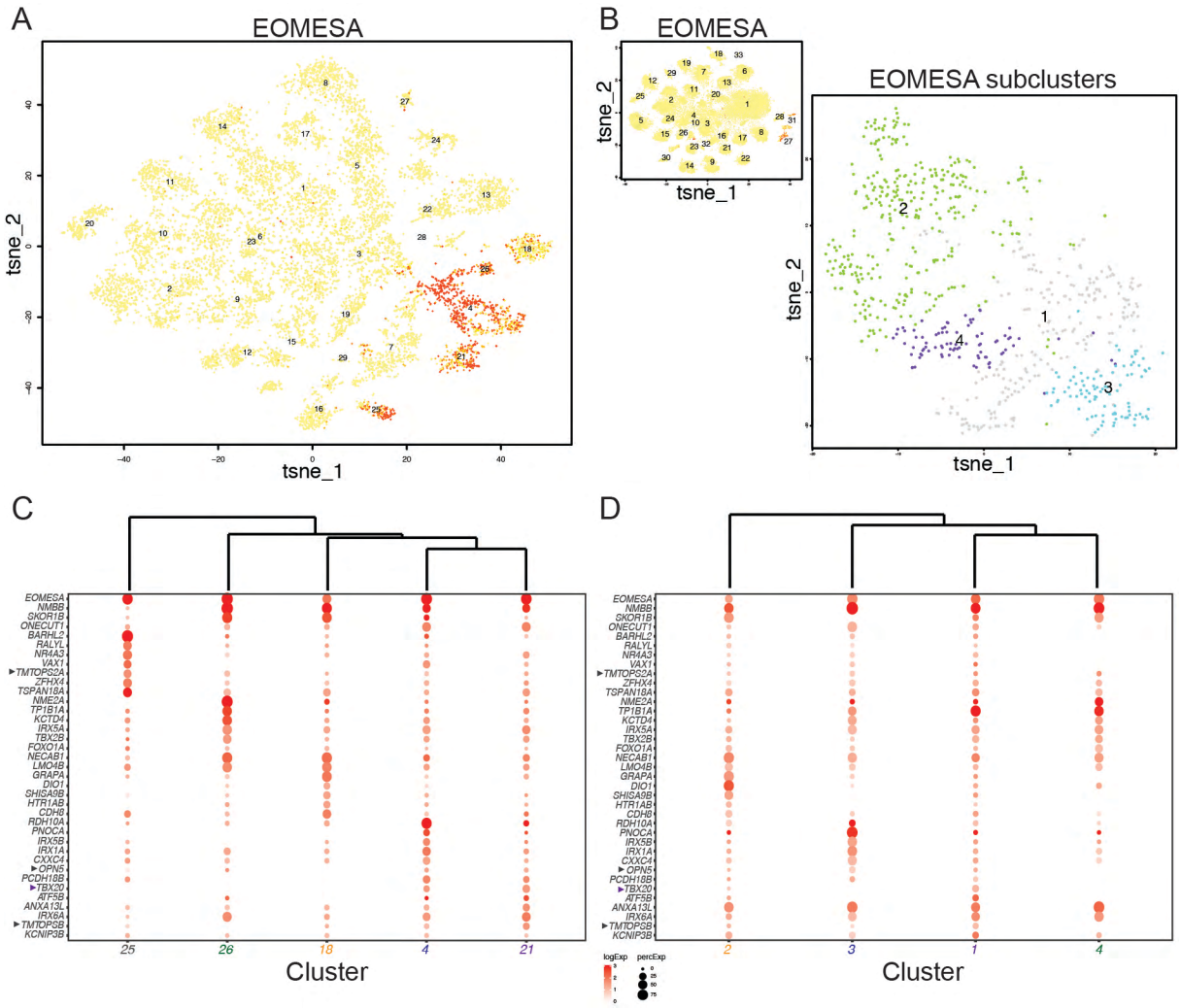

Figure 15: Molecular identity is maintained throughout larval and adult stages.

A) Visualization of *eomesa* expression in red across the larval RGC clusters. *eomesa*$^{+}$ RGC types are transcriptionally distinct and form five clusters: 4, 18, 21, 25 and 26. **B)** *eomesa*$^{+}$ RGC types clustered into two domains in the adult dataset (cluster 27 and 31) probably due to higher transcriptional similarity. A supervised second iteration of clustering segregates heterogeneity of *eomesa*$^{+}$ clusters and retrieves four molecularly distinct subclusters. **C)** Relationship of larval *eomesa*$^{+}$ clusters and top markers for each individual cluster. *eomesa*$^{+}$ RGCs express opsin family genes (grey arrows) and *tbx20* is a marker for specific clusters within this family (purple arrow). **D)** Relationship of the four adult *eomesa*$^{+}$ subclusters, which maintain core molecular identity so that top markers identified in the larval *eomesa*$^{+}$ clusters can be used to correspond adult subclusters and larval clusters. The *eomesa*$^{+}$ precursor cluster is not present in the adult data.

4.2 Mapping novel molecular markers to RGC morphotypes

At this point, we presume that the genetic distinctions between RGC clusters arise by nature of type-specific molecular repertoires. In other words, we hypothesize that transcriptionally distinct RGC clusters represent, and directly correspond to, putative RGC types. However, the approach of large-scale transcriptome profiling lacks biological information, in particular morphological features, which would facilitate unambiguous identification of actual cell types. In addition, because no prior knowledge on RGC subclass or type markers is available, clusters cannot be readily assigned a morphological type identity *in silico* with the exception of differentiating RGCs in adult cluster 10.

How do transcriptionally distinct RGC clusters relate to morphologically classified types? To determine the correspondence between molecularly and morphologically classified cell types, I exploited cluster-specific markers as genetic entry points to label cellular morphology. In the following sections, I describe experimental procedures and findings.

Acknowledgement
The results presented in Part II "Mapping novel molecular markers to RGC morphotypes" were obtained together with Manuel Stemmer to design and establish a CRISPR-Cas9 knockin approach and Shriya Lele and Irene Arnold-Ammer to perform microinjections.

4.2.1 *tbx20* is a RGC type marker and corresponds to a transcriptional cluster

The first evidence that transcriptional clusters represent distinct RGC morphotypes stems from a transgenic BAC line based on the promoter elements of the transcription factor *tbx20*. This *tbx20:Gal4* transgene [77] labels a morphologically distinctive RGC type previously described as a unique and rare RGC type in the retinal projectome [16] (Figure 16A-B). *tbx20*+ RGCs exhibit monostratified dendrites within the ON region of the IPL (M3; retinal projectome [16]) and their axons extend collaterals into AF4 and terminate in AF9 (PC15; retinal projectome [16]). Importantly, the gene *tbx20* is a cluster-specific marker that is differentially expressed between all transcriptional clusters and specific to a cluster in the *eomesa*$^{+}$ subclass. Across all larval RGC clusters, *tbx20* transcripts were detected in cluster 4 and 21, while *tbx20*$^{+}$ RGCs localize to the adult *eomesa*$^{+}$ cluster 27 or rather its derivate subcluster (Figure 15).

In conclusion, this finding is a first case of evidence that distinctive transcriptional clusters truly represent morphologically diverse RGC types.

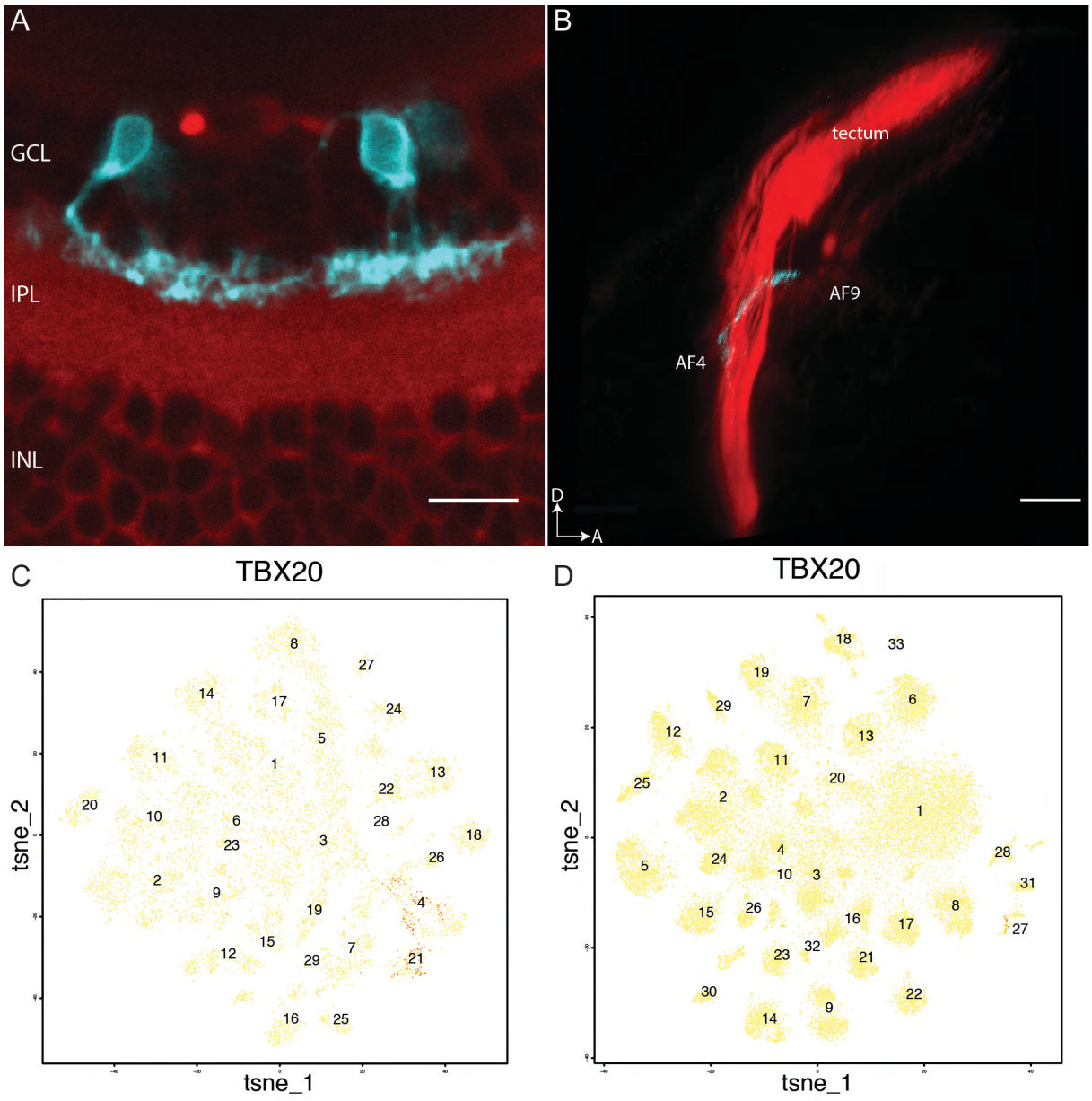

Figure 16: The RGC type marker *tbx20* maps to a transcriptional cluster.

A) Dendritic structure of *tbx20*$^{+}$ RGCs was imaged *in vivo* in 6 dpf transgenic *tbx20:Gal4, UAS:Dendra* retinas and can be classified as monostratified ON. Retinal IPL was counterstained with BODIPY. **B)** *tbx20*$^{+}$ RGCs project to AF4 and terminate in AF9 as illustrated in this 3D side view of *tbx20:Gal4, UAS:Dendra*, where *is2b:tagRFP* serves as a reference for all RGC projections. **C)** *tbx20* transcripts map to larval cluster 4 and 21, which form part of the *eomesa*$^{+}$ RGC subclass. **D)** *tbx20*$^{+}$ RGCs localize to cluster 27 in the adult transcriptome clusters and indicate transcriptional architecture of *eomesa*$^{+}$ clusters. Scale bar in A is 10 µm, in B 50 µm.

4.2.2 The Q-system offers an improved binary transgenic toolbox

Unlike for *tbx20*$^{+}$ clusters, however, transgenic reporter lines for other clusters are lacking. Taking into account that variegation and silencing effects inherent to the Gal4/UAS-system [55,241,242] may provide tools unsatisfactory for manipulation of specific cell types, I first set out to establish improved transgenic methods.

The Q-system is expected to show less variegation effects and enhanced stability over the course of generations [58–61]. Commensurate to other binary expression systems, the exogenous transcription factor QF2 can be expressed by a tissue- or ideally cell type-specific promoters. QF2 in turn acts on its QUAS consensus sequence, a promoter consisting of five interspaced copies of the naturally occurring QF2 binding sites, to activate expression of a desired reporter (Figure 17A). I generated the RGC-specific driver line *ath5:QF2* and three different QUAS reporter lines allowing for expression of membrane-tagged GFP (Figure 17B) for visualization of neuronal morphology or the RFP-fused enhanced potency version of nitroreductase (epNTR) for chemogenetic cell ablation (Figure 17C) or the calcium reporter GCaMP6s for functional imaging (Figure 17D). The functionality of both epNTR and GCaMP6s was confirmed by a visual background adaptation assay and visual stimulation during functional imaging from RGC axons, respectively (data not shown). Indeed, by visual inspection transgenic components of the Q-system appear less variegated between individuals.

By and large, the establishment of improved transgenic methods using the Q-system set groundwork for transgenic validation of candidate RGC type markers.

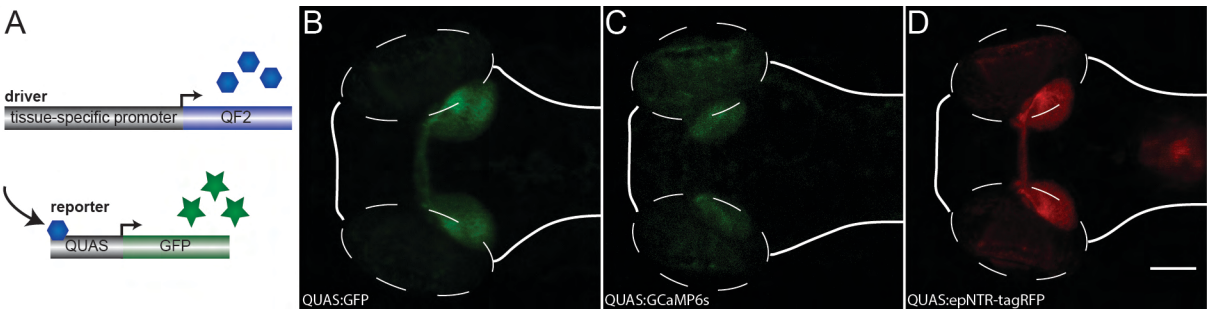

Figure 17: Robust reporter expression using the Q-system.

A) Schematic of the Q-system as an alternate binary expression system. A tissue specific promoter drives expression of a transcription factor, named QF2, which in turn activates reporter expression from its QUAS binding sequence. The transgenic *ath5:QF2* BAC driver line drives expression of **B)** *QUAS:GFPcaax*, **C)** *QUAS:GCaMP6s* or **D)** *QUAS:epNTR-tagRFP*. Scale bar in D is 100 µm.

4.2.3 Validation of novel markers by cluster-specific labeling of RGC types

Next, I aimed to generate candidate-specific QF2 driver lines to label the corresponding RGC type's morphology. The most faithful recapitulation of a candidate marker's expression is achieved by a direct knockin to the endogenous genomic locus of the gene.

To this end, I harnessed the CRISPR-Cas9 genome editing toolbox to integrate the coding sequence of QF2 to native promoter sites of cluster-specific markers. Specifically, a homologous-independent targeted integration, abbreviated HITI, strategy [243] was implemented. Here, the ribonucleoprotein (RNP) complex of Cas9 protein and target-specific gRNA cuts genomic DNA and donor DNA concurrently as illustrated in Figure 18A. This cleavage results in linearized donor DNA encoding QF2 and makes the target genomic DNA site accessible. In the unfavorable event of reverse integration of QF2, the gRNA target sites are reconstituted leading to recurrent cleavage and ultimate removal of donor DNA from the genome. If, however, donor DNA integrates in the desired forward direction, gRNA target sites are lost and integration remains stable. Thus, the HITI strategy favors forward integration allowing for efficient expression of QF2 under the promoter of candidate markers.

To establish a pipeline for transgenic validation, three different knockin positions were tested (Figure 18B): First, we targeted the region up to 500bp upstream of a candidate gene and inserted a e1b:QF2 fragment with a basal promoter to enhance expression. Second, we targeted the first exon of the candidate gene for in-frame integration of a QF2 fragment shortly after the start codon. Third, we targeted the first intron of the candidate gene to insert a QF2 fragment flanked by splicing sites. The latter two integration sites result in gene disruption due to a terminating polyA-signal in the donor construct. We tested the knockin strategies by injection of a RNP/donor DNA cocktail into transgenic *QUAS:loxP-GFP-loxP-epNTR-tagRFP* (*QUAS:switchNTR*) reporter eggs.

In Figure 18C, I quantified efficiencies using different gRNAs targeting selected candidates as measured by transient GFP expression. Overall, it is noticeable that knockin efficiency varies between gRNAs. Some exhibit a transient integration rate as low as 0.4%, others are with 4.9% more efficient. The average of measured efficiencies of all gRNAs used in this study lies at 2%.

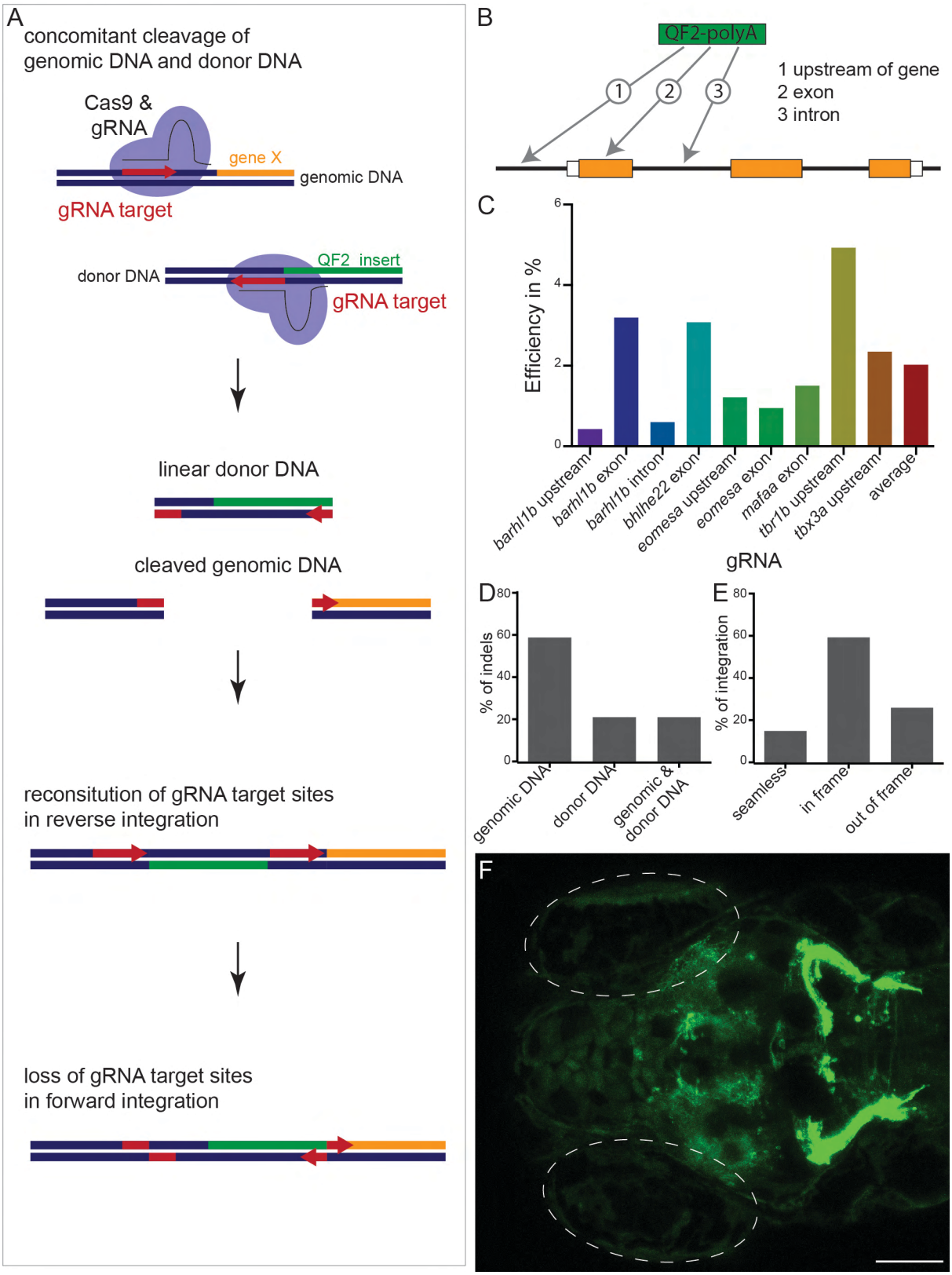

Figure 18: Locus-specific knockin via CRISPR-Cas9 enables validation of novel RGC type markers.

A) Schematic of the working principle of homologous-independent targeted integration (HITI) using CRISPR-Cas9. Genomic DNA and donor DNA are cleaved concomitantly through recognition of the same gRNA target sequence (indicated by red arrow). For a knockin event, the linearized donor DNA integrates into the cleaved genomic position. In case of a reverse integration gRNA target sites are reconstituted and mediate recurrent cleavage, whereas gRNA target sites are lost with forward integration and stabilize the knockin. **B)** Schematic indicating three approaches for knockin of QF2 to different gene structures: 1) up to 500bp upstream of the translation start. 2) into the first exon and 3) into the first intron flanked with splicing sites. **C)** Various gRNAs differ in knockin efficiency as measured by transient GFP expression. The average efficiency is 2%. **D)** Characterization of knockin events showed that indels occur predominantly on the genomic DNA, but also on donor DNA or both. **E)** Characterization of knockin events targeting the first exon showed that most knockins are in frame. **F)** Transient mosaic expression pattern reflects the endogenous expression pattern as exemplified by knockin to *barhl1b* expressed by tectal and cerebellar neurons. Scale bar in F is 100 µm.

I next characterized the nature of successful QF2 integration. Single amplicon sequencing revealed that genome engineering via CRISPR-Cas9 is associated with insertions and deletions (indels) at the target site. I quantified the occurrence of indels (Figure 18D) and found that most indels occur solely at the genomic DNA. Only 20% of the characterized cases showed indels on only the donor DNA or both genomic DNA and donor DNA. Figure 18E depicts further characterization of knockins targeted to the exon, which require in-frame integration for QF2 expression. A mere 15% of knockin events integrated exactly as designed and in frame with no indels at the flanking integration sites. However, the majority of knockin events (59.2%) exhibited indels but integrated in frame, whereas 25.9% of cases were out of frame.

Most importantly, knockin of QF2 via CRISPR-Cas9 to the genomic locus of a candidate gene results in transient expression of GFP that recapitulates the endogenous expression pattern. Figure 18F shows a representative larva injected for targeted knockin to the first exon of *barhl1b*. The candidate *barhl1b* is specific to adult cluster 5 and expressed in forebrain, tectum, cerebellum, hindbrain, and retina [244]. Consistent with this expression pattern, we observed GFP labeling in *barhl1b*-expressing brain areas in injected larvae. In fact, labeling of structures outside the expression domain of candidate genes was observed rarely and such larvae were discarded.

Taken together, locus-specific transgene knockin via CRISPR-Cas9 genome engineering allows to label genetically defined neurons in a fashion that recapitulates the endogenous expression pattern.

4.2.4 Genetic intersection refines expression to specific cell types

Cluster-specific genetic markers hold functions outside the retina and often are broadly expressed throughout the organism. Thus, the complete labeling of the endogenous expression pattern challenges the morphological classification of RGC types as RGC axons cannot be differentiated from neuronal processes of other origins. This obstacle can be exemplified using the marker *barhl1b* shown in Figure 18F. Because neurites of *barhl1b*$^{+}$ tectal neurons are intermingled in the tectal neuropil, it is impossible to determine morphology of *barhl1b*$^{+}$ RGCs. Is there a measure to refine transgene expression specifically to RGCs?

As a matter of fact, genetic intersection offers an elegant solution to label RGCs out of any given expression pattern. Central to this approach is the overlapping expression of two genes as illustrated in Figure 19A. Reporter expression can be restricted to cells of interest via driver and Cre intersection. A driver line activates expression of an intersectional reporter that consists of a floxed default cassette followed by a conditional cassette. The default cassette is removed through Cre-mediated recombination via the flanking loxP sites, which leads to activation of the conditional cassette in cells that share driver and Cre expression while other cells remain labeled by the default reporter.

To refine expression to RGCs, I generated the RGC-specific *ath5:Cre* line, which provides an essential component necessary for the intersectional transgenic validation of marker genes. *ath5* encodes a transcription factor, which is necessary for RGC neurogenesis and is also expressed in some amacrine cells, horizontal cells and photoreceptors [212,234,245]. To examine the pattern of recombination, I intersected *ath5:Cre* with the *ß-actin:loxP-GFP-loxP-tagRFP* [79] transgene. As shown in Figure 19B, *ath5:Cre* mediates recombination specifically in RGCs, but not in any other areas of the nervous system. Consistent with the reported expression of *ath5*, I observed Cre-mediated conversion of GFP to RFP in all RGCs as well as a subset of ACs, HC and photoreceptors within the retina (Figure 19C).

Conclusively, transgenic intersection via *ath5:Cre* refines expression to RGCs in broad patterns and aids genetic identification of RGC processes in the brain.

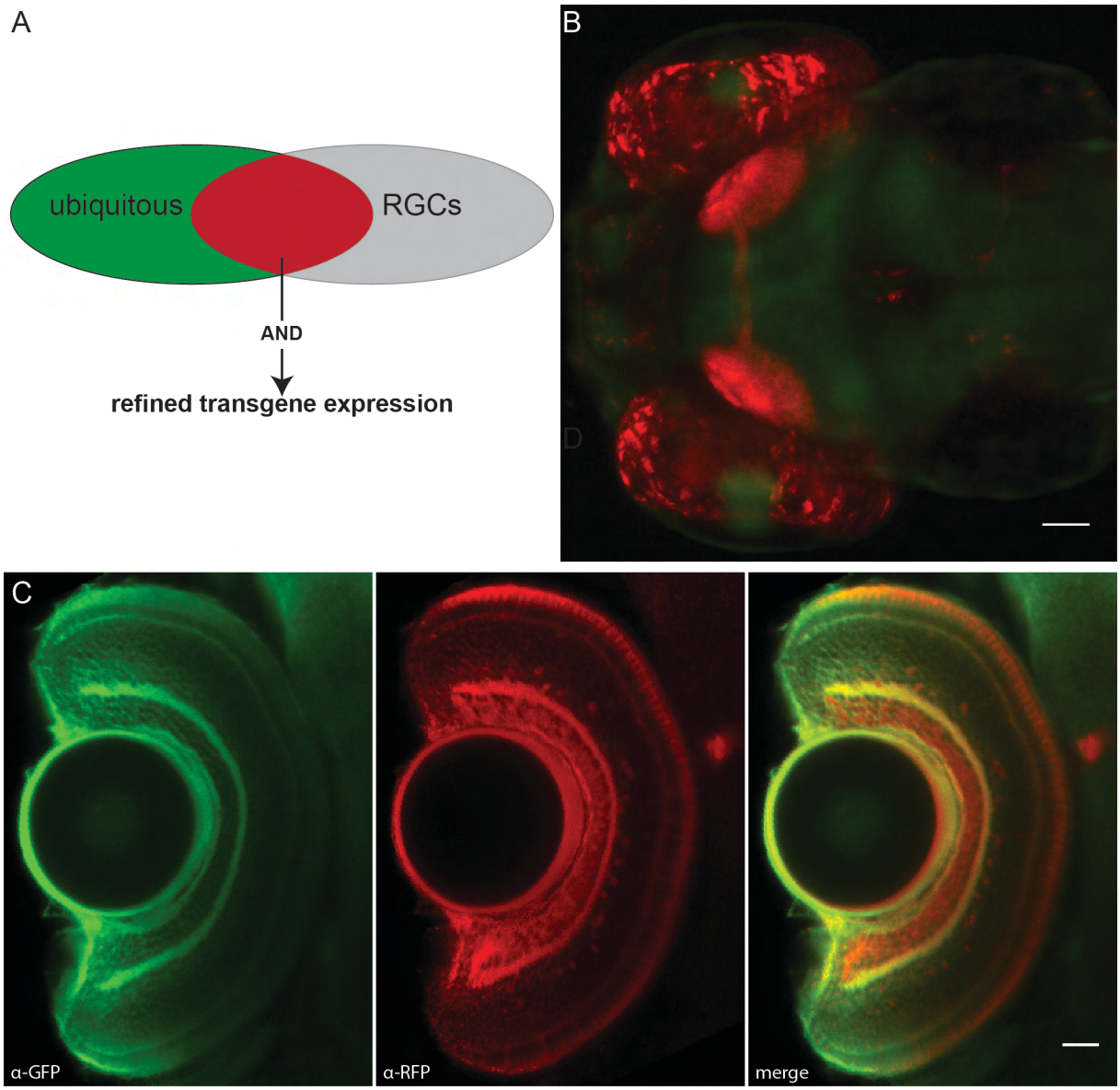

Figure 19: Genetic intersection restricts expression to RGCs.

A) Principle of the intersectional approach, in which the overlapping expression pattern of two genes is exploited in a logic AND gate to refine transgene expression. For example a ubiquitously expressed gene, such as *β-actin* can be intersected with *ath5* to refine expression to RGCs. **B)** A 5dpf larvae showing intersection of *β-actin:loxP-GFP-loxP-tagRFP* and *ath5:Cre*. Cre-mediated recombination is specific to RGCs and does not occur in other brain areas. **C)** Retina section of a *β-actin:loxP-GFP-loxP-tagRFP*, *ath5:Cre* larva. Consistent with endogenous *ath5* expression, the *ath5:Cre* transgene drives recombination in all RGCs, some ACs and HCs. Scale bar in B is 50 µm, in C 20 µm.

4.2.5 Distinct transcriptional cluster relate to diverse RGC morphotypes

The establishment of a CRISPR-Cas9 technique for candidate-specific generation of driver lines in conjunction with RGC-specific genetic intersection is elementary for the validation of novel RGC type markers. Figure 20 presents a strategy for mapping

transcriptional RGC clusters derived from single cell transcriptomics to morphological RGC type identity as classified by the retinal projectome.

To clarify, we crossed transgenic *ath5:Cre* fish to *QUAS:loxP-GFP-loxP-epNTR-tagRFP*, hereafter abbreviated *QUAS:switchNTR*, and injected a locus-specific CRISPR-Cas9 cocktail into zygotes. We screened injected larvae at 5 dpf for transient mosaic expression and imaged labeled RGCs *in vivo* before raising fish into adulthood. Importantly, integration of QF2 to the *barhl1b* locus in this intersectional background resulted in GFP expression outside the retina while *barhl1b*$^{+}$ RGCs were RFP-labeled (see Figure 20 to be compared with Figure 18F).

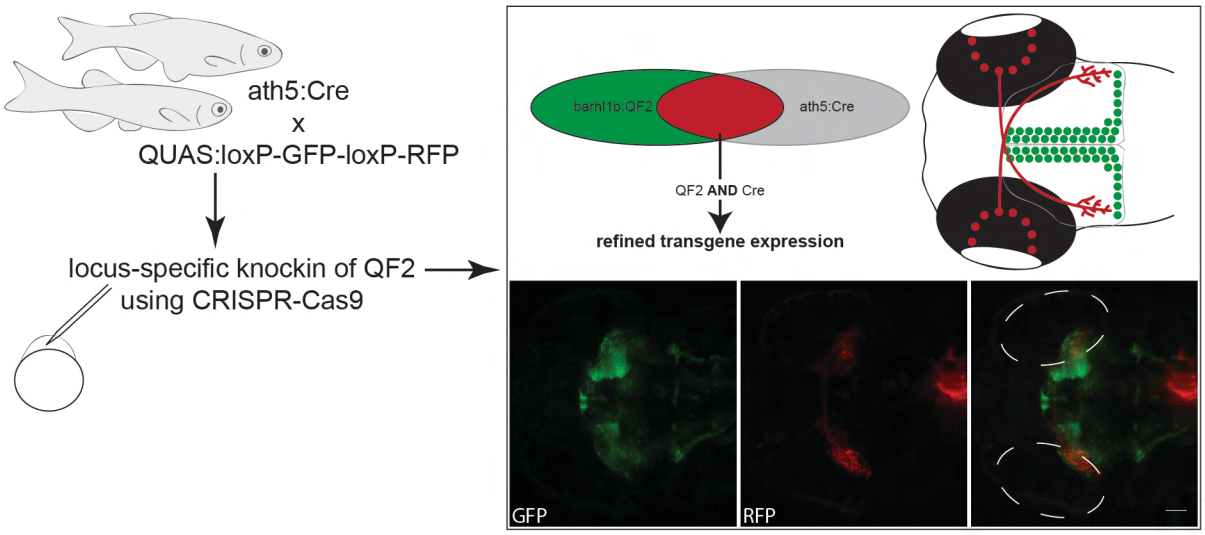

Figure 20: Workflow for mapping cluster-specific markers onto RGC morphology.

Cluster-specific genes were used to intersectionally label corresponding RGC types and map morphological identity to transcriptomic clusters. *ath5:Cre* transgenic fish were crossed to a *QUAS:loxP-GFP-loxP-RFP* intersectional reporter. Eggs were collected and injected with locus-specific CRISPR-Cas9/gRNA complexes and donor DNA yielding transient cluster-specific labeling of RGC types. Transiently expressing larvae were analyzed by *in vivo* imaging prior to raising. The provided example is a *barhl1b:QF2* larva showing GFP labeling outside of the retina, while *barhl1b*-expressing RGCs are labeled by RFP and their axonal morphology can be characterized. For clarity, GFP-labeled neurites of tectal cells are omitted in the schematic. Scale bar is 50 µm.

Next, we implemented this strategy to validate various selected candidates. The identified differentially expressed genes provide a roadmap for gerating RGC type specific transgenic lines. I specifically focused on transcription factors (TFs) specifically, because they have been established as major determinants of neuronal cell type identity [4]. I present selected TF candidates in feature plots in Figure 21. Here, red dots correspond to single cells expressing the gene. Gene expression, however, should

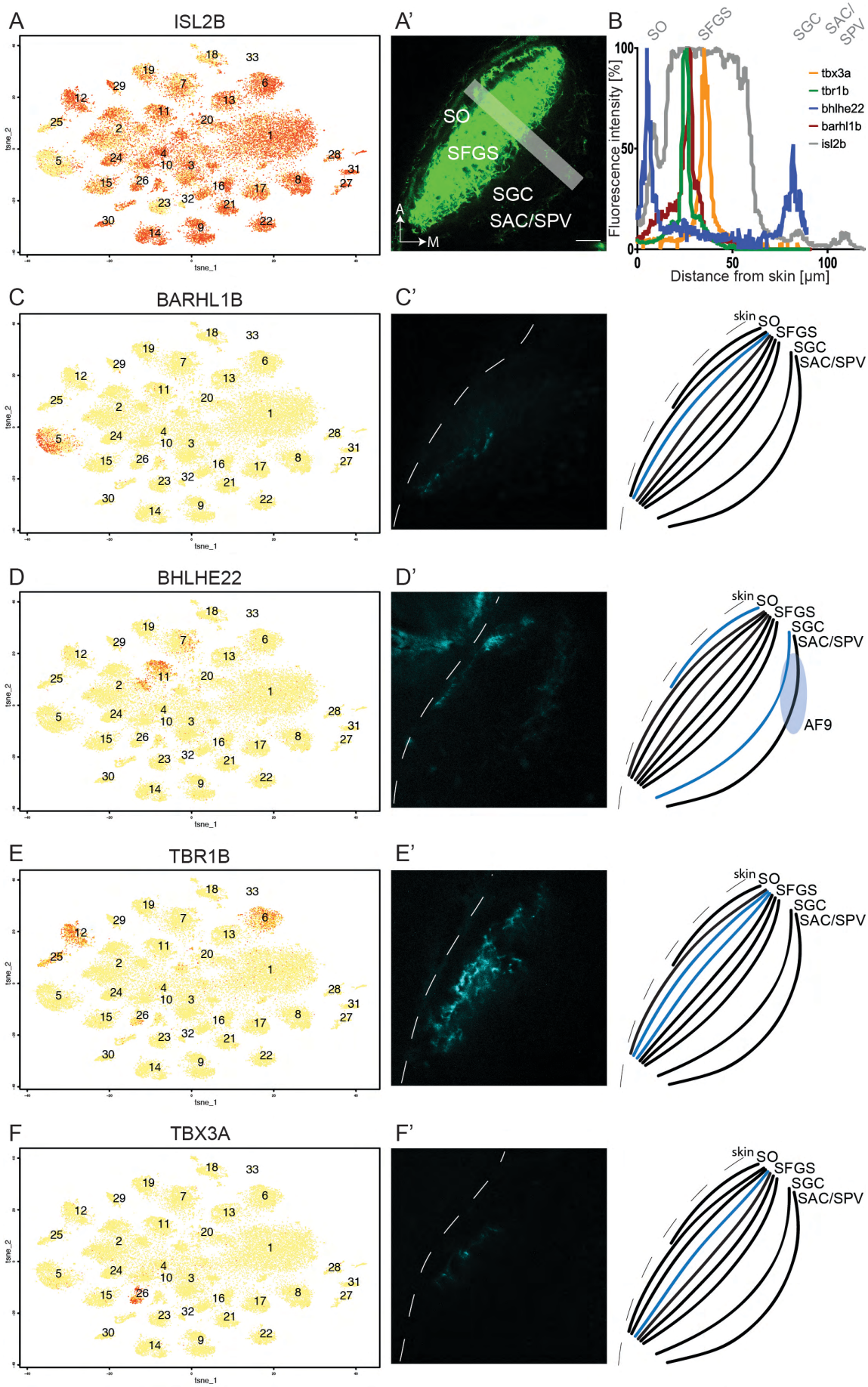

Figure 21: Different cluster represent different RGC types.

A) The pan-RGC marker *isl2b* is broadly expressed across adult RGC clusters. **A')** Transgenic expression in *isl2b*$^{+}$ RGCs labels all retinotectal innervation domains: stratum opticum (SO), stratum fibrosum et griseum superficiale (SFGS), stratum griseum centrale (SGC) and stratum album centrale/stratum periventriculare (SAC/SPV). Layers can be distinguished in a fluorescence plot across layers created by drawing a bar as indicated. **B)** Fluorescence profiles derived from transient labeling are indicative of marker-specific termination sites within retinotectal innervation domains. *isl2b* profile serves as a reference. **C)** Expression pattern of *barhl1b* across adult clusters and **C')** corresponding labeled RGC processes. **D)** Expression pattern of *bhlhe22* across adult clusters and **D')** corresponding labeled RGC processes. **E)** Expression pattern of *tbr1b* across adult clusters and **E')** corresponding labeled RGC processes. **F)** Expression pattern of *tbx3a* across adult clusters and **F')** corresponding labeled RGC processes. Scale bar in A' is 20 µm.

be qualitatively examined on the basis of collective correlation of cells within clusters. This is to say that the shallow sequencing approach leads to dropouts at individual cell level so that actually expressed transcripts have not been detected in a fraction of cells within a cluster.

To better compare RGC type specificity of candidate markers, I first describe expression of the pan-RGC marker *isl2b*. This transcription factor is broadly expressed across adult RGC clusters (Figure 21A). Accordingly, *isl2b* labels all retinal projections and innervation domains in the tectum: SO, SFGS, SGC and SAC/SPV as annotated in Figure 21A'. Individual retinotectal layers can be discriminated and measured in a fluorescence profile across the neuropil area. The *isl2b*-derived fluorescence plot in Figure 21B thus serves a s a reference label to compare to the termination of marker-specific RGC types.

The adult RGC cluster 5 specifically expresses the TF *barhl1b* (Figure 21C) and transient mosaic labeling facilitated examination of retinotectal projection pattern of *barhl1b*$^{+}$ RGCs as demonstrated in Figure 21C'. I generated a fluorescenec profile from skin to deep tectum and manually aligned *barhl1b*$^{+}$ RGC signal to the pan-RGC reference (Figure 21B). The overlay indicates that *barhl1b*$^{+}$ RGCs terminate in the SFGS innervation domain, most likely SFGS2.

The TF *bhlhe22* is expressed in two adult RGC clusters (Figure 21D), namely cluster 7 and 11. This marker appears to label two distinct retinotectal projections shown in Figure 21D': One routing directly to the superficial layer and one targeting a deep tectal layer via AF9. The fluorescence signals of RFP-labeled *bhlhe22*$^{+}$ retinal processes coincide well with the SO and SGC innervation domains in the tectum (Figure 21B).

As shown in Figure 21E, *tbr1b* is strongly enriched in multiple clusters (adult cluster 6, 12 and 25), though these clusters are not closely related with regard to

molecular taxonomy. In mouse retina, this TF is expressed by four RGC types and guides their dendritic stratification to the OFF region within IPL layers [246]. In transient validation experiments, RFP-labeled *tbr1b*$^{+}$ RGC axons terminated in the SFGS domain spanning at least two SFGS sublayers (Figure 21E'). The fluorescence profile in Figure 21B indicates innervation of SFGS2/3 by *tbr1b*$^{+}$ RGCs.

Last, the TF *tbx3a* is a marker for adult RGC cluster 28 (Figure 21F) and transient labeling showed few RGC axons in the SFGS domain (Figure 21F'), presumably SFGS3.

Together, these findings show to a certain level of confidence that distinct transcriptional RGC clusters directly correspond to different RGC morphotypes, which form visual pathways with termination sites in various retinotectal innervation domains.

4.2.6 The RGC subclass marker *mafaa* is specific to superficial visual pathways

Mosaic transient labeling supports that transcriptional clusters represent RGC types. Yet, a stable transgenic reporter line will present a more compelling evidence and are necessary to unequivocally confirm this hypothesis. Do marker genes remain specific to RGC types when labeled in their full expression pattern?

The transcription factor *mafaa*, homologue to mouse MafA [247], is a marker for a subclass comprising multiple clusters: cluster 5, 8, 17 and 24 in the larval RGC dataset, cluster 8, 29, 30, 32 in the adult RGC dataset (Figure 13). The close relationships of these putative RGC types thus appear to be maintained from larval to mature retina. We identified a stable founder for a *mafaa:QF2* line. In this particular case, integration of QF2 was targeted to the first exon of the *mafaa* gene as designed during initial iterations of CRISPR-Cas9 knockins. The precise insertion of QF2 at the desired locus was verified by PCR and sequencing (data not shown).

In addition to the retina, *mafaa* is reported to be expressed by myotomes, the olfactory system and in hindbrain and midbrain neurons [248] and, accordingly, *mafaa:QF2* drives expression in these tissues. Importantly, the genetic intersection with *ath5:Cre* uncovered specific labeling of *mafaa*$^{+}$ RGCs as shown in Figure 22A. To examine these RGC projections morphologically, I crossed fish intersectionally labeling *mafaa*$^{+}$ RGCs (*mafaa:QF2, QUAS:loxP-GFP-loxP-epNTR-tagRFP, ath5:Cre*) to the pan-RGC marker *isl2b:GFP* and imaged the entire optic tract in the 6 dpf larva. The 3D view in Figure 22B thus shows GFP-labeled RGC landmarks and RFP-expressing *mafaa*$^{+}$ RGCs. It is evident from these images that *mafaa* is a marker for specific visual

pathways with similar axonal routings to superficial layers. A group of *mafaa*$^+$ RGCs projects to the SO layer and extends axon collaterals to AF7, while the remainder of *mafaa*$^+$ RGCs terminate in the SFGS innervation domain. To determine precisely which layers are targeted by *mafaa*$^+$ RGCs, I analyzed as before a fluorescence plot across RGC layers in the tectum (Figure 22C) with *isl2b:GFP* signal serving as a reference. Consistent with the expression of *mafaa* by multiple clusters, transgenic labeling indicated multiple morphotypes. *mafaa*$^+$ RGC axons coincide with signal of the SO and SFGS2 layer. Figure 22D and 22E demonstrate specific labeling of *mafaa*$^+$ RGCs in the tectum and AF7 neuropil, respectively. These axonal morphologies correspond with projection class 2 (AF7-SO) and 5 (SFGS2) as classified by the retinal projectome [67].

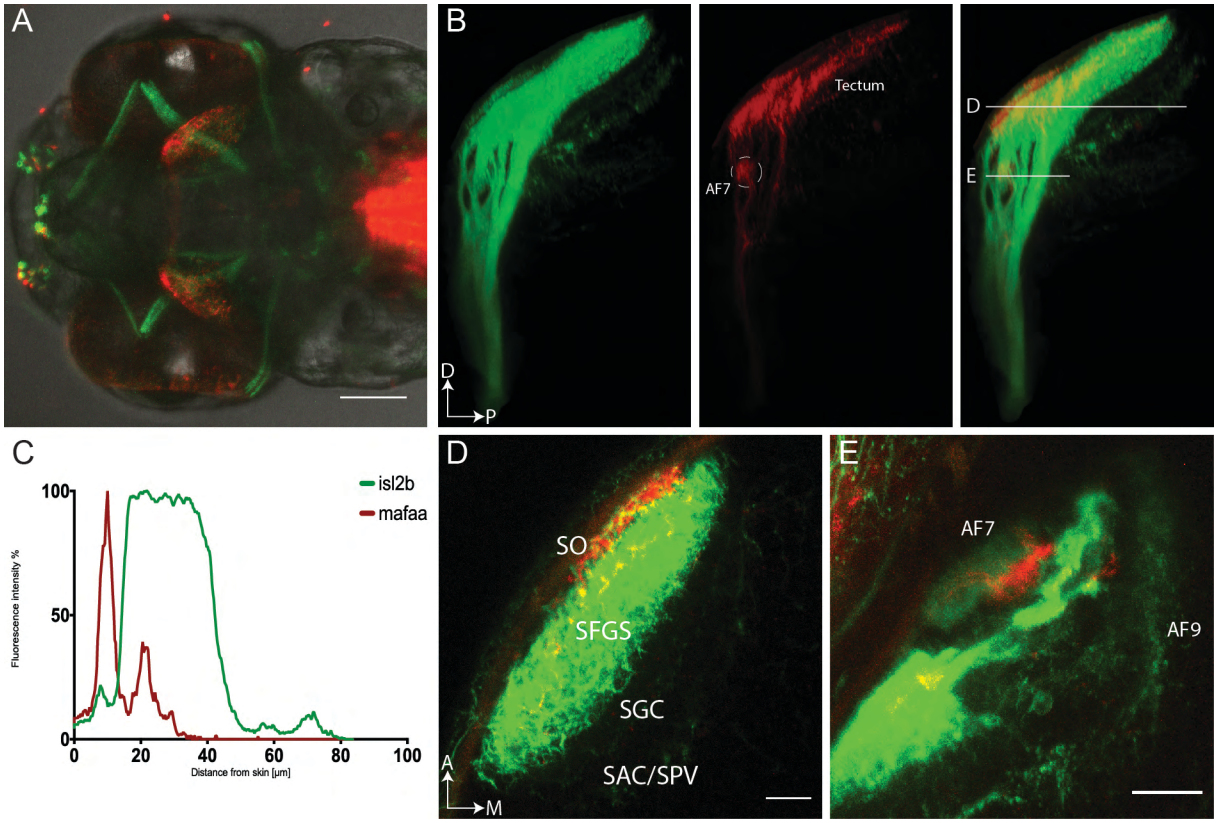

Figure 22: *mafaa* labels a RGC subclass forming superficial visual pathways.

A) *mafaa:QF2, QUAS:switchNTR, ath5:Cre* transgenic 6 dpf larva expresses GFP in *mafaa*$^+$ cells, while *mafaa*$^+$ RGCs are RFP-labeled. The transgene reflects endogenous expression pattern of *mafaa*. **B)** 3D view of *mafaa*$^+$ retinal projections expressing RFP in a *mafaa:QF2, QUAS:switchNTR, ath5:Cre, isl2b:GFP* larva. GFP is expressed by all RGCs and serves as a reference for major anatomical landmarks. *mafaa*$^+$ RGCs terminate in SO with axon collaterals in AF7, and in SFGS. **C)** Fluorescence profile analysis of *mafaa*$^+$ RGC innervation across retinotectal layers reveals that *mafaa*$^+$ RGCs target SO and SFGS2. **D)** Plane view of *mafaa*$^+$ RGCs in the tectum. **E)** Plane view of *mafaa*$^+$ RGC axon collaterals to AF7. Scale bar in A is 50µm, in D and E 20 µm.

In essence, these observations provide compelling evidence that transcriptionally distinct RGC clusters derived from single cell transcriptomics do indeed correspond to specific RGC morphotypes. Hence, there is a strong relation between the molecular composition and morphology of RGC types.

4.2.7 The RGC subclass marker *eomesa* defines a deep visual pathway

A striking discovery based on morphological examination of *mafaa*$^{+}$ RGCs is that the axonal routings from clusters within a RGC subclass are highly similar. This observation is a first indication that molecularly related clusters also share morphological features. Do transcriptionally related RGC clusters generally share morphological features? Is this similarity a prevailing principle governing RGC diversification patterns? If yes, is axonal projection superior to dendritic stratification in determining RGC taxonomy?

I chose to investigate these questions by looking at a different RGC subclass marker. The best candidate we have thus far uncovered is the previously discussed subclass defined by the T-box transcription factor *eomesa*, which comprises four RGC clusters (Figure 13 and 15). The integrity of this subclass remains maintained from larval to adult stages as in effect *eomesa* is continuously expressed by four putative RGC types, which remain each other's closest relatives in both larval and adult datasets. Furthermore, this particular candidate became focus of my attention for an unrelated reason: *eomesa* (better known as Tbr2 in mammals) is a well characterized marker for intrinsically photosensitive RGCs in mouse and other species [49,50,159,160,249] and may hold conserved functions in zebrafish.

We obtained germline transmitted carriers of *eomesa:QF2* from targeted insertion of QF2 to both the region upstream and the first exon of *eomesa*. Correct insertion was verified by PCR and sequencing. Both lines showed a consistent expression pattern. Because the basal promotor included in the knockin targeted upstream of *eomesa* appears to result in slightly boosted expression, I restricted further investigations to this transgene.

In the zebrafish nervous system, *eomesa* is best known for its expression in the pallium [250] and cerebellar granule cells [251]. Consistent with these reports, the stable *eomesa:QF2* line drives expression in forebrain and cerebellum. Importantly, there is additional labeling of a specific subset of RGCs (Figure 23A). To classify axonal projections of *eomesa*$^{+}$ RGCs, I crossed *eomesa:QF2, QUAS:switchNTR, ath5:Cre* fish to the pan-RGC marker *isl2b:GFP*. Figure 23B demonstrates a 3D view with GFP labeling

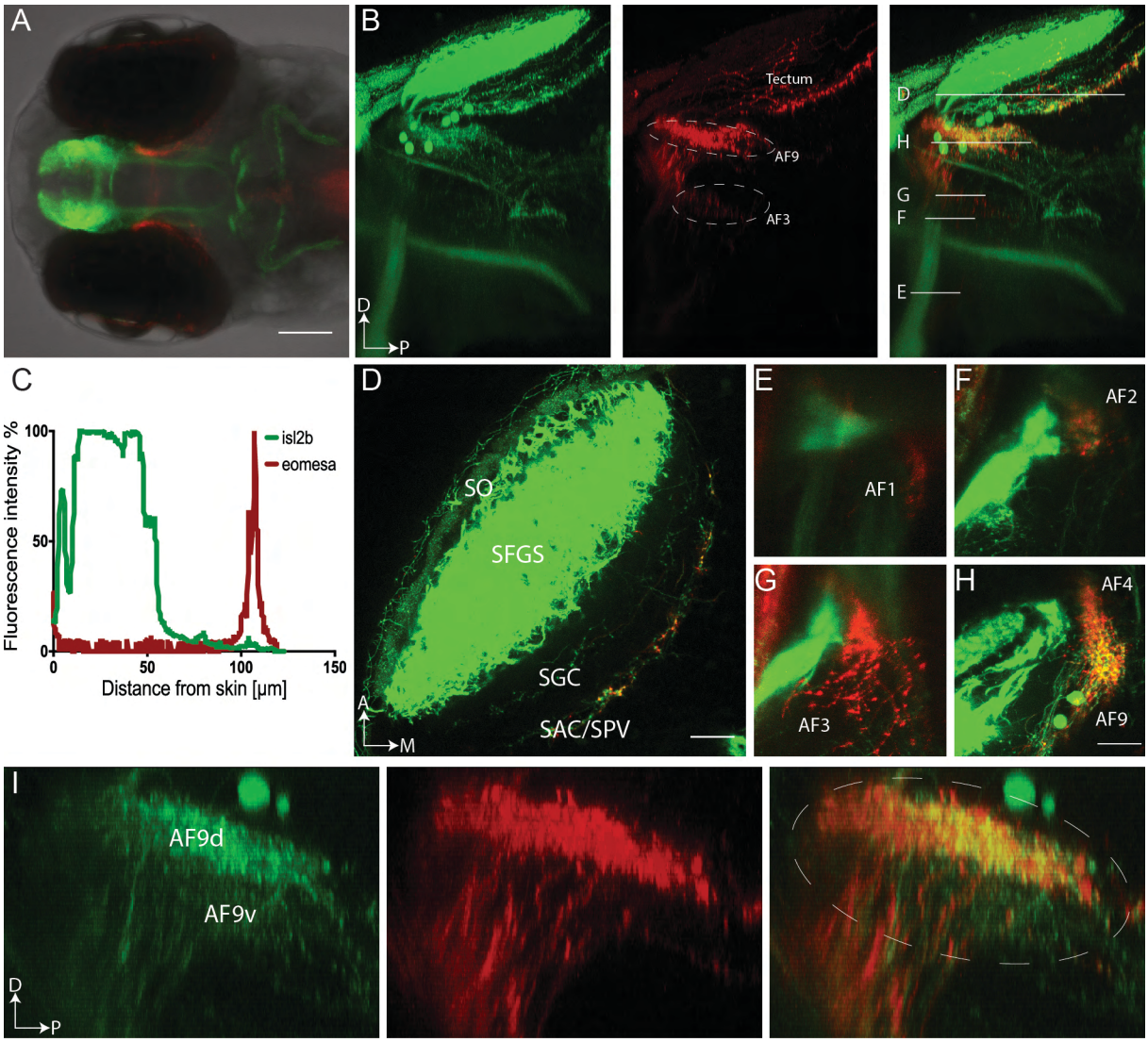

Figure 23: *eomesa* is specifically expressed by a RGC subclass forming deep visual pathways.

A) A transgenic *eomesa:QF2, QUAS:switchNTR, ath5:Cre* 6 dpf larva expressing GFP in *eomesa*$^+$ cells outside the retina, while *eomesa*$^+$ RGCs are RFP-labeled. The transgene reflects the endogenous expression pattern. **B)** 3D view of *eomesa*$^+$ retinal projections expressing RFP in a *eomesa:QF2, QUAS:switchNTR, ath5:Cre, isl2b:GFP* larva. GFP is expressed by all RGCs and serves as a reference for major anatomical landmarks. *eomesa*$^+$ RGCs terminate in SAC/SPV and form axon collaterals to AF1, AF2, AF3, AF4 and AF9 en route to tectum. **C)** RFP signal from *eomesa*$^+$ RGCs coincides with SAC/SPV signal in a fluorescence profile across tectal layers. **D)** Plane view of *eomesa*$^+$ RGCs in the tectum. Plane views of *eomesa*$^+$ axon collaterals to extratectal **E)** AF1, **F)** AF2, **G)** AF3 and **H)** AF4 and AF9. **I)** 3D side view to AF9 neuropil. *eomesa*$^+$ RGCs specifically innervate dorsal AF9. Scale bar in A is 50 µm, in D and H 20 µm.

of the major RGC termination sites and RFP-expressing *eomesa*$^+$ RGCs. This co-labeling clearly demonstrated that *eomesa*$^+$ RGCs form a visual pathway to a set of extratectal AFs, in particular AF9, and the SAC/SPV layer. The fluorescence profile across the

tectal layers shown in Figure 23C further corroborates innervation of SAC/SPV by *eomesa*$^+$ RGCs as RFP signals coincide with the deepest tectal layer. Of note, *eomesa*$^+$ RGCs are a subset of SAC/SPV innervating types. Thus, there are RFP-negative RGC axons intermingled with *eomesa*$^+$ RGC axons in the tectal neuropil (Figure 23D). Based on the GFP-labeled landmarks, I determined *eomesa*$^+$ axon collaterals to AF1 (Figure 23E), AF2 (Figure 23F), AF3 (Figure 23G) and AF4 and AF9 (Figure 23H). This axonal projection pattern corresponds to projection class 20 (PC20) described by the retinal projectome [16]. The breadth of *eomesa*$^+$ RGC terminations may all be attributed PC20 or may as well mask a combination of projection classes. Whether or not *eomesa*$^+$ RGCs differentially innervate the observed brain targets will be investigated below.

Interestingly, AF9 is composed of a dorsal and a ventral subdivision, which are distinguished by the manner of encoding luminance changes (ON versus OFF) [16,139]. I investigated specificity of *eomesa*$^+$ RGC axons within the AF9 neuropil and found that axon collaterals are exclusively extended within the dorsal neuropil of AF9 (Figure 23I) suggesting that they are primarily involved in ON visual pathways.

In conclusion, similar to the case of *mafaa*, a stable transgenic reporter for the subclass marker *eomesa* proves that segregated transcriptional RGC clusters correspond to distinct RGC morphotypes. Most intriguingly, types within the *eomesa*$^+$ RGC subclass form a deep visual pathway. Their axons innervate the deepest tectal layer SAC/SPV layer and route via dorsal AF9. These findings, together with morphological examination of the *mafaa*$^+$ RGC subclass, provide mounting evidence that transcriptionally related RGC types are also morphologically related. Based on these insights, it is conceivable to postulate that taxonomic diversification pattern of RGCs corresponds with global axonal projection properties.

4.2.8 Morphological dissection of *eomesa*$^+$ RGC types

The RGC subclass defined by *eomesa* comprises four transcriptionally distinct types, which project to a variety of AFs (AF1, AF2, AF3, AF4, AF9 and tectal SAC/SPV). But do all four possible *eomesa*$^+$ RGC types exhibit same axonal morphologies to all these AFs or do distinct types innervate these AFs differentially? And, if the latter is the case, which cluster corresponds to which morphotype?

To molecularly decipher the *eomesa*$^+$ RGC subclass, I exploited the individual cluster marker *tbx20* presented in Figure 15. In fact, one of the clusters within the *eomesa* subclass expresses *tbx20* discussed above. *tbx20*$^+$ RGCs are unique in that they

do not innervate the main retinorecipient brain area – the tectum. Rather, *tbx20*$^{+}$ RGCs form axonal projections to AF4 and terminate in AF9 corresponding to a unique projection class (PC15) as characterized in Figure 16. To confirm that *eomesa*$^{+}$ RGC types are comprised of distinct morphotypes, I investigated *tbx20*$^{+}$ RGC morphology within *eomesa*$^{+}$ RGCs. The fact that there is no crosstalk between the Gal4/UAS-system and the Q-system allowed me to simultaneously visualize RGCs of both markers in the same larvae. Figure 24A thus shows a representative example of a *eomesa:QF2, QUAS:switchNTR, tbx20:Gal4, UAS:Dendra* larva, in which Dendra-labeled *tbx20*$^{+}$ axons were photoconverted to red and *eomesa*$^{+}$ axons are labeled in GFP. First to mention, *tbx20*$^{+}$ RGCs terminate in AF9 and do not innervate the SAC/SPV layer. Hence, there is no *tbx20*$^{+}$ signal within the *eomesa*$^{+}$ labeled RGC axons in the tectum. Within the AF9 neuropil, the *tbx20*$^{+}$ axons form a subset of the *eomesa*$^{+}$ RGC axons, directly corresponding to the representations of these markers in RGC transcriptional clusters.

Next, stochastic sparse labeling of RGCs in the *eomesa:QF2* line allowed to investigate axonal projection patterns of individual *eomesa*$^{+}$ RGC morphotypes. A total of five single RGCs, labeled by mosaic expression of *QUAS:tdTomatocaax* injected into *eomesa:QF2*, could be imaged *in vivo* and reconstructed by tracing in three dimensions. Figure 24B shows single RGC traces and an overlaid reconstruction of their projections. Three of the sparsely labeled RGCs terminated in AF9, while two of them projected further to tectal SAC/SPV. Axon collaterals in AF1 could not be observed in our samples, possibly due to imaging limitations based on weak fluorescence and depth of AF1. With exception of one trace, the RGC projection types can be associated with previously classified morphologies. RGC traces innervating AF4 and AF9 correspond to PC 15. Remaining traces with SAC/SPV innervation likely can be attributed to PC 17. The third trace, however, showed an atypical projection pattern with an axon extension into tectal SAC/SPV returning to AF9. It is possible that this RGC sample showed an erroneous development of axonal projections, which best corresponds to PC 18 or 20. Of note, this morphological dissection of *eomesa*$^{+}$ RGCs is not saturated and needs to be extended to dendritic morphologies.

Together, the current data suggest a model in which *eomesa*$^{+}$ RGCs comprise distinct morphotypes, which differentially innervate AF1, AF2, AF3, AF4, AF9 and tectal SAC/SPV. Therefore, it can be concluded, with highest confidence for *tbx20*$^{+}$ clusters, that distinct molecular clusters within the *eomesa*$^{+}$ RGC subclass correspond to distinct morphologies.

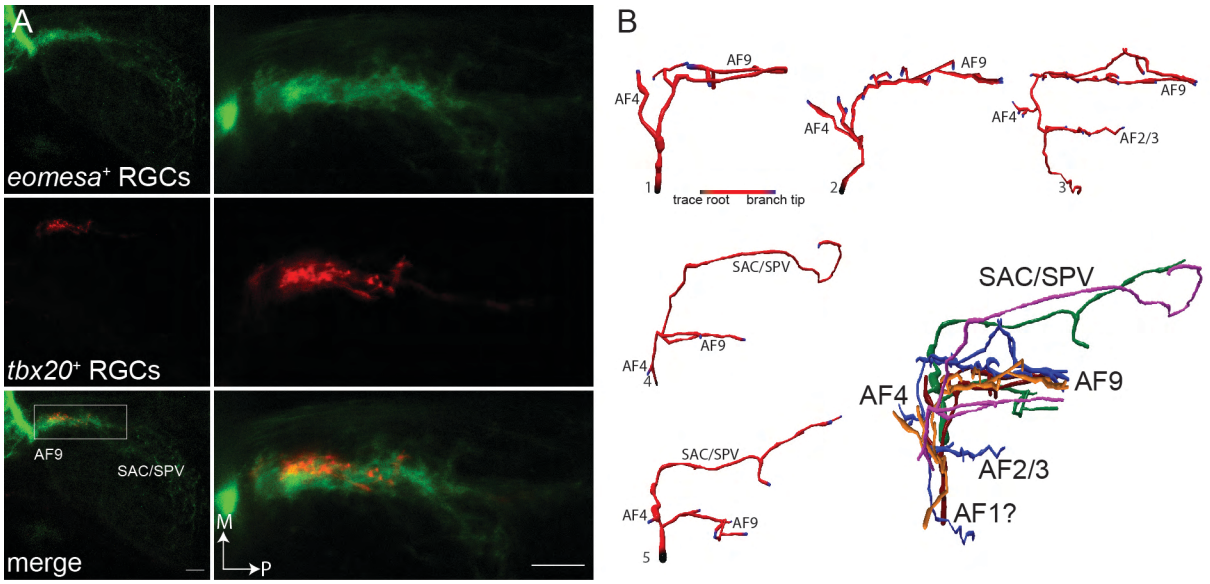

Figure 24: Dissection of individual types within the *eomesa*$^+$ RGC subclass.

A) Co-localization of *eomesa*$^+$ and *tbx20*$^+$ RGCs in a *eomesa:QF2, QUAS:switchNTR, tbx20:Gal4, UAS:Dendra* (photoconverted to red) 6 dpf larva. *tbx20*$^+$ RGCs form a subpopulation of the RGC subclass marked by *eomesa* as accurately represented in transcriptional RGC clusters. The *eomesa* retinal projection pattern masks differential innervation formed by RGC types comprising this subclass. **B)** Traces of sparse, stochastically labeled *eomesa*$^+$ RGCs demonstrate diversity of RGC morphotypes in this subclass. Scale bar in A is 20 µm.

4.3 Functional characterization of RGC types

Eomes (also known as Tbr2), the mouse homolog to zebrafish *eomesa*, is a well characterized marker for intrinsically photosensitive RGCs (ipRGCs) [22,34,49,159,160]. ipRGCs are evolutionary ancient and have been shown to be conserved between mouse to primates [50].In mouse, approximately 10% of RGCs express Eomes [160,252] and project to non-image forming brain nuclei [160]. Eomes is expressed by all five known types of ipRGCs, but also labels additional non-photosensitive types [159,160]. Moreover, studies show that Eomes is required for proper development as well as maintenance of ipRGCs [159,160]. Intriguingly, mouse ipRGCs and the zebrafish *eomesa*$^+$ RGC subclass share not only expression of this transcription factor, but also other genetic components: Most importantly, *eomesa*$^+$ clusters show enrichment of opsin genes (Figure 15), which is a fundamental requirement of ipRGCs physiology [154,253]. Furthermore, genes enriched in zebrafish individual *eomesa*$^+$ RGC clusters, in particular *onecut1*, *tbx20*, *irx5* and *irx6*, were also found to be co-expressed by Eomes RGC types specifically [21].

These conserved features are a first strong molecular correlation between the zebrafish *eomesa*$^+$ RGC subclass and mouse ipRGCs. Other accumulating observations point to a potential function of *eomesa*$^+$ RGCs as ipRGCs: First, *eomesa*$^+$ RGCs are enriched in the ventral half of the retina [254], an additional property they have in common with mouse ipRGCs [255]. It is hypothesized that this anatomical asymmetry aids to specifically survey luminance levels. Second, *eomesa*$^+$ RGCs extend axon collaterals into AF1 - the only hypothalamic retinorecipient brain nucleus [16,139], which is thought to be involved in non-image forming functions.

Based on these parallels, I hypothesized that *eomesa*$^+$ RGCs constitute ipRGCs in zebrafish and regulate non-image forming functions. In the following paragraphs, I describe two complementary experiments to test this hypothesis.

Acknowledgement

The results presented in Part III “Functional characterization of RGC types” were obtained in collaboration with Thomas Helmbrecht, who analyzed functional imaging data using custom-written Python algorithms and Shriya Lele, who helped perform behavioral tests.

4.3.1 Characterization of tuning types of genetically-defined RGC populations

ipRGCs encode global levels of ambient illumination and are primarily known to not function in pattern vision. Is this also the case for *eomesa*$^{+}$ RGCs in zebrafish? What are functional properties of *eomesa*$^{+}$ RGCs? Also, is there a one-to-one correspondence of a molecularly defined and morphologically classified RGC type to functional tuning type?

To test tuning properties of RGC types, I designed a battery of visual stimuli including ON and OFF stimuli, dimming and brightening as well as moving gratings, virtual prey or approaching objects. I immobilized 5 to 7 dpf larvae for *in vivo* imaging at a two-photon microscope as illustrated in Figure 25A. I presented visual stimuli monocularly on a screen that covers approximately 120° of the fish's eye, corresponding to roughly 80% of its field of view. During visual stimulation, I recorded responses from RGC axons within the AF9 neuropil and the tectum. To rigorously characterize RGC types within AF9, I recorded from various planes spanning the entire depth of AF9 (Figure 25B). Here, I imaged neuronal activity from all RGCs using *isl2b:Gal4, UAS:GCaMP6s* larvae as a pan-RGC reference as well as the *eomesa*$^{+}$ RGC subclass using *eomesa:QF2, QUAS:switchGCaMP6s, ath5:Cre* and from the definite *tbx20*$^{+}$ RGC type using *tbx20:Gal4, UAS:GCaMP6s*.

The recorded GCaMP6s fluorescence intensities served as a proxy for neuronal activity and were analyzed using custom-written python scripts. A total of eleven regressors were designed to assess responses of individual pixels originating from individual RGC axons to each stimulus feature. To evaluate tuning properties to sustained or transient ON and OFF stimuli or to presented patterned stimulation, all pixels were scored based on their responses to all regressors. A positive score value indicates increased neuronal activity when a certain stimulus is presented, while a negative score specifies anti-correlation to a stimulus feature.

Pixel-wise clustering of normalized regressor scores across the three reporter lines (24.368 pixels for *isl2b*, 14659 pixels for *eomesa*, 10049 pixels for *tbx20*) revealed distinct response types (Figure 25C). The identified response types can be classified as sustained ON (cluster 4 in blue), transient ON (cluster 5 in purple), sustained ON - transient OFF (cluster 3 in green), sustained OFF (cluster 2 in yellow) and transient OFF types (cluster 1 in red) (Figure 25D). While recordings from *isl2b*$^{+}$ RGC axons in tectum revealed traces tuned to patterns such as direction-selectivity, orientation-selectivity, prey- or loom-sensitive (data not shown), no such responses were found in

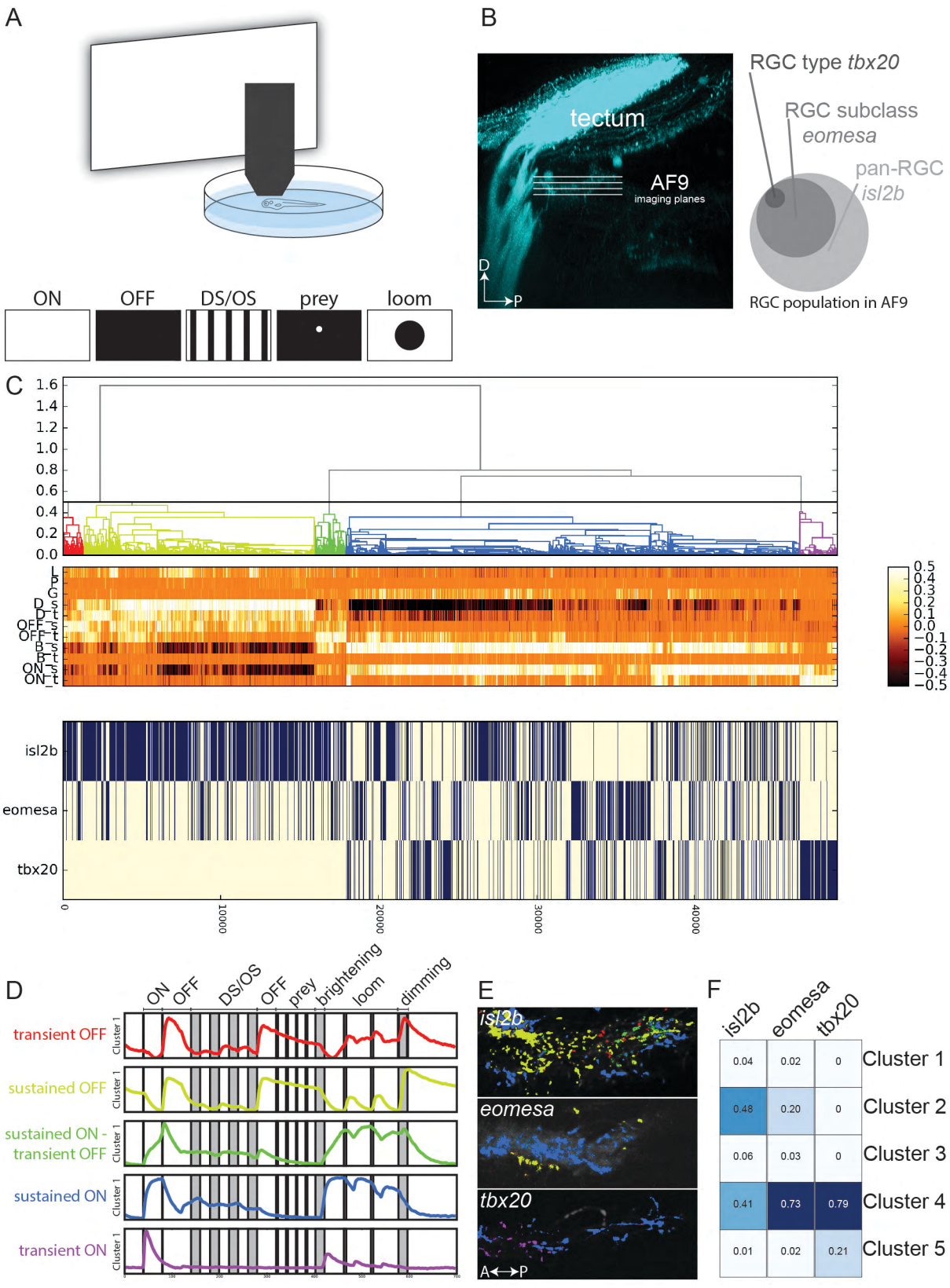

Figure 25: Genetically-defined RGC types in AF9 encode ambient luminance.

A) Setup for functional characterization of RGC types by two-photon calcium imaging from RGC axons during monocular visual stimulation probing ON and OFF responses and sensitivity for direction (DS), orientation (OS), prey or looming stimuli. **B)** Functional recordings were taken from planes at 5µm Z-steps through AF9. Responses were characterized from distinct genetically-defined RGC populations using the pan-RGC marker *isl2b*, the subclass marker *eomesa* and the type marker *tbx20*. **C)** Clustering using correlation scores of about 50.000 pixels to built regressors identifies five major functional types. Heatmap shows correlation of pixels with each regressor to L: loom; P: prey; G: grating (direction or orientation selectivity); D: dimming; B: brightening; _s: sustained; _t: transient. Bottom map indicates pixel origin. **D)** Average traces of five main functional clusters aligned to stimulus sequence. RGCs in pretectum show no activity during presentation of patterns (moving grating, prey or loom) but rather encode ambient luminance levels through predominant ON and OFF responses. **E)** Individual pixels in AF9 neuropil were color-coded by cluster correspondence. *isl2b* labels all RGCs and a mix of functional types, whereas *eomesa*$^{+}$ RGCs mostly show sustained ON and OFF responses and the single RGC type labeled by *tbx20* exclusively exhibits ON responses. **F)** Relative correspondences of pixels to functional types found in different genetically-defined RGC populations. Each column sums up to 100%.

AF9 neuropil suggesting that RGC types projecting to pretectum mainly encode ambient luminance levels in form of predominant ON and OFF responses.

Responses recorded from the pan-RGC marker *isl2b* are represented in all functional types (Figure 25E). Main functional types are sustained OFF (cluster 2) and sustained ON (cluster 4) representing 48% and 41% of *isl2b* traces, respectively (Figure 25F). Similarly, cell types of the *eomesa*$^{+}$ RGC subclass show mixed functional ON and OFF responses and form part of all five identified response types. The majority of *eomesa*$^{+}$ pixels, however, can be attributed to sustained ON cluster 4. Intriguingly, *tbx20*$^{+}$ RGCs are specifically tuned to ON stimuli. Of note, *tbx20*$^{+}$ ON responses can be distinguished into a sustained (cluster 4) and a transient type (cluster 5). The latter is a minority cluster with respect to the entire dataset and originates to large extent from *tbx20*$^{+}$ recordings.

In conclusion, distinct functional types innervate AF9 neuropil, none of which appear to directly encode visual features from the presented patterns such as direction, size or local edges. Rather than carrying extracted spatial information, AF9 RGCs report ambient luminance levels to the brain. In particular, these experiments allow to correlate physiological properties with genetically-defined RGC populations. As predicted by transcriptional profiling and morphological analysis, *eomesa*$^{+}$ RGCs comprise mixed functional response types. In contrast, the single type identified by *tbx20*$^{+}$ expression corresponds exclusively to ON responses, which at increased level of detail can be further divided into sustained and transient ON categories. More importantly, the observation that *eomesa*$^{+}$ RGCs do not directly contribute to pattern

vision supports the idea that they play a role in non-image forming functions of the visual system.

4.3.2 Testing behavioral relevance of *eomesa*$^+$ RGCs

What is the behavioral relevance of *eomesa*$^+$ RGCs? Zebrafish mutants with defective photoreceptors are still capable to adapt to their visual background [180], hinting at an alternate light-sensing RGC population such as ipRGCs driving this neuroendocrine camouflage response. Resting on the hypothesis that *eomesa*$^+$ RGCs are intrinsically photosensitive, I tested their role in regulation of VBA.

The nitroreductase/metronidazole cell ablation system is contained within in the intersectional transgenic reporter described previously facilitating physical disruption of specific RGC populations while other tissues remain unaffected. Specifically, the bacterial enzyme nitroreductase is only expressed by *eomesa*$^+$ RGCs and converts the substrate metronidazole into a DNA-intercalating compound, which ultimately causes cell death. First, I validated efficiency of induced cell ablation of *eomesa*$^+$ RGCs. Figure 26A shows that treatment of *eomesa:QF2, QUAS:switchNTR, ath5:Cre* fish with metronidazole for 24 hours damages *eomesa*$^+$ RGC axons as indicated by progressing degradation in AF9 neuropil (compare RFP aggregates after MTZ treatment). In contrast, sibling control larvae treated with DMSO do not show induced cell ablation.

Using the intersectional expression of nitroreductase, *eomesa*$^+$ RGCs were chemo-genetically ablated to test for their necessity in VBA. Larvae were treated at 4 dpf for 24 hours and then allowed to recover overnight. The VBA test was performed at 6 dpf by placing dark-adapted larvae onto bright background and scoring their appearance after 45 minutes adaptation. Wildtype and *lakritz* mutants, which lack all RGCs and remain dark against bright background [180] were used as controls and reference for visual inspection. Larvae were scored on a range from 0 to 10, where 0 was assigned to pale larvae showing contracted melanophores, whereas dark larvae with dispersed melanophores were scored 10. RGC-ablated *ath5:QF2, QUAS:epNTR-tagRFP* larvae appeared very dark and are comparable to *lakritz* (mean score is 9.42 ± 0.12 SEM, n=108) demonstrating successful cell ablation and RGC dependency of VBA. DMSO and MTZ control groups appeared pale and bright adapted with few outliers (mean score is 1.24 ± 0.1 SEM, n=108 for DMSO group; mean score is 0.53 ± 0.1 SEM,

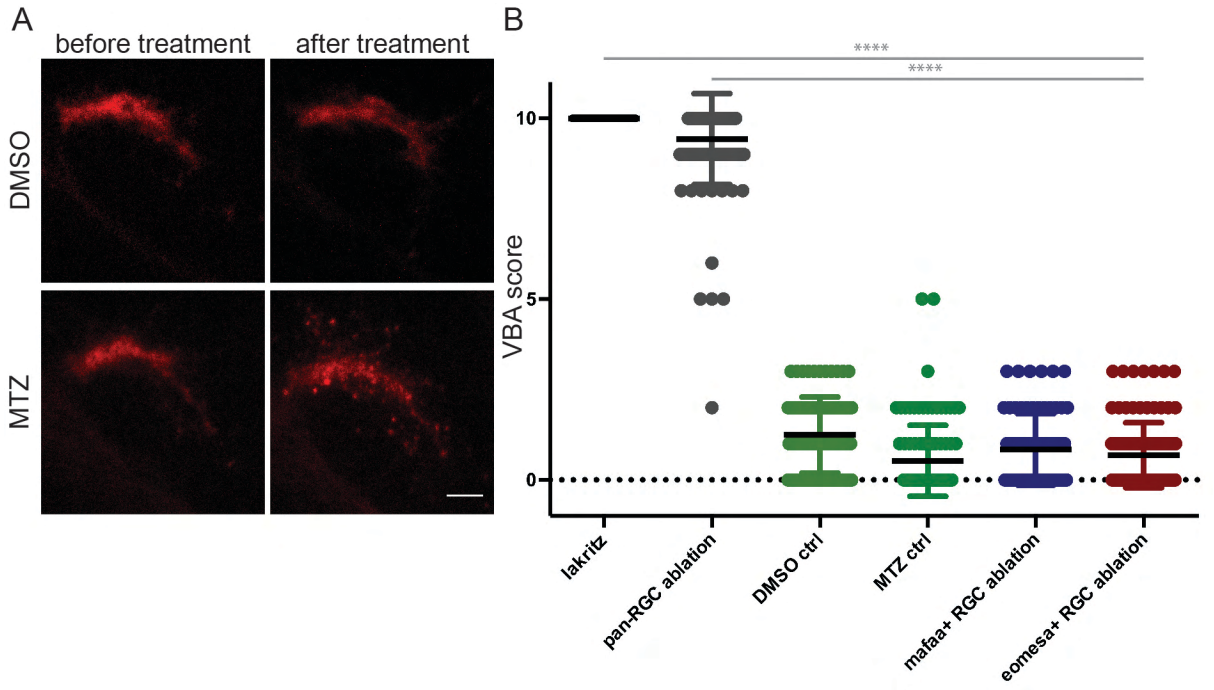

Figure 26: Intersectional ablation of *eomesa*$^+$ RGCs enables behavioral necessity tests.

A) Metronidazole (MTZ) treatment of larvae expressing nitroreductase in *eomesa*$^+$ RGCs mediates specific induced cell ablation. Left panel shows AF9 neuropil in the 4 dpf larvae before treatment. Right panel shows AF9 neuropil in 5 dpf larvae after treatment with MTZ or DMSO (control). Control larvae exhibit intact AF9 neuropil, whereas MTZ-treated larvae show progressing decomposition of AF9 neuropil as indicated by RFP aggregates. **B)** Visual background adaptation appears not affected by physical disruption of *eomesa*$^+$ RGCs in initial behavioral assays. Dark adapted test and control larvae were allowed to adapt to bright background and scored on a range from 0 to 10 (0 is pale, 10 is dark). Genetic or physical ablation of all RGCs strongly impairs larva's ability to camouflage to the bright background. Ablation of *eomesa*$^+$ or *mafaa*$^+$ RGCs by MTZ treatment for 24 hours does not affect VBA. Dots correspond to individually scored larvae. Lines show mean with standard deviation.

n=108 for MTZ group). Larvae show ability to adapt to bright background when *mafaa*$^+$ RGCs, which project to superficial layers, are ablated (mean score is 0.85 ± 0.12 SEM, n=72). The test group of *eomesa*$^+$ RGC ablated larvae appeared to have no deficits in VBA. The larvae in this group showed contracted melanophores and were scored as bright adapted (mean score is 0.68 ± 0.01 SEM, n=107). Successful ablation of *eomesa*$^+$ RGCs was confirmed by confocal imaging immediately after the behavioral assay. I confirmed these results by measuring the mean grey value of individual larvae from images taken after 45 minutes bright adaptation (data not shown).

In summary, transgenic intersection using a nitroreductase cassette facilitates efficient cell ablation of specific RGC subpopulations for testing their behavioral relevance. The hypothesis that *eomesa*$^+$ RGCs regulate VBA could not be affirmed by

these initial behavioral tests. Nonetheless, based on these results a possible contribution of *eomesa*$^{+}$ RGCs cannot be ruled out, because, for one, the induced physical disruption might have been incomplete and, for another, there might be other RGC types compensating their function. Also, other aspects of the behavior such as temporal kinetics of VBA have not been assessed.

5 DISCUSSION

5.1 Summary of key findings

In this thesis, I optimized a protocol to capture single zebrafish neurons from larval and adult retinas. I show that large-scale transcriptomic profiling can be applied to molecularly classify bipolar cells and retrieve transcriptional domains representing distinct cell types. Next, in a collaborative effort, I generated a comprehensive cell type atlas for RGCs, the output neurons of the eye. The results provide the following main advances:

First, analysis of transcriptome profiles of thousands of RGCs during both larval and adult stages classified distinct types of unique molecular composition. The data support the notion that transcriptional diversity during development eases type segregation, albeit RGC types indeed maintain molecular identity throughout life stages. Second, investigation of global inter-cluster relationships revealed a hierarchical organizing principle of RGC types. In a taxonomic pattern, RGC diversity is structured into major groups comprising RGC subclasses, which further split into individual RGC clusters. Third, dozens of novel molecular markers for zebrafish RGC types were identified at unprecedented high resolution. Fourth, distinct molecular RGC subclasses or types directly corresponded to defined RGC morphotypes. Specifically, cluster-specific markers were exploited as genetic entry points in a CRISPR-Cas9 knockin approach to label axonal projections to retinorecipient brain targets that correspond to previously classified RGC morphotypes. This approach resulted in the generation of novel robust driver lines for genetically-defined RGC populations. One such transgene labels a RGC subclass defined by the transcription factor *eomesa*, which projects to a select set of retinorecipient brain areas including pretectum and deep tectal structures. Fifth, accurate representation of transcriptional composition in RGC clusters was further corroborated by detailed anatomical characterization of the *tbx20* type marker within the *eomesa*$^{+}$ subclass. Sixth, genetically and anatomically defined RGC populations were correlated with functional response types suggesting a tight correlation between molecular, morphological and functional definitions of a cell type. Seventh, a hypothesis-driven approach begins to elucidate the behavioral relevance of *eomesa*$^{+}$ RGCs in non-image forming functions of the visual system.

In conclusion, the molecular classification of diverse RGC types builds a taxonomic cell type atlas, which serves as a foundation to map corresponding morphotypes and integrate functional properties. The identified novel molecular markers, as well as the established transgenic lines and tools, present an extensive resource for future systematic investigations of structure and function of the visual system.

5.2 Building a comprehensive catalog of RGC types

Large-scale single cell transcriptome profiling together with bioinformatic clustering reliably and accurately classifies neuronal cell types. For example, recent work using this approach resolved monkey and mouse retinal cell types [46,49,50] or neuronal types in the zebrafish habenula [215]. In the present work, known and novel markers for zebrafish bipolar cell types could be identified from derived transcriptional clusters demonstrating the power of this approach in cell type classification studies.

In a collaborative effort, I generated an atlas of zebrafish retinal ganglion cells (RGCs) by capturing and analyzing transcriptome profiles of thousands of larval and adult cells. I consider this atlas comprehensive enough to disentangle RGC types at high resolution for two main reasons: First, we profiled a transcriptomic snapshot from different life stages, larval and adult, to obtain a fully-featured characterization of molecular composition of diverse RGC types. Second, we detected *tbx20*$^{+}$ types associated to a rare morphotype within both larval and adult RGC clusters.

Anatomically, the retinal output channels in zebrafish do not undergo significant changes from larval to adult stages with the same RGC morphologies and innervation sites found in both the larva and the adult [67,124,139]. In spite of morphological stability, integrating developmental gene expression profiles appears advantageous in resolving molecularly related RGC types. In the larval retina, *eomesa*$^{+}$ RGCs have segregated into five clusters, possibly due to higher transcriptional diversity during development as reported in a similar case for Drosophila olfactory projection neurons [230]. However, clustering analysis classified adult *eomesa*$^{+}$ RGCs into two clusters, likely because they exhibit high transcriptional similarities. The heterogeneity of RGC types masked by *eomesa* were resolved by a supervised second iteration of clustering showcasing how classification of developing neurons can inform interpretation of mature systems.

The retinal projectome has classified more than fifty distinct RGC morphotypes counting defined morphologies as a type when observed for at least three times [16]. How does this great diversity match with the twenty-nine transcriptional clusters obtained from larval RGCs and the thirty-three domains derived from adult RGCs? First, it must be remembered that bioinformatical clustering is strongly dependent on transcriptional diversity, which is with over 4.000 highly variable genes much higher in the larval dataset, and sampling magnitude, which is with close to 40.000 cells much higher in the adult dataset. This variation explains the outcome of different cluster numbers between larval and adult RGCs. Because RGC morphologies are stereotyped and have been observed repeatedly, the most likely scenario that explains the deviation of fifty morphotypes versus about thirty transcriptional clusters is that further heterogeneity is yet to be uncovered in transcriptional clusters. Such heterogeneity is well exemplified by the case of the *eomesa*$^{+}$ RGC subclass in the adult, supervised clustering segregated multiple types that inadequately have been merged together. It is well possible that further clusters may be split into more homogenous subclusters so that ultimate representation of transcriptional clusters is a close one-on-one correspondence with RGC morphotypes.

Interestingly, the molecular identity of a RGC type is maintained from early establishment during larval stages to the adult life. This continuity of molecular composition was self-evident in the maintenance of the *eomesa*$^{+}$ RGC subclass. The same set of molecular markers distinguishes and identifies larval and adult *eomesa*$^{+}$ RGCs demonstrating a one-to-one correspondence between transcriptional clusters obtained from different stages. This tight correspondence between larval and adult RGC types is further supported by additional genetic markers such as *mafaa*, *lmo1* or *c1ql3a*, which are also expressed in a cluster-specific fashion in both larval and adult RGC clusters. Yet, it remains to be tested if global molecular composition and morphological identity confirms this predicted relation between larva and adult RGC types. In a similar manner, analogies from larval to adult type identities were reported for zebrafish habenular neuron types [215].

We obtained a molecularly derived taxonomy of RGC clusters by investigating overall relatedness of gene signatures. This taxonomy revealed higher-order organizing principles as evidenced by the arrangement of clusters into groups branching into subclasses and diverging further into types. Strikingly, taxonomic organization is accompanied by underlying genetic commonalities - in particular shared expression of transcription factors - within groups and subclasses. This diversification pattern may, at a more global level, correspond to major morphological

and physiological distinctions as in the case of mouse BCs, where a molecularly derived taxonomy splits BC clusters into major ON and OFF branches [46]. In other words, RGC clusters that are more closely related may share physiological and/or morphological features, whereas RGC clusters that are positioned in more distant groups may exhibit more divergent or even opposing properties. What exactly the main distinctions are in regard to morphological or physiological features remains to be further investigated. It is possible that, similar to mouse BCs [46], certain groups correspond to the coarse ON and OFF physiological differences amongst RGC types. Likewise, it could be theorized that the level of complexity rises from outer to inner retina and, for RGCs, main distinctions are governed by other properties such as axonal projection patterns are main distinguishing features.

Collectively, I propose that this molecularly-derived taxonomy of segregated RGC types should be used as a compendium for a hierarchical atlas and for prospective integration of other modalities, for example developmental lineage, morphology, connectivity and physiology.

5.3 Genetic markers provide cell type specific access

Up to now, molecular markers, and thus genetic access, for discrete zebrafish RGC types has been scarce. Based on differential gene expression analysis across RGC single cell transcriptional clusters, we have ascertained dozens of novel genetic markers for RGC types. Consistent with previous literature [4,25,46,215,256], I conclude from our observations that certain gene ontologies, in particular transcription factors, cell surface molecules and neuropeptides, account for the majority of type-specific markers. In regard to their cellular function, it is conceivable that these gene categories fall into key determinants of cell type identity. Transcription factors establish and maintain cell type identity in addition to regulating their molecular composition by activation or repression of gene expression [4]. Across the presented data, a number of TFs (such as *eomesa*, *irx5b*, *foxp4*, *lmo1*, *mafaa*, *tbr1b*, *tbx3a*, *tbx20*, to name a few) are specific to RGC clusters. Moreover, cell surface molecules are known to mediate neuronal connectivity. Cadherins, for example, mediate specific cell-cell adhesion [257,258] and *cdh6* was identified with specific expression in restricted RGC clusters. Falling into a similar category, the synapse organizing protein *c1ql3a* [237,259] is specifically enriched in a single RGC cluster. Lastly, neuropeptides recently receive increased attention as type markers and show high type-specific expression in the zebrafish habenula [215].

Similarly, in RGCs, the neuropeptides *pdyn* (prodynorphin) and *tac1* (tachykinin, also known as substance P) each specify an adult cluster. Neuropeptides have wide-ranging functions such as modulating neural activity [260] so that their RGC type-specific expression is likely implicated in physiology. The fact that neuropeptides are not highly represented across larval RGC clusters, however, might indicate that their function is inherent to the mature visual system.

How many of such genetic markers are necessary to define a cell type? Drosophila olfactory neurons appear to require a highly intersecting pattern of genetic markers in order to be defined [230]. For virtually every zebrafish RGC cluster, however, a potentially sole genetic marker, which is highly enriched and differentially expressed in a given cluster, was identified. Nonetheless, the vast majority of cluster-specific RGC markers hold functions outside of the retina, which makes genetic intersection a prerequisite for type-specific access. Here, I established genetic intersection using a pan-RGC gene and demonstrate its merit to RGC-restricted gene expression. Future endeavors should probe even higher specificity by combining subclass and type markers.

Taken together, my results substantiate previous notions that particularly transcription factors and cell adhesion molecules are common markers with high type specificity. Identification of type-specific markers in conjunction with an intersectional paradigm provides unprecedented genetic access to RGC types, which I hope will pave way for future research.

5.4 Defined molecular clusters relate to RGC morphotypes

Known molecular markers are an invaluable asset to assign transcriptional clusters to individual cell types [34,46,49,50]. Due to lack of known markers for zebrafish RGCs, I could merely assign progenitor identity to adult RGC cluster 10 *in silico* based on prior knowledge. Therefore, the veracity of transcriptional clusters remained elusive and experimental validation became indispensable for further interpretation. To this end, I employed a transgenic validation strategy utilizing CRISPR-Cas9 guided knockin in conjunction with intersectional labeling to determine RGC morphologies associated to transcriptional clusters. This transient and mosaic labelling allowed me to map a selection of cluster-specific transcription factors to different RGC morphotypes. I tentatively assign these clusters to the labeled visual pathways, but stable transgenic reporter lines will provide more confident inferences. Overall, the collected data prove

accurate representation of gene expression in RGC transcriptional clusters and support a tight correlation of molecular composition and morphology of RGC types. Such close interrelation of transcriptional and morphological or histological definitions of cell types was also found in Drosophila olfactory neurons [230], zebrafish habenula [215], mouse bipolar neurons [46] or monkey retinal cells [50].

For two subclass markers, *mafaa* and *eomesa*, I generated stable reporter lines, which allowed me to unequivocally map the respective clusters to morphological RGC subsets. I found that while *mafaa*$^+$ clusters relate to previously described RGC types targeting superficial tectal layers, *eomesa*$^+$ clusters are associated with a unique class of RGC types projecting to a set of termination sites in hypothalamus, thalamus, pretectum and the deep tectal layer. Notably, these observations are coherent with transcriptomic data in that molecularly unrelated clusters can be assigned to distant, morphologically segregated RGC types. Importantly, anatomical characterization of *tbx20*$^+$ RGC types within the *eomesa*$^+$ RGC subclass proves high accuracy of RNA-Sequencing clusters. Put differently, distinct gene expression profiles across RGC transcriptional clusters reflect natural expression with high confidence and do relate to actual morphological differences.

Strikingly, molecularly related RGC types also appeared to share morphological features, specifically axonal projections. That is to say that, in the case of *eomesa*, the four *eomesa*$^+$ types are each other's transcriptionally closest relatives and all follow the same projection route along pretectal AF9 and SAC/SPV layer. In the same fashion, the molecularly related *mafaa*$^+$ types share similar projections dedicated to superficial tectal layers including SO and superficial SFGS domains. Given these points, it is possible that these transcription factors regulate gene pathways that determine axonal projection patterns to these specific brain targets.

In conclusion, all empirical validation provides compelling evidence that distinct RGC clusters do indeed correspond to distinct morphologically classified RGC types. Importantly, this means that molecular diversity underlies morphological diversity or, in other words, different RGC morphotypes exhibit distinct molecular compositions.

5.5 A cell type atlas paves way for dissection of complex neural circuits

Why do we need cell type atlases? Generating a catalog of diverse neurons is argued to have several key benefits to science: First, understanding how the brain functions, as the most complex organ, is unattainable without a description of all its constituents. Second, the naming and characterization of cell types facilitates scientific conduct in its reproducibility and knowledge exchange across laboratories worldwide. Third, genetic access gained through identification of differentially expressed genes by transcriptional profiling is invaluable to investigating the structure and function of specific types. Fourth, once a cell type atlas has been generated it allows for an evolutionary comparison with that of other species. Altogether, a cell type atlas allows to orthogonally investigate different features of cell types and, thus, draw conclusions about causal relationships of gene expression to morphology and function.

In this work, I demonstrate that the generation of a zebrafish RGC atlas is a productive strategy towards dissection of complex visual circuits. In an unbiased fashion, RGC types were classified based on transcriptional composition and dozens of novel unique genetic markers for individual types were identified. Mapping of diverse molecularly defined types to the pre-existing morphological RGC type atlas showed that, in all cases investigated here, these two modalities can be harmonized. To ease communication and reproducibility, I propose to refer to anatomically diverging visual pathways by molecular definitions as in their core genetic markers.

Moreover, evolutionary conserved molecular features with mouse RGCs were a Rosetta stone in hypothesizing that *eomesa*$^{+}$ RGCs identify as intrinsically-photosensitive RGCs in zebrafish – an aspect of my work, which I discuss below. However, this specific case provides a prime example for how comparative studies can drive hypothesis generation. In contrast to *eomesa*, where there appear to be close type homologs, the gene orthologues to *mafaa* have not been detected in mouse or primate RGC clusters in a corresponding cluster-specific fashion. Thus, *mafaa*$^{+}$ RGCs do not appear evolutionary conserved and may constitute a teleost-specific RGC subclass.

The unprecedented genetic access broke new ground to label, characterize and manipulate specific RGC types in zebrafish. The specific investigation of *eomesa*$^{+}$ RGCs in this thesis should be instructive for future studies that seek to functionally dissect additional visual pathways. Based on the taxonomy established here, future functional studies can be guided by this classification and approached systematically.

5.6 Causal relationship of molecular composition, cellular anatomy and function

Transcriptional differences between cell types not only underlie different morphological features but also may imply different functionalities. In this thesis, I investigated the causal relationship between molecular composition, cellular anatomy and neural function.

Mounting parallels to intrinsically photosensitive RGCs described in other species [49,50] led me to speculate that *eomesa*$^{+}$ RGCs may function similarly in zebrafish. Because investigations can be driven by this hypothesis and realized using transgenic tools, I will focus my discussions on the case of *eomesa*$^{+}$ RGCs. How do molecular, morphological and functional properties of cell types relate?

From a molecular perspective, several genetic signatures strike as causally relevant for anatomy and function. To begin, the transcription factor *eomesa* likely is involved in cell fate determination and maintenance of the expressing RGC subclass as evidenced in mouse, where ipRGCs are not formed when Eomes function is genetically disrupted, demonstrating its essential role in establishing this specific subclass [159]. Next, mouse ipRGCs are unique among RGCs in their expression of opsins, which is pivotal to their characteristic physiological property: intrinsic photosensitivity [153–155]. Likewise, opsin transcripts are co-expressed in *eomesa*$^{+}$ RGC clusters linking specific molecules to predicted physiological function. Besides the transcription factor *eomesa*, these clusters show strong differential expression of the neuropeptide neuromedin b (nmbb). The exact function of *nmbb* in zebrafish is not known, but the peptide is speculated to evoke endocrine responses in hypothalamus, where its receptor is expressed [261], and thus could exert effects to a variety of basal functions from energy homeostasis to circadian rhythm. Notably, the larval RGC clusters also revealed high enrichment of an axon guidance receptor, plexin A4, specifically in *eomesa*$^{+}$ RGCs and points to a RGC subclass-specific function during development.

Interestingly, *eomesa*$^{+}$ RGCs innervate a combinatorial set of AFs including AF1, AF2, AF3, AF4, AF9 and SAC/SPV. Signal divergence to these distinct AFs may, as proposed previously [16], serve the efficient utilization of the same input to drive distinct behaviors. In fact, it is hypothesized that AF1, the only hypothalamic retinorecipient brain area [16,139], mediates circadian photoentrainment [16,262] or visual background adaptation [194,262]. The function of AF2 and AF3 is currently unknown. AF4, however, has recently been linked to light-seeking behavior specifically mediated by sustained

ON-RGCs, which express opsins [176]. The function of AF9 is an interesting point of discussion, because the role in visuomotor transformation of this large retinorecipient nucleus with anatomical and functional subdivisions remains to be identified. AF9 was first argued to mediate OKR [181], but optic flow stimuli were later shown to activate RGCs in AF6 [263] leaving AF9 function unresolved.

Functional imaging of *eomesa*$^{+}$ RGCs revealed mixed ON and OFF response types, which are consistent with previous functional analyses [16,176]. In fact, same classes of sustained ON, transient ON, sustained OFF and sustained ON - transient OFF have been anatomically and molecularly identified as AF4-projecting melanopsin RGCs [176]. The revealed sustained ON types, which form the majority of *eomesa*$^{+}$ RGCs, mirror mouse ipRGCs, which exhibit characteristic long-lasting sustained ON responses [153–155]. A minor population of the *eomesa*$^{+}$ RGC subclass, however, relates to OFF functional types. This observation may indicate labeling of other RGC types in addition to ipRGCs. Indeed, such additional labeling would correspond to findings in mouse, where Eomes labels additional non-ipRGCs types [160]. The fact that *eomesa*$^{+}$ RGCs, and AF9 RGCs in general, are not tuned to patterns contributes further compelling evidence that they execute non-image forming functions.

Reconciling molecular signature, anatomy and function, the data could be interpreted as follows: Expression of opsins confers *eomesa*$^{+}$ RGCs the ability to encode ambient luminance levels. This information is relayed in parallel to various brain nuclei in hypothalamus, thalamus, pretectum and tectum. Downstream of AF1 *eomesa*$^{+}$ RGCs could mediate VBA, while they drive light-seeking behavior via AF4, whereas tectal neurons use this information to compute contrast and form images.

Motivated by reports suggesting a role of ipRGCs in VBA, I tested VBA performance following physical disruption of *eomesa*$^{+}$ RGCs. Although a conclusive necessity of *eomesa*$^{+}$ RGCs in VBA could not be established by these initial experiments, the hypothesis should be pursued further for several reasons. First, we have not tested the temporal kinematics of the VBA, which often occurs within few minutes. It is possible that physical loss of *eomesa*$^{+}$ RGCs leads to a much slower adaptation. Second, the exact mechanism of VBA is unknown and it is possible that few ipRGCs remaining after ablation can still mediate VBA. Third, as the mechanism is unknown, it is possible that VBA is mediated synergistically by multiple (*eomesa*$^{+}$ and *eomesa*$^{-}$) RGC types and disruption of one component is not sufficient to result in VBA deficits. In addition to expanding upon these initial experimental VBA tests, other behavioral assays studying circadian rhythm and phototaxis should be performed.

In conclusion, a tight causal relation of molecular composition, cellular anatomy, physiology and potentially behavioral relevance of cell types in the visual system exists. In this specific case, *eomesa*$^{+}$ RGCs express opsins and relay luminance information to various non-image forming brain targets, where signals are transformed into adequate behavior.

5.7 Rigid classification by harmonization of distinct cell type properties

Can different cellular modalities be reconciled into a unique, unambiguous definition of a cell type? As I discuss above, molecular differences observed between transcriptional clusters imply morphological and functional differences. However, it is unclear how stable and robust these direct correspondences are. For most of the empirical observations presented in this thesis, cell types could be uniquely identified and related by molecular and morphological means supporting coherent and unified cell type definitions. However, the case of *tbx20*$^{+}$ RGCs discloses possible conceptual challenges.

Across RGC transcriptional clusters, *tbx20* transcripts show high differential expression. Morphologically, *tbx20*$^{+}$ RGCs define a unique RGC type. In contrast, functional characterization of *tbx20*$^{+}$ RGCs classified them into two response types. Depending on the level of detail, they can be distinguished into a transient and a sustained ON response type.

This observation of multiple functional neuronal definitions within a single morphological type is not without precedent [7,121]. The correlation of cell type definition by morphology and physiology was recently investigated in zebrafish bipolar neurons [121] using a transgenic enhancer trap line that labels three morphologically classified BC types [264]. The study revealed that a single morphological type can fall into multiple functional classes depending on its position within the retina. Conclusively, the physiology of a cell type may be dictated by its local surround network inputs and a defined morphotype can traverse across different functional types. It is possible that *tbx20*$^{+}$ RGC sustained versus transient ON responses originate from similar asymmetric retinal inputs.

For full satisfaction, however, a cell type atlas should integrate and harmonize all phenotypic modalities. Therefore, should *tbx20*$^{+}$ RGC functional types be lumped into a main ON type or remain split? One opportunity to address this matter is to unite discreteness and continuity of cell type properties [265]. In this recent bioinformatic

advancement, topologies map discrete cell types by branching end points, which are connected to each other through continuous properties. Hypothetically, such a model could split *tbx20*$^{+}$ RGCs into a sustained and transient ON type, which remain closely connected.

Taken together, whether or not RGC types can be rigidly defined across their modalities in a type atlas will require future investigation. Prospectively, integration and reconciliation of different modalities will refine and manifest cell type definitions proposed in this thesis.

6 CONCLUSION AND OUTLOOK

Retinal ganglion cells, the output neurons of the eye, are a highly diverse neuronal population. While cell type diversity was well exhaustively classified at the morphological level, we had no knowledge of cellular taxonomy, molecular composition or genetic distinctions, and hence no genetic access to systematically interrogate function of specific RGC types. The presented collaborative research closed this gap of our understanding by generating a molecular RGC type atlas and integrating morphological and functional features. Using unprecedented genetic access and intersectional transgenic tools, we began to elucidate the functional role of genetically defined visual pathways.

This RGC type atlas, in conjunction with the transgenic tools established herein, provides a rich resource for RGC type-specific access and nomenclature. This atlas sets groundwork for systematic investigation of RGC type contribution to visual system function across neuroscientific fields from developmental biology to psychophysics.

Regarding developmental biology, it will be particularly interesting to dissect how distinct RGC types selectively innervate tectal layers during development. This hard-wired process is thought to be guided by axon guidance molecules secreted by tectal cells. However, how distinct RGC types are rendered differentially sensitive to this cue remains obscure [65,266]. Today, the transgenic lines can be used to purify RGC populations for deeper RNA-Sequencing experiments to identify candidate molecules involved in lamina-specific assembly of visual circuits. Moreover, development of defined RGC populations can be visualized, observed and ultimately manipulated to test mechanisms of laminar guidance.

Regarding psychophysics, future research will be aimed at functional investigations of a variety of genetically encoded visual pathways using the identified marker genes. In addition to the transgenes provided here, our established CRISPR-Cas9 knockin method may be used to expand the available RGC-specific driver lines for thorough characterization by functional imaging and other techniques.

An attractive prospect, for example, is to investigate the role of *mafaa*$^{+}$ RGCs in prey capture behavior. Two prey-selective RGC types route to AF7 and SO, a visual pathway that is represented in the *mafaa* line. It is believed that a conjunction of several specific visual features (specifically size, speed, direction and contrast) needs to be relayed to these processing centers in order to initiate a hunting behavior [141,189,190]. However, how each of these features is encoded by the prey-sensitive RGC types is poorly understood. It will be interesting to perform functional imaging from *mafaa*$^{+}$

RGC axons to probe their tuning selectivity to varying feature compounds of prey-like stimuli. Similarly, ablations of *mafaa*$^{+}$ RGCs can be performed to assess their role in driving the natural prey capture behavior of the zebrafish larva.

Furthermore, it is highly debated where in the brain optic flow stimuli are integrated and transformed into the optokinetic or optomotor response [181,263] (publication in submission, Baier lab). It is, however, postulated that direction-selective RGCs play a pivotal role in these reflex circuits. Thus, the generation of a specific driver line would allow for genetic and morphological identification of DS-RGCs and promises to solve the enigma of which visual pathway relays whole-field motion to the brain and drives these reflexive behaviors.

BIBLIOGRAPHY

1. Ramón y Cajal, S. *Histology of the Nervous System*. (Springer, 1899).
2. Ramón y Cajal, S. Structure of the mammalian retina. (1900).
3. Piccolino, M. Cajal and the retina: a 100-year retrospective. *Trends Neurosci.* **11,** 521–525 (1988).
4. Fishell, G. & Heintz, N. The neuron identity problem: Form meets function. *Neuron* **80,** 602–612 (2013).
5. Zeng, H. & Sanes, J. R. Neuronal cell-type classification: challenges, opportunities and the path forward. *Nat. Rev. Neurosci.* (2017). doi:10.1038/nrn.2017.85
6. Benoist, C. *et al.* The Human Cell Atlas. 1–30 (2017). doi:10.7554/eLife.27041
7. Vlasits, A. L., Euler, T. & Franke, K. Function first: classifying cell types and circuits of the retina. *Curr. Opin. Neurobiol.* **56,** 8–15 (2019).
8. Bota, M. & Swanson, L. W. The neuron classification problem. *Brain Res. Rev.* **56,** 79–88 (2007).
9. Nelson, S. B., Sugino, K. & Hempel, C. M. The problem of neuronal cell types: a physiological genomics approach. *Trends Neurosci.* **29,** 339–345 (2006).
10. Luo, L., Callaway, E. M. & Svoboda, K. Genetic Dissection of Neural Circuits: A Decade of Progress. *Neuron* **98,** 256–281 (2018).
11. Luo, L., Callaway, E. M. & Svoboda, K. Genetic Dissection of Neural Circuits. *Neuron* **57,** 634–660 (2008).
12. Masland, R. H. Neuronal cell types. *Curr. Biol.* **14,** R497–R500 (2004).
13. Helmstaedter, M. *et al.* Connectomic reconstruction of the inner plexiform layer in the mouse retina. *Nature* **500,** 168–74 (2013).
14. Baden, T. *et al.* The functional diversity of mouse retinal ganglion cells. *Nature* 1–21 (2016). doi:10.1038/nature16468
15. Franke, K. *et al.* Inhibition decorrelates visual feature representations in the inner retina. *Nature* **542,** 439–444 (2017).
16. Robles, E., Laurell, E. & Baier, H. The Retinal Projectome Reveals Brain-Area-Specific Visual Representations Generated by Ganglion Cell Diversity. *Curr. Biol.* **24,** 2085–2096 (2014).
17. Helmbrecht, T. O., dal Maschio, M., Donovan, J. C., Koutsouli, S. & Baier, H. Topography of a Visuomotor Transformation. *Neuron* **100,** 1429–1445.e4 (2018).
18. Arlotta, P. *et al.* Neuronal subtype-specific genes that control corticospinal motor neuron development in vivo. *Neuron* **45,** 207–221 (2005).
19. Sugino, K. *et al.* Molecular taxonomy of major neuronal classes in the adult mouse forebrain. *Nat. Neurosci.* **9,** 99–107 (2006).
20. Kay, J. N. *et al.* Retinal ganglion cells with distinct directional preferences differ in molecular identity, structure, and central projections. *J. Neurosci.* **31,** 7753–7762 (2011).
21. Sajgo, S. *et al.* Molecular codes for cell type specification in Brn3 retinal ganglion cells. *Proc. Natl. Acad. Sci.* **114,** E3974–E3983 (2017).
22. Siegert, S. *et al.* Transcriptional code and disease map for adult retinal cell types. *Nat Neurosci* **15,** 487–95, S1-2 (2012).
23. Tang, F. *et al.* mRNA-Seq whole-transcriptome analysis of a single cell. *Nat. Methods* **6,** 377–382 (2009).

24. Tang, F. *et al.* Tracing the derivation of embryonic stem cells from the inner cell mass by single-cell RNA-seq analysis. *Cell Stem Cell* **6,** 468–478 (2010).
25. Tasic, B. *et al.* Adult mouse cortical cell taxonomy revealed by single cell transcriptomics. *Nat. Neurosci.* **19,** 335–346 (2016).
26. Ramsköld, D. *et al.* Full-length mRNA-Seq from single-cell levels of RNA and individual circulating tumor cells. *Nat. Biotechnol.* **30,** 777–782 (2012).
27. Picelli, S. *et al.* Smart-seq2 for sensitive full-length transcriptome profiling in single cells. *Nat. Methods* **10,** 1096–8 (2013).
28. Hashimshony, T., Wagner, F., Sher, N. & Yanai, I. CEL-Seq: Single-Cell RNA-Seq by Multiplexed Linear Amplification. *Cell Rep.* **2,** 666–673 (2012).
29. Fluidigm. Single-Cell Whole Genome Sequencing on the C1 System: a Performance Evaluation. *Tech. Note* 1–7 (2014).
30. Jaitin, D. A. *et al.* Massively Parallel Single-Cell RNA-Seq for Marker-Free Decomposition of Tissues into Cell Types. *Science (80-.).* **343,** 776–779 (2014).
31. Darmanis, S. *et al.* A survey of human brain transcriptome diversity at the single cell level. *Proc. Natl. Acad. Sci.* **112,** 7285–7290 (2015).
32. Zeisel, A. *et al.* Cell types in the mouse cortex and hippocampus revealed by single-cell RNA-seq. *Science (80-.).* **347,** 0–5 (2015).
33. Pollen, A. A. *et al.* Low-coverage single-cell mRNA sequencing reveals cellular heterogeneity and activated signaling pathways in developing cerebral cortex. *Nat. Biotechnol.* **32,** 1053–1058 (2014).
34. Macosko, E. Z. Z. *et al.* Highly Parallel Genome-wide Expression Profiling of Individual Cells Using Nanoliter Droplets. *Cell* **161,** 1202–1214 (2015).
35. Klein, A. M. *et al.* Droplet barcoding for single-cell transcriptomics applied to embryonic stem cells. *Cell* **161,** 1187–1201 (2015).
36. Zheng, G. X. Y. *et al.* Massively parallel digital transcriptional profiling of single cells. *Nat. Commun.* **8,** 14049 (2017).
37. Chen, J. *et al.* PBMC fixation and processing for Chromium single-cell RNA sequencing. *J. Transl. Med.* **16,** 1–11 (2018).
38. Fan, H. C., Fu, G. K. & Fodor, S. P. A. Combinatorial labeling of single cells for gene expression cytometry. *Science (80-.).* **347,** (2015).
39. Yuan, J. & Sims, P. A. An Automated Microwell Platform for Large-Scale Single Cell RNA-Seq. *Sci. Rep.* **6,** 1–10 (2016).
40. Shah, S., Lubeck, E., Zhou, W. & Cai, L. In Situ Transcription Profiling of Single Cells Reveals Spatial Organization of Cells in the Mouse Hippocampus. *Neuron* **92,** 342–357 (2016).
41. Moffitt, J. R. *et al.* High-throughput single-cell gene-expression profiling with multiplexed error-robust fluorescence in situ hybridization. *Proc. Natl. Acad. Sci.* **113,** 11046–11051 (2016).
42. Quadrato, G. *et al.* Cell diversity and network dynamics in photosensitive human brain organoids. *Nature* **545,** 48–53 (2017).
43. Tepe, B. *et al.* Single-Cell RNA-Seq of Mouse Olfactory Bulb Reveals Cellular Heterogeneity and Activity-Dependent Molecular Census of Adult-Born Neurons. *Cell Rep.* **25,** 2689–2703.e3 (2018).
44. Vento-Tormo, R. *et al.* Single-cell reconstruction of the early maternal–fetal interface in humans. *Nature* **563,** 347–353 (2018).

45. Jeon, C. J., Strettoi, E. & Masland, R. H. The major cell populations of the mouse retina. *J. Neurosci.* **18,** 8936–8946 (1998).
46. Shekhar, K. *et al.* Comprehensive Classification of Retinal Bipolar Neurons by Single-Cell Transcriptomics. *Cell* **166,** 1308–1323.e30 (2016).
47. Kim, J. S. *et al.* Space-time wiring specificity supports direction selectivity in the retina. *Nature* **509,** 331–336 (2014).
48. Greene, M. J., Kim, J. S. & Seung, H. S. Analogous Convergence of Sustained and Transient Inputs in Parallel On and Off Pathways for Retinal Motion Computation. *Cell Rep.* **14,** 1892–1900 (2016).
49. Rheaume, B. A. *et al.* Single cell transcriptome profiling of retinal ganglion cells identifies cellular subtypes. *Nat. Commun.* **9,** (2018).
50. Peng, Y.-R. *et al.* Molecular Classification and Comparative Taxonomics of Foveal and Peripheral Cells in Primate Retina. *Cell* **176,** 1–16 (2019).
51. Streisinger, G., Walker, C., Dower, N., Knauber, D. & Singer, F. Production of clones of homozygous diploid zebra fish (Brachydanio rerio). *Nature* **291,** (1981).
52. Howe, K. *et al.* The zebrafish reference genome sequence and its relationship to the human genome. *Nature* **496,** 498–503 (2013).
53. Dooley, K. & Zon, L. I. Zebrafish: a model system for the study of human disease. *Curr. Opin. Genet. Dev.* **10,** 252–256 (2000).
54. Scheer, N. & Campos-Ortega, J. A. Use of the Gal4-UAS technique for targeted gene expression in the zebrafish. *Mech. Dev.* **80,** 153–158 (1999).
55. Halpern, M. E. *et al.* Gal4/UAS Transgenic Tools and Their Application to Zebrafish. **5,** (2008).
56. Scott, E. K. The Gal4/UAS toolbox in zebrafish: new approaches for defining behavioral circuits. *J. Neurochem.* **110,** 441–56 (2009).
57. Asakawa, K. & Kawakami, K. Targeted gene expression by the Gal4-UAS system in zebrafish. *Dev. Growth Differ.* **50,** 391–399 (2008).
58. Subedi, A. *et al.* Adoption of the Q transcriptional regulatory system for zebrafish transgenesis. *Methods* **66,** 433–440 (2014).
59. Ghosh, A. & Halpern, M. E. *Transcriptional regulation using the Q system in transgenic zebrafish*. *Methods in Cell Biology* **135,** (Elsevier Ltd, 2016).
60. Potter, C. J., Tasic, B., Russler, E. V., Liang, L. & Luo, L. The Q system: A repressible binary system for transgene expression, lineage tracing, and mosaic analysis. *Cell* **141,** 536–548 (2010).
61. Riabinina, O. *et al.* Improved and expanded Q-system reagents for genetic manipulations. *Nat. Methods* **12,** (2015).
62. Livet, J. *et al.* Transgenic strategies for combinatorial expression of fluorescent proteins in the nervous system. *Nature* **450,** 56–62 (2007).
63. Robles, E., Filosa, A. & Baier, H. Precise lamination of retinal axons generates multiple parallel input pathways in the tectum. *J. Neurosci.* **33,** 5027–39 (2013).
64. Pan, Y. A. *et al.* Zebrabow: multispectral cell labeling for cell tracing and lineage analysis in zebrafish. *Development* **140,** 2835–2846 (2013).
65. Xiao, T. & Baier, H. Lamina-specific axonal projections in the zebrafish tectum require the type IV collagen Dragnet. *Nat. Neurosci.* **10,** 1529–1537 (2007).

66. Scott, E. K. *et al.* Targeting neural circuitry in zebrafish using GAL4 enhancer trapping. *Nat. Methods* **4,** 323–326 (2007).
67. Robles, E., Laurell, E. & Baier, H. The Retinal Projectome Reveals Brain- Area-Specific Visual Representations Generated by Ganglion Cell Diversity. *Curr. Biol.* **24,** 2085–2096 (2014).
68. Nagai, T., Sawano, A., Park, E. S. & Miyawaki, A. Circularly permuted green fluorescent proteins engineered to sense Ca2+. *Proc. Natl. Acad. Sci.* **98,** 3197–3202 (2001).
69. Akerboom, J. *et al.* Optimization of a GCaMP Calcium Indicator for Neural Activity Imaging. *J. Neurosci.* **32,** 13819–13840 (2012).
70. Randlett, O. *et al.* Whole-brain activity mapping onto a zebrafish brain atlas. *Nat. Methods* **12,** 1–12 (2015).
71. Ahrens, M. B., Orger, M. B., Robson, D. N., Li, J. M. & Keller, P. J. Whole-brain functional imaging at cellular resolution using light-sheet microscopy. *Nat. Methods* **10,** 413–420 (2013).
72. Curado, S., Stainier, D. Y. R. & Anderson, R. M. Nitroreductase-mediated cell/tissue ablation in zebrafish: a spatially and temporally controlled ablation method with applications in developmental and regeneration studies. *Nat. Protoc.* **3,** 948–954 (2008).
73. Curado, S. *et al.* Conditional targeted cell ablation in zebrafish: A new tool for regeneration studies. *Dev. Dyn.* **236,** 1025–1035 (2007).
74. Mathias, J. R., Zhang, Z., Saxena, M. T. & Mumm, J. S. Enhanced Cell-Specific Ablation in Zebrafish Using a Triple Mutant of Escherichia Coli Nitroreductase. *Zebrafish* **00,** 1–13 (2014).
75. Asakawa, K. *et al.* Genetic dissection of neural circuits by Tol2 transposon-mediated Gal4 gene and enhancer trapping in zebrafish. *Proc. Natl. Acad. Sci. U. S. A.* **105,** 1255–1260 (2008).
76. Suster, M. L., Abe, G., Schouw, A. & Kawakami, K. Transposon-mediated BAC transgenesis in zebrafish. *Nat. Protoc.* **6,** 1998–2021 (2011).
77. Förster, D. *et al.* Genetic targeting and anatomical registration of neuronal populations in the zebrafish brain with a new set of BAC transgenic tools. *Sci. Rep.* **7,** 1–11 (2017).
78. Ronneberger, O. *et al.* ViBE-Z: A framework for 3D virtual colocalization analysis in zebrafish larval brains. *Nat. Methods* **9,** 735–742 (2012).
79. Marquart, G. D. *et al.* A 3D Searchable Database of Transgenic Zebrafish Gal4 and Cre Lines for Functional Neuroanatomy Studies. *Front. Neural Circuits* **9,** 78 (2015).
80. Tabor, K. M. *et al. Brain-wide cellular resolution imaging of Cre transgenic zebrafish lines for functional circuit-mapping*. *bioRxiv* (2018). doi:10.1101/444075
81. Kunst, M. *et al.* A Cellular-Resolution Atlas of the Larval Zebrafish Brain.
82. Satou, C. *et al.* Transgenic tools to characterize neuronal properties of discrete populations of zebrafish neurons. *Development* **140,** 3927–31 (2013).
83. Kimura, Y., Hisano, Y., Kawahara, A. & Higashijima, S. I. Efficient generation of knock-in transgenic zebrafish carrying reporter/driver genes by CRISPR/Cas9-mediated genome engineering. *Sci. Rep.* **4,** 6545 (2015).
84. Zu, Y. *et al.* TALEN-mediated precise genome modification by homologous recombination in zebrafish. *Nat. Methods* **10,** 329–331 (2013).
85. Meng, X., Noyes, M. B., Zhu, L. J., Lawson, N. D. & Wolfe, S. A. Targeted gene inactivation in zebrafish using engineered zinc-finger nucleases. *Nat. Biotechnol.* **26,** 695–701 (2008).
86. Hwang, W. Y. *et al.* Heritable and Precise Zebrafish Genome Editing Using a CRISPR-Cas System. *PLoS One* **8,** 1–9 (2013).

87. Doudna, J. A. & Charpentier, E. The new frontier of genome engineering with CRISPR-Cas9. *Science (80-.).* **346,** (2014).
88. Hsu, P. D., Lander, E. S. & Zhang, F. Development and applications of CRISPR-Cas9 for genome engineering. *Cell* **157,** 1262–1278 (2014).
89. Boyaval, P., Moineau, S., Romero, D. a & Horvath, P. CRISPR Provides Acquired Resistance Against Viruses in Prokaryotes. *Science (80-.).* **315,** 1709–1712 (2007).
90. Jinek, M. *et al.* A Programmable Dual-RNA – Guided. *Science (80-.).* **337,** 816–822 (2012).
91. Cong, L. *et al.* Multiplex Genome Engineering Using CRISPR/Cas Systems. 819–824 (2013).
92. Mali, P. *et al.* RNA-Guided Human Genome Engineering via Cas9. *Science (80-.).* **823,** 823–827 (2013).
93. Jinek, M. *et al.* RNA-programmed genome editing in human cells. *Elife* **2013,** 1–9 (2013).
94. Kesavan, G., Chekuru, A., Machate, A. & Brand, M. CRISPR/Cas9-Mediated Zebrafish Knock-in as a Novel Strategy to Study Midbrain-Hindbrain Boundary Development. *Front. Neuroanat.* **11,** 1–14 (2017).
95. Ota, S. *et al.* Functional visualization and disruption of targeted genes using CRISPR/Cas9-mediated eGFP reporter integration in zebrafish. *Sci. Rep.* **6,** 1–10 (2016).
96. Auer, T. O., Duroure, K., Cian, A. De, Concordet, J. & Bene, F. Del. Highly efficient CRISPR / Cas9-mediated knock-in in zebrafish by homology-independent DNA repair. *Genome Res.* **24,** 142–153 (2014).
97. Albadri, S., Del Bene, F. & Revenu, C. Genome editing using CRISPR/Cas9-based knock-in approaches in zebrafish. *Methods* **121–122,** 77–85 (2017).
98. Dowling, J. *The Retina - an approachable part of the brain*. (1987).
99. Kolb, H. How the retina works. *Am. Sci.* **91,** 28–35 (2003).
100. Wässle, H. Parallel processing in the mammalian retina. *Nat. Rev. Neurosci.* **5,** 747–757 (2004).
101. Roska, B. & Meister, M. in *The new visual neurosciences* 163–182 (2014).
102. Portugues, R. & Engert, F. The neural basis of visual behaviors in the larval zebrafish. *Curr. Opin. Neurobiol.* **19,** 644–647 (2009).
103. Sanes, J. R. & Zipursky, S. L. Design Principles of Insect and Vertebrate Visual Systems. *Neuron* **66,** 15–36 (2010).
104. Masland, R. H. Neuronal diversity in the retina. 431–436 (2001).
105. Masland, R. H. The fundamental plan of the retina. *Nat. Neurosci.* **4,** 877–886 (2001).
106. Wässle, H. & Baycott, B. Functional Architecture of the Mammalian Retina. *Physiol. Rev.* **71,** 447–480 (1991).
107. Masland, R. H. The Neuronal Organization of the Retina. *Neuron* **76,** 266–280 (2012).
108. Morris, A. C. & Fadool, J. M. Studying rod photoreceptor development in zebrafish. *Physiol. Behav.* **86,** 306–313 (2005).
109. Nawrocki, L., BreMiller, R., Streisinger, G. & Kaplan, M. Larval and adult visual pigments of the zebrafish, Brachydanio rerio. *Vision Res.* **25,** 1569–76 (1985).
110. Marc, R. & Cameron, D. A molecular phenotype atlas of the zebrafish retina. *J. Neurocytol.* **30,** 593–654 (2002).
111. Li, Y. N., Tsujimura, T., Kawamura, S. & Dowling, J. E. Bipolar cell-photoreceptor connectivity in the zebrafish (Danio rerio) retina. *J. Comp. Neurol.* **520,** 3786–3802 (2012).

112. Bloomfield, S. A. & Dacheux, R. F. Rod vision: Pathways and processing in the mammalian retina. *Prog. Retin. Eye Res.* **20,** 351–384 (2001).
113. Euler, T., Haverkamp, S., Schubert, T. & Baden, T. Retinal bipolar cells: elementary building blocks of vision. *Nat. Rev. Neurosci.* **15,** 507–19 (2014).
114. Connaughton, V. P., Graham, D. & Nelson, R. Identification and morphological classification of horizontal, bipolar, and amacrine cells within the zebrafish retina. *J. Comp. Neurol.* **477,** 371–385 (2004).
115. Vitorino, M. *et al.* Vsx2 in the zebrafish retina: Restricted lineages through derepression. *Neural Dev.* **4,** (2009).
116. Song, P., Matsui, J. & Dowling, J. E. Morphological types and connectivity of horizontal cells found in the adult zebrafish retina. *J. Comp. Neurol.* **506,** 287–297 (2008).
117. Li, Y. N., Matsui, J. I. & Dowling, J. E. Specificity of the horizontal cell-photoreceptor connections in the zebrafish (Danio rerio) retina. *J. Comp. Neurol.* **516,** 442–453 (2009).
118. Twig, G., Levy, H. & Perlman, I. Color opponency in horizontal cells of the vertebrate retina. *Prog. Retin. Eye Res.* **22,** 31–68 (2003).
119. Connaughton, V. P. & Nelson, R. Spectral Responses in Zebrafish Horizontal Cells Include a Tetraphasic Response and a Novel UV-Dominated Triphasic Response. *J. Neurophysiol.* **104,** 2407–2422 (2010).
120. Nikolaev, A., Leung, K.-M., Odermatt, B. & Lagnado, L. Synaptic mechanisms of adaptation and sensitization in the retina. *Nat. Neurosci.* **16,** 934–41 (2013).
121. Zimmermann, M. J. Y. *et al.* Zebrafish Differentially Process Color across Visual Space to Match Natural Scenes. *Curr. Biol.* 1–15 (2018). doi:10.1016/j.cub.2018.04.075
122. Macneil, M. A. & Masland, R. H. Extreme Diversity among Amacrine Cells: Implications for Function. *Cell* **20,** 971–982 (1998).
123. Jusuf, P. R. & Harris, W. a. Ptf1a is expressed transiently in all types of amacrine cells in the embryonic zebrafish retina. *Neural Dev.* **4,** 34 (2009).
124. Mangrum, W. I., Dowling, J. E. & Cohen, E. D. A morphological classification of ganglion cells in the zebrafish retina. *Vis. Neurosci.* **19,** 767–779 (2002).
125. Ott, M., Walz, B., Paulsen, U., Mack, A. & Wagner, H. Retinotectal Ganglion Cells in the Zebrafish, Danio rerio. *J. Comp. Neurol.* **504,** 287–297 (2007).
126. Famiglietti, E. & Kolb, H. Structural basis for ON- and OFF-center responses in retinal ganglion cells. *Science (80-.).* **4261,** 193–195 (1976).
127. Kuffler, S. W. Discharge Patterns and Functional of Mammalian Retina. *J. Neurophysiol.* **16,** 37–68 (1953).
128. Gollisch, T. & Meister, M. Eye Smarter than Scientists Believed: Neural Computations in Circuits of the Retina. *Neuron* **65,** 150–164 (2010).
129. Weng, S., Sun, W. & He, S. Identification of ON-OFF direction-selective ganglion cells in the mouse retina. *J. Physiol.* **562,** 915–923 (2005).
130. Vaney, D. I., Sivyer, B. & Taylor, W. R. Direction selectivity in the retina: symmetry and asymmetry in structure and function. *Nat. Rev. Neurosci.* **13,** 194–208 (2012).
131. Wei, W. & Feller, M. B. Organization and development of direction-selective circuits in the retina. *Trends Neurosci.* **34,** 638–645 (2011).

132. Piscopo, D. M., El-Danaf, R. N., Huberman, a. D. & Niell, C. M. Diverse Visual Features Encoded in Mouse Lateral Geniculate Nucleus. *J. Neurosci.* **33,** 4642–4656 (2013).
133. Zhao, X., Chen, H., Liu, X. & Cang, J. Orientation-selective Responses in the Mouse Lateral Geniculate Nucleus. *J. Neurosci.* **33,** 12751–12763 (2013).
134. Zhang, Y., Kim, I.-J., Sanes, J. R. & Meister, M. PNAS Plus: The most numerous ganglion cell type of the mouse retina is a selective feature detector. *Proc. Natl. Acad. Sci.* **109,** E2391–E2398 (2012).
135. Olveczky, B. P., Baccus, S. a & Meister, M. Segregation of object and background motion in the retina. *Nature* **423,** 401–408 (2003).
136. Baccus, S. a, Olveczky, B. P., Manu, M. & Meister, M. A retinal circuit that computes object motion. *J. Neurosci.* **28,** 6807–6817 (2008).
137. Ölveczky, B. P., Baccus, S. a. & Meister, M. Retinal Adaptation to Object Motion. *Neuron* **56,** 689–700 (2007).
138. Baier, H. Synaptic laminae in the visual system: molecular mechanisms forming layers of perception. *Annu. Rev. Cell Dev. Biol.* **29,** 385–416 (2013).
139. Burrill, J. D. & Easter, S. S. Development of the retinofugal projections in the embryonic and larval zebrafish (Brachydanio rerio). *J. Comp. Neurol.* **346,** 583–600 (1994).
140. Karlstrom, R. O., Trowe, T. & Bonhoeffer, F. Genetic analysis of axon guidance and mapping in the zebrafish. *Trends Neurosci.* **20,** 3–8 (1997).
141. Semmelhack, J. L. *et al.* A dedicated visual pathway for prey detection in larval zebrafish. *Elife* **3,** (2014).
142. Dhande, O. S. & Huberman, A. D. Retinal ganglion cell maps in the brain: Implications for visual processing. *Curr. Opin. Neurobiol.* **24,** 133–142 (2014).
143. Sanes, J. R. & Masland, R. H. The Types of Retinal Ganglion Cells: Current Status and Implications for Neuronal Classification. *Annu. Rev. Neurosci.* **38,** 150421150146009 (2014).
144. Dhande, O. S. *et al.* Genetic Dissection of Retinal Inputs to Brainstem Nuclei Controlling Image Stabilization. *J. Neurosci.* **33,** 17797–17813 (2013).
145. Nikolaou, N. *et al.* Parametric Functional Maps of Visual Inputs to the Tectum. *Neuron* **76,** 317–324 (2012).
146. Gabriel, J. P., Trivedi, C. A., Maurer, C. M., Ryu, S. & Bollmann, J. H. Layer-Specific Targeting of Direction-Selective Neurons in the Zebrafish Optic Tectum. *Neuron* **76,** 1147–1160 (2012).
147. Do, M. T. H. & Yau, K.-W. Intrinsically photosensitive retinal ganglion cells. *Physiol. Rev.* **90,** 1547–1581 (2010).
148. Jiang, Z., Yue, W. W. S., Chen, L., Sheng, Y. & Yau, K. W. Cyclic-Nucleotide- and HCN-Channel-Mediated Phototransduction in Intrinsically Photosensitive Retinal Ganglion Cells. *Cell* **175,** 652–664.e12 (2018).
149. Fiske, S. *et al.* Circadian photoreception in the retinally degenerate mouse (rd/rd). *J. Comp. Physiol. A* **169,** 39–50 (2004).
150. Freedman, M. S. *et al.* Circadian behavior by non-rod, non-cone, ocular photoreceptors. *Science (80-.).* **284,** 502–504 (1999).
151. Lucas, R. J., Freedman, M. S., Mun, M. & Foster, R. G. Regulation of the Mammalian Pineal by Non-rod , Non-cone , Ocular Photoreceptors. *Science (80-.).* **505,** 505–508 (2007).

152. Lucas, R. J., Douglas, R. H. & Foster, R. G. Characterization of an ocular photopigment capable of driving pupillary constriction in mice. *Nat. Neurosci.* **4,** 621–626 (2001).
153. Provencio, I., Rollag, M. D. & Castrucci, A. M. Photoreceptive net in the mammalian retina. *Nature* **415,** 493–493 (2002).
154. Berson, D. M., Dunn, F. a & Takao, M. Phototransduction by retinal ganglion cells that set the circadian clock. *Science* **295,** 1070–1073 (2002).
155. Gooley, J. J. *et al.* A broad role for melanopsin in nonvisual photoreception. *J. Neurosci.* **23,** 7093–106 (2003).
156. Pickard, G. E. & Sollars, P. J. Intrinsically Photosensitive Retinal Ganglion Cells. *Rev. Physiol. Biochem. Pharmacol.* **162,** 59–90 (2012).
157. Schmidt, T. M., Chen, S. K. & Hattar, S. Intrinsically photosensitive retinal ganglion cells: Many subtypes, diverse functions. *Trends Neurosci.* **34,** 572–580 (2011).
158. Hattar, S. *et al.* Melanopsin-Containing Retinal Ganglion Cells: Architecture, Projections, and Intrinsic Photosensitivity. *Science (80-.).* **295,** 1065–1070 (2002).
159. Mao, C.-A. *et al.* T-box Transcription Regulator Tbr2 Is Essential for the Formation and Maintenance of Opn4/Melanopsin-Expressing Intrinsically Photosensitive Retinal Ganglion Cells. *J. Neurosci.* **34,** 13083–13095 (2014).
160. Sweeney, N. T., Tierney, H. & Feldheim, D. A. Tbr2 Is Required to Generate a Neural Circuit Mediating the Pupillary Light Reflex. *J. Neurosci.* **34,** 5447–5453 (2014).
161. Belenky, M. A., Smeraski, C. A., Provencio, I., Sollars, P. J. & Pickard, G. E. Melanopsin retinal ganglion cells receive bipolar and amacrine cell synapses. *J. Comp. Neurol.* **460,** 380–393 (2003).
162. Schmidt, T. M. & Kofuji, P. Differential Cone Pathway Influence on Intrinsically Photosensitive Retinal Ganglion Cell Subtypes. *J. Neurosci.* **30,** 16262–16271 (2010).
163. Pickard, G. E., Baver, S. B., Ogilvie, M. D. & Sollars, P. J. Light-induced Fos expression in intrinsically photosensitive retinal ganglion cells in melanopsin knockout (Opn4-/-) mice. *PLoS One* **4,** (2009).
164. Dumitrescu, O. N., Pucci, F. G., Wong, K. Y. & Berson, D. M. Ectopic retinal ON bipolar cell synapses in the OFF inner plexiform layer: Contacts with dopaminergic amacrine cells and melanopsin ganglion cells. *J. Comp. Neurol.* **517,** 226–244 (2009).
165. Hoshi, H., Liu, W.-L., Massey, S. C. & Mills, S. L. ON Inputs to the OFF Layer: Bipolar Cells That Break the Stratification Rules of the Retina. *J. Neurosci.* **29,** 8875–8883 (2009).
166. Wong, K. Y. A Retinal Ganglion Cell That Can Signal Irradiance Continuously for 10 Hours. *J. Neurosci.* **32,** 11478–11485 (2012).
167. Hatter, S. *et al.* Central Projections of Melanopsin- Expressing Retinal Ganglion Cells in the Mouse. *J. Comp. Neurol.* **497,** 326–349 (2006).
168. Hattar, S. *et al.* Melanopsin and rod–cone photoreceptive systems account for all major accessory visual functions in mice. *Nature* **424,** 75–81 (2003).
169. Güler, A. D. *et al.* Melanopsin cells are the principal conduits for rod–cone input to non-image-forming vision. *Nature* **453,** 102–105 (2008).
170. Hatori, M. *et al.* Inducible ablation of melanopsin-expressing retinal ganglion cells reveals their central role in non-image forming visual responses. *PLoS One* **3,** (2008).
171. Chen, S.-K., Badea, T. C. & Hattar, S. Photoentrainment and pupillary light reflex are mediated by distinct populations of ipRGCs. *Nature* **476,** 92–5 (2011).

172. Ecker, J. L. *et al.* Melanopsin-expressing retinal ganglion-cell photoreceptors: Cellular diversity and role in pattern vision. *Neuron* **67,** 49–60 (2010).
173. Stabio, M. E. *et al.* Erratum: The M5 Cell: A Color-Opponent Intrinsically Photosensitive Retinal Ganglion Cell (S0896627317310838 (2018) 97(1) (150–163.e4) (S0896627317310838) (10.1016/j.neuron.2017.11.030)). *Neuron* **97,** 251 (2018).
174. Matos-Cruz, V. *et al.* Unexpected Diversity and Photoperiod Dependence of the Zebrafish Melanopsin System. *PLoS One* **6,** e25111 (2011).
175. Davies, W. I. L. *et al.* An extended family of novel vertebrate photopigments is widely expressed and displays a diversity of function An extended family of novel vertebrate photopigments is widely expressed and displays a diversity of function. *Genome Res.* **25,** 1–14 (2015).
176. Zhang, B. bing, Yao, Y. yuan, Zhang, H. fei, Kawakami, K. & Du, J. lin. Left Habenula Mediates Light-Preference Behavior in Zebrafish via an Asymmetrical Visual Pathway. *Neuron* **93,** 914–928.e4 (2017).
177. Fleisch, V. C. & Neuhauss, S. C. F. Visual behavior in zebrafish. *Zebrafish* **3,** 191–201 (2006).
178. Baier, H. Zebrafish on the move : towards a behavior – genetic analysis of vertebrate vision. 451–455 (2000).
179. Neuhauss, S. C. *et al.* Genetic disorders of vision revealed by a behavioral screen of 400 essential loci in zebrafish. *J. Neurosci.* **19,** 8603–8615 (1999).
180. Muto, A. *et al.* Forward genetic analysis of visual behavior in zebrafish. *PLoS Genet* **1,** e66 (2005).
181. Kubo, F. *et al.* Functional architecture of an optic flow-responsive area that drives horizontal eye movements in zebrafish. *Neuron* **81,** 1344–1359 (2014).
182. Huang, Y.-Y. & Neuhauss, S. C. F. The optokinetic response in zebrafish and its applications. *Front. Biosci.* **13,** 68–74 (2008).
183. Brockerhoff, S. E. *et al.* A behavioral screen for isolating zebrafish mutants with visual system defects. **92,** 10545–10549 (1995).
184. Burgess, H. A., Schoch, H. & Granato, M. Distinct Retinal Pathways Drive Spatial Orientation Behaviors in Zebrafish Navigation. *Curr. Biol.* **20,** 381–386 (2010).
185. Fernandes, A. M. *et al.* Deep brain photoreceptors control light-seeking behavior in zebrafish larvae. *Curr. Biol.* **22,** 2042–2047 (2012).
186. Roeser, T. & Baier, H. Visuomotor behaviors in larval zebrafish after GFP-guided laser ablation of the optic tectum. *J. Neurosci.* **23,** 3726–3734 (2003).
187. Gahtan, E., Tanger, P. & Baier, H. Visual prey capture in larval zebrafish is controlled by identified reticulospinal neurons downstream of the tectum. *J. Neurosci.* **25,** 9294–9303 (2005).
188. Patterson, B. W., Abraham, A. O., MacIver, M. a & McLean, D. L. Visually guided gradation of prey capture movements in larval zebrafish. *J. Exp. Biol.* **216,** 3071–83 (2013).
189. Bianco, I. H., Kampff, A. R. & Engert, F. Prey Capture Behavior Evoked by Simple Visual Stimuli in Larval Zebrafish. *Front. Syst. Neurosci.* **5,** 1–13 (2011).
190. Bianco, I. H. & Engert, F. Visuomotor Transformations Underlying Hunting Behavior in Zebrafish. *Curr. Biol.* **25,** 831–846 (2015).
191. Temizer, I., Donovan, J. C., Baier, H. & Semmelhack, J. L. A Visual Pathway for Looming-Evoked Escape in Larval Zebrafish. *Curr. Biol.* 1–12 (2015). doi:10.1016/j.cub.2015.06.002
192. Dunn, T. W. *et al.* Neural Circuits Underlying Visually Evoked Escapes in Larval Zebrafish. *Neuron* 1–16 (2016). doi:10.1016/j.neuron.2015.12.021

193. Barker, A. J. & Baier, H. Sensorimotor Decision Making in the Zebrafish Tectum. *Curr. Biol.* **25,** 2804–2814 (2015).
194. Neuhauss, S. C. F. F. Behavioral genetic approaches to visual system development and function in zebrafish. *J. Neurobiol.* **54,** 148–160 (2003).
195. Baier, H. *et al.* Genetic dissection of the retinotectal projection. *Development* **123,** 415–425 (1996).
196. Wolman, M. & Granato, M. Behavioral genetics in larval zebrafish: Learning from the young. *Dev. Neurobiol.* **72,** 366–372 (2012).
197. Allwardt, B. A., Lall, A. B., Brockerhoff, S. E. & Dowling, J. E. Synapse formation is arrested in retinal photoreceptors of the zebrafish nrc mutant. *J. Neurosci.* **21,** 2330–42 (2001).
198. Emran, F. *et al.* OFF ganglion cells cannot drive the optokinetic reflex in zebrafish. *Proc. Natl. Acad. Sci. U. S. A.* **104,** 19126–19131 (2007).
199. Odenthal, J. *et al.* Mutations affecting the formation of the notochord in the zebrafish, Danio rerio. *Development* **123,** 103–115 (1996).
200. Karlstrom, R. O. *et al.* Zebrafish mutations affecting retinotectal axon pathfinding. *Development* **123,** 427–438 (1996).
201. Pittman, A. J., Law, M.-Y. & Chien, C.-B. Pathfinding in a large vertebrate axon tract: isotypic interactions guide retinotectal axons at multiple choice points. *Development* **135,** 2865–71 (2008).
202. Horndli, C. S. & Chien, C.-B. Sonic hedgehog is indirectly required for intraretinal axon pathfinding by regulating chemokine expression in the optic stalk. *Development* **139,** 2604–2613 (2012).
203. Arrenberg, A. B., Del Bene, F. & Baier, H. Optical control of zebrafish behavior with halorhodopsin. *Proc. Natl. Acad. Sci.* **106,** 17968–17973 (2009).
204. Kimura, Y., Satou, C. & Higashijima, S. -i. V2a and V2b neurons are generated by the final divisions of pair-producing progenitors in the zebrafish spinal cord. *Development* **135,** 3001–3005 (2008).
205. 10X Cell Ranger.
206. Tabor, K. M. *et al.* Direct activation of the Mauthner cell by electric field pulses drives ultra-rapid escape responses. *J. Neurophysiol.* 834–844 (2014). doi:10.1152/jn.00228.2014
207. Thiele, T. R., Donovan, J. C. & Baier, H. Descending Control of Swim Posture by a Midbrain Nucleus in Zebrafish. *Neuron* **83,** 679–691 (2014).
208. Kirchmaier, S., Lust, K. & Wittbrodt, J. Golden GATEway cloning--a combinatorial approach to generate fusion and recombination constructs. *PLoS One* **8,** 1–9 (2013).
209. Stemmer, M., Thumberger, T., Del Sol Keyer, M., Wittbrodt, J. & Mateo, J. L. CCTop: An intuitive, flexible and reliable CRISPR/Cas9 target prediction tool. *PLoS One* **10,** 1–11 (2015).
210. Schindelin, J. *et al.* Fiji: An open-source platform for biological-image analysis. *Nat. Methods* **9,** 676–682 (2012).
211. Peirce, J. W. PsychoPy-Psychophysics software in Python. *J. Neurosci. Methods* **162,** 8–13 (2007).
212. Jusuf, P. R. *et al.* Origin and Determination of Inhibitory Cell Lineages in the Vertebrate Retina. **31,** 2549–2562 (2011).
213. Poulain, F. E. & Chien, C. Bin. Proteoglycan-Mediated Axon Degeneration Corrects Pretarget Topographic Sorting Errors. *Neuron* **78,** 49–56 (2013).

214. Boije, H., Rulands, S., Dudczig, S., Simons, B. D. & Harris, W. A. The Independent Probabilistic Firing of Transcription Factors: A Paradigm for Clonal Variability in the Zebrafish Retina. *Dev. Cell* **34,** 532–543 (2015).
215. Pandey, S., Shekhar, K., Regev, A. & Schier, A. F. Comprehensive Identification and Spatial Mapping of Habenular Neuronal Types Using Single-Cell RNA-Seq. *Curr. Biol.* **28,** 1052–1065.e7 (2018).
216. Smear, M. C. *et al.* Vesicular Glutamate Transport at a Central Synapse Limits the Acuity of Visual Perception in Zebrafish. *Neuron* **53,** 65–77 (2007).
217. Wan, L., Almers, W. & Chen, W. Two ribeye Genes in Teleosts: The Role of Ribeye in Ribbon Formation and Bipolar Cell Development. *J. Neurosci.* **25,** 941–949 (2005).
218. Di Donato, V., Auer, T. O., Duroure, K. & Del Bene, F. Characterization of the Calcium Binding Protein Family in Zebrafish. *PLoS One* **8,** 1–13 (2013).
219. Marquardt, T. *et al.* Pax6 Is Required for the Multipotent State of Retinal Progenitor Cells. *Trends Biochem. Sci.* **30,** i (2005).
220. Raymond, P. A., Barthel, L. K., Bernardos, R. L. & Perkowski, J. J. Molecular characterization of retinal stem cells and their niches in adult zebrafish. *BMC Dev. Biol.* **6,** 1–17 (2006).
221. Lakowski, J., Majumder, A. & Lauderdale, J. D. Mechanisms controlling Pax6 isoform expression in the retina have been conserved between teleosts and mammals. *Dev. Biol.* **307,** 498–520 (2007).
222. Yazulla, S. & Studholme, K. M. Neurochemical anatomy of the zebrafish retina as determined by immunocytochemistry. *J. Neurocytol.* **30,** 551–592 (2001).
223. Elshatory, Y., Deng, M., Xie, X. & Gan, L. Expression of the LIM-Homeodomain Protein Isl1 in the Developing and Mature Mouse Retina. *J. Comp. Neurol.* **504,** 287–297 (2007).
224. Gregg, R. G. *et al.* Nyctalopin Expression in Retinal Bipolar Cells Restores Visual Function in a Mouse Model of Complete X-Linked Congenital Stationary Night Blindness. *J. Neurophysiol.* **98,** 3023–3033 (2007).
225. Schroeter, E. H., Wong, R. O. L. & Gregg, R. G. In vivo development of retinal ON-bipolar cell axonal terminals visualized in nyx::MYFP transgenic zebrafish. *Vis. Neurosci.* **23,** 833–843 (2006).
226. Bahadori, R. *et al.* Nyctalopin is essential for synaptic transmission in the cone dominated zebrafish retina. *Eur. J. Neurosci.* **24,** 1664–1674 (2006).
227. Biehlmaier, O., Neuhauss, S. C. F. & Kohler, K. Synaptic plasticity and functionality at the cone terminal of the developing zebrafish retina. *J. Neurobiol.* **56,** 222–236 (2003).
228. Liao, M. L., Peng, W. H., Kan, D. & Chien, C. L. Developmental pattern of the neuronal intermediate filament inaa in the zebrafish retina. *J. Comp. Neurol.* **524,** 3810–3826 (2016).
229. CONNAUGHTON, V. P. P. Bipolar cells in the zebrafish retina. *Vis. Neurosci.* **28,** 77–93 (2011).
230. Li, H. *et al.* Classifying Drosophila Olfactory Projection Neuron Subtypes by Single-Cell RNA Sequencing. *Cell* **171,** 1206.e22-1207 (2017).
231. Hörnberg, H. *et al.* RNA-Binding Protein Hermes/RBPMS Inversely Affects Synapse Density and Axon Arbor Formation in Retinal Ganglion Cells In Vivo. *J. Neurosci.* **33,** 10384–10395 (2013).
232. Campbell, D. S. *et al.* Slit1a inhibits retinal ganglion cell arborization and synaptogenesis via Robo2-dependent and -independent pathways. *Neuron* **55,** 231–45 (2007).
233. Xiao, T., Roeser, T., Staub, W. & Baier, H. A GFP-based genetic screen reveals mutations that disrupt the architecture of the zebrafish retinotectal projection. *Development* **132,** 2955–67 (2005).

234. Kay, J. N., Finger-Baier, K. C., Roeser, T., Staub, W. & Baier, H. Retinal ganglion cell genesis requires lakritz, a Zebrafish atonal Homolog. *Neuron* **30,** 725–36 (2001).
235. Zhang, J. Disruption of gradient expression of Zic3 resulted in abnormal intra-retinal axon projection. *Development* **131,** 1553–1562 (2004).
236. Diekmann, H. & Stuermer, C. A. O. Zebrafish neurolin-a and -b, orthologs of ALCAM, are involved in retinal ganglion cell differentiation and retinal axon pathfinding. *J. Comp. Neurol.* **513,** 38–50 (2009).
237. Martinelli, D. C. *et al.* Expression of C1ql3 in Discrete Neuronal Populations Controls Efferent Synapse Numbers and Diverse Behaviors. *Neuron* **91,** 1034–1051 (2016).
238. Moutsaki, P. *et al.* Teleost multiple tissue (tmt) opsin: A candidate photopigment regulating the peripheral clocks of zebrafish? *Mol. Brain Res.* **112,** 135–145 (2003).
239. Ding, Q. *et al.* BARHL2 Differentially Regulates the Development of Retinal Amacrine and Ganglion Neurons. *J. Neurosci.* **29,** 3992–4003 (2009).
240. Raj, B. *et al.* Simultaneous single-cell profiling of lineages and cell types in the vertebrate brain. *Nat. Biotechnol.* **36,** 442–450 (2018).
241. Gonçalves, P. J., Arrenberg, A. B., Hablitzel, B., Baier, H. & Machens, C. K. Optogenetic perturbations reveal the dynamics of an oculomotor integrator. *Front. Neural Circuits* **8,** 10 (2014).
242. Akitake, C. M., Macurak, M., Halpern, M. E. & Goll, M. G. Transgenerational analysis of transcriptional silencing in zebrafish. *Dev. Biol.* **352,** 191–201 (2011).
243. Suzuki, K. *et al.* In vivo genome editing via CRISPR/Cas9 mediated homology-independent targeted integration. *Nature* **540,** 144–149 (2016).
244. Colombo, A., Reig, G., Mione, M. & Concha, M. L. Zebrafish BarH-like genes define discrete neural domains in the early embryo. *Gene Expr. Patterns* **6,** 347–352 (2006).
245. Poggi, L., Vitorino, M., Masai, I. & Harris, W. A. Influences on neural lineage and mode of division in the zebrafish retina in vivo. *J. Cell Biol.* **171,** 991–999 (2005).
246. Liu, J. *et al.* Tbr1 instructs laminar patterning of retinal ganglion cell dendrites. *Nat. Neurosci.* **21,** (2018).
247. Kajihara, M. *et al.* Mouse MafA, homologue of zebrafish somite Maf 1, contributes to the specific transcriptional activity through the insulin promoter. *Biochem. Biophys. Res. Commun.* **312,** 831–842 (2003).
248. Thisse, B. & Thisse, C. Fast Release Clones: A High Throughput Expression Analysis. (2004). Available at: www.zfin.org.
249. Sweeney, N. T., James, K. N., Nistorica, A. & Feldheim, D. A. Expression of transcription factors divides retinal ganglion cells into distinct classes. (2019). doi:10.1002/cne.24172
250. Ganz, J. *et al.* Subdivisions of the adult zebrafish pallium based on molecular marker analysis. *F1000Research* 1–20 (2015). doi:10.12688/f1000research.5595.2
251. Bae, Y. K. *et al.* Anatomy of zebrafish cerebellum and screen for mutations affecting its development. *Dev. Biol.* **330,** 406–426 (2009).
252. Mao, C.-A. *et al.* Eomesodermin, a target gene of Pou4f2, is required for retinal ganglion cell and optic nerve development in the mouse. *Development* **135,** 271–280 (2007).
253. Hattar, S. Melanopsin-Containing Retinal Ganglion Cells: Architecture, Projections, and Intrinsic Photosensitivity. *Science (80-.).* **295,** 1065–1070 (2002).

254. Thisse, C. & Thisse, B. High Throughput Expression Analysis of ZF-Models Consortium Clones. (2005).
255. Lin, B., Wang, S. W. & Masland, R. H. Retinal Ganglion Cell Type , Size , Report and Spacing Can Be Specified Independent of Homotypic Dendritic Contacts. **43,** 475–485 (2004).
256. Doyle, J. P. *et al.* Application of a Translational Profiling Approach for the Comparative Analysis of CNS Cell Types. *Cell* **135,** 749–762 (2008).
257. Sanes, J. R. & Yamagata, M. Many Paths to Synaptic Specificity. *Annu. Rev. Cell Dev. Biol.* **25,** 161–195 (2009).
258. Yamagata, M., Sanes, J. R. & Weiner, J. A. Synaptic adhesion molecules. *Curr. Opin. Cell Biol.* **15,** 621–632 (2003).
259. Chew, K. S., Fernandez, D. C., Hattar, S., Südhof, T. C. & Martinelli, D. C. Anatomical and Behavioral Investigation of C1ql3 in the Mouse Suprachiasmatic Nucleus. *J. Biol. Rhythms* **32,** 222–236 (2017).
260. Hökfelt, T. *et al.* Neuropeptides — an overview. *Neuropharmacology* **39,** 1337–1356 (2000).
261. Kurrasch, D. M. *et al.* The Neonatal Ventromedial Hypothalamus Transcriptome Reveals Novel Markers with Spatially Distinct Patterning. *J. Neurosci.* **27,** 13624–13634 (2007).
262. Nevin, L. M., Robles, E., Baier, H. & Scott, E. K. Focusing on optic tectum circuitry through the lens of genetics. *BMC Biol.* **8,** 126 (2010).
263. Naumann, E. A. *et al.* From Whole-Brain Data to Functional Circuit Models: The Zebrafish Optomotor Response. *Cell* **167,** 947–960.e20 (2016).
264. D'Orazi, F. D., Zhao, X. F., Wong, R. O. & Yoshimatsu, T. Mismatch of Synaptic Patterns between Neurons Produced in Regeneration and during Development of the Vertebrate Retina. *Curr. Biol.* **26,** 2268–2279 (2016).
265. Wolf, F. A. *et al.* Graph abstraction reconciles clustering with trajectory inference through a topology preserving map of single cells. *bioRxiv* **1,** 208819 (2018).
266. Xiao, T. *et al.* Assembly of lamina-specific neuronal connections by slit bound to type IV collagen. *Cell* **146,** 164–76 (2011).

APPENDIX

List of publications

Koelzer, S., **Kölsch, Y.** & Panfilio, K. A. Visualizing late insect embryogenesis: Extraembryonic and mesodermal enhancer trap expression in the beetle Tribolium castaneum. PLoS One 9, (2014).

Förster, D., Arnold-Ammer, I., Laurell, E., Barker A.J., Fernandes A.M., Finger-Baier, K., Filosa, A., Helmbrecht, T.O., **Kölsch, Y.**, Kühn, E., Robles, E., Slanchev, K., Thiele, T.R., Baier, H., Kubo, F. Genetic targeting and anatomical registration of neuronal populations in the zebrafish brain with a new set of BAC transgenic tools. Sci. Rep. 7, 1–11 (2017).

Submitted

Fernandes, A.M., Larsch, J., Helmbrecht, T., **Kölsch, Y.**, Mearns, D., Donovan, J.C., Dal Maschio, M., Baier, H. Neuronal circuitry for stimulus competition in the visual system.

In preparation for submission in 2019

Kölsch et al. "Genetic specification of labeled lines in the visual system"

Declaration of author contributions

Herwig Baier[1], Joshua Sanes[2], Yvonne Kölsch[1] and Karthik Shekhar[3] designed this study. Yvonne Kölsch carried out single cell RNA-Sequencing experiments with guidance of Irene Whitney[2]. Bioinformatic analysis was performed by Karthik Shekhar and Anna Sappington[3]. Yvonne Kölsch, Manuel Stemmer[1], Shriya Lele[1] and Irene Arnold-Ammer[1] established knockin methods using CRISPR-Cas9 and generated cluster-specific transgenes. Yvonne Kölsch generated transgenic lines used in the intersectional approaches. Functional experiments were carried out by Yvonne Kölsch and analyzed by Thomas Helmbrecht[1]. Yvonne Kölsch and Shriya Lele performed behavioral experiments.

Author affiliations:

[1] Max Planck Institute of Neurobiology, Department Genes - Circuits - Behavior, Am Klopferspitz 18, D-82152, Martinsried, Germany.

[2] Center for Brain Science and Department of Molecular and Cellular Biology, Harvard University, Cambridge, MA, United States.

[3] Klarman Cell Observatory, Broad Institute of MIT and Harvard, 7 Cambridge Center, Cambridge, MA 02142, USA.

Yvonne Kölsch

Prof. Dr. Herwig Baier


SIGILL: UNIVERSI TAT: LUDOVIC: MAXIM:

Affidavit / Eidesstattliche Versicherung

Hiermit versichere ich an Eides statt, dass ich die vorliegende Dissertation "Molecular dissection of the retinal projectome" selbstständig angefertigt habe, mich außer der angegebenen keiner weiteren Hilfsmittel bedient und alle Erkenntnisse, die aus dem Schrifttum ganz oder annähernd übernommen sind, als solche kenntlich gemacht und nach ihrer Herkunft unter Bezeichnung der Fundstelle einzeln nachgewiesen habe.

I hereby confirm that the dissertation " Molecular dissection of the retinal projectome" is the result of my own work and that I have only used sources or materials listed and specified in the dissertation.

München, den
Munich, date

_____

Yvonne Kölsch